

Washington University in St. Louis

Washington University Open Scholarship

Arts & Sciences Electronic Theses and
Dissertations

Arts & Sciences

Spring 5-15-2022

Disuse-Driven Plasticity in the Human Brain

Dillan James Newbold

Washington University in St. Louis

Follow this and additional works at: https://openscholarship.wustl.edu/art_sci_etds



Part of the [Neurosciences Commons](#)

Recommended Citation

Newbold, Dillan James, "Disuse-Driven Plasticity in the Human Brain" (2022). *Arts & Sciences Electronic Theses and Dissertations*. 2684.

https://openscholarship.wustl.edu/art_sci_etds/2684

This Dissertation is brought to you for free and open access by the Arts & Sciences at Washington University Open Scholarship. It has been accepted for inclusion in Arts & Sciences Electronic Theses and Dissertations by an authorized administrator of Washington University Open Scholarship. For more information, please contact digital@wumail.wustl.edu.

WASHINGTON UNIVERSITY IN ST. LOUIS

Division of Biology and Biomedical Sciences

Neurosciences

Dissertation Examination Committee:

Nico Dosenbach, Chair

Deanna Barch

Jin-Moo Lee

Steven Petersen

Marcus Raichle

Abraham Snyder

Disuse-Driven Plasticity in the Human Brain

by

Dillan Jacob Newbold

A dissertation presented to
The Graduate School
of Washington University in
partial fulfillment of the
requirements for the degree
of Doctor of Philosophy

May 2022

St. Louis, Missouri

© 2022, Dillan Newbold

Table of Contents

List of Figures.....	vi
List of Tables	v
Acknowledgements	vi
Abstract.....	xvi
Chapter 1: Introduction.....	1
1.1 Disuse-Driven Neural Plasticity	1
1.1.1 Remapping the Cerebral Cortex	1
1.1.2 Disinhibition of Disused Circuits	3
1.2 Spontaneous Activity and Plasticity	5
1.2.1 Spontaneous Waves of Activity and Early Brain Development	5
1.2.2 Spontaneous Activity During Developmental Critical Periods and Adulthood.....	8
1.3 Tracking Plasticity in the Human Brain.....	9
1.3.1 Recording of Human Brain Activity	9
1.3.2 Large-Scale Functional Networks	10
1.3.3 Precision Functional Mapping.....	12
1.3.4 Plasticity of Human Brain Networks.....	14
Chapter 2: Plasticity and Spontaneous Activity Pulses in Disused Human Brain Circuits.....	17
2.1 Preface.....	17
2.2 Abstract.....	20
2.3 Introduction	20
2.4 Results	22
2.4.1 Casting Caused Disuse and Reduced Strength of the Dominant Upper Extremity....	22
2.4.2 Disused Somatomotor Regions Became Functionally Uncoupled from the Remainder of the Somatomotor System.....	24
2.4.3 Spontaneous Activity Pulses Emerged in the Disused Somatomotor Cortex During Casting.....	27
2.4.4 Disuse Pulses Propagated Throughout the Disused Somatomotor Sub-Circuit.....	30
2.5 Discussion	32
2.5.1 Disuse Drives Large Decreases in Functional Connectivity	32
2.5.2 Functional Connectivity Can Change Rapidly Over a Span of Days.....	32
2.5.3 Disused Sub-Circuits Maintain Internal Connectivity	33
2.5.4 Spontaneous Activity Shapes Neural Circuits During Development.....	34
2.5.5 Focal Disinhibition May Allow the Emergence of Spontaneous Activity Pulses.....	35
2.6.6 The Human Brain – Plastic yet Stable.....	36
2.6 Methods.....	37
2.7 Supplementary Figures	53
2.8 Acknowledgements	65

Chapter 3: Cingulo-Opercular Control Network Supports Disused Motor Circuits in Standby Mode	66
3.1 Preface.....	66
3.2 Abstract.....	69
3.3 Introduction.....	69
3.4 Results	73
3.4.1 Disuse Caused Both Increases and Decreases in Functional Connectivity	73
3.4.2 Disuse-Driven Functional Connectivity Changes Were Highly Focal in Network Space	75
3.4.3 Plasticity Was Restricted to the Somatomotor and Cingulo-Opercular Networks	77
3.4.4 Increased Somatomotor Connectivity with the CON Depended on a History of Disuse	79
3.4.5 Network-Specific Connectivity Changes Reflect Spontaneous Activity Pulses	81
3.5 Discussion	87
3.5.1 Disuse Drives Plasticity of Functional Networks.....	87
3.5.2 Spontaneous Activity Pulses Alter Functional Connectivity	88
3.5.3 Disuse Impacts Cingulo-Opercular Network Important for Executive Control.....	88
3.5.4 Two Complementary Mechanisms for Functional Network Plasticity	92
3.6 Methods.....	93
3.7 Supplementary Figures	105
3.8 Acknowledgements	117
 Chapter 4: Conclusions	 118
4.1 Summary of results	118
4.1.1 Casting Degraded Strength and Fine Motor Skill	118
4.1.2 Spontaneous Activity Pulses Propagated through Disused Brain Circuits	118
4.1.3 Disuse Caused Rapid, Anatomically Specific Changes in Functional Connectivity	119
4.1.4 Functional Connectivity Increases Resulted from Spontaneous Activity Pulses.....	120
4.2 Brain Circuits Require Regular Use to Maintain Their Functional Architecture ..	121
4.3 Disuse Drives Systems-Level Plasticity of Brain Networks.....	125
4.4 Precision Functional Mapping Allows Reliable Measurement of Plasticity.....	126
4.5 Individual Differences in Disuse-Driven Plasticity	127
4.6 Spontaneous Activity Pulses May Help to Maintain Disused Circuits	129
4.6 Relationship between Pulses and Ongoing Spontaneous Activity	132
 References	 134

List of Figures

Figure 2-1. Casting Caused Disuse and Reduced Strength of the Dominant Upper Extremity	23
Figure 2-2. Disused Somatomotor Regions Became Functionally Uncoupled from the Opposite Hemisphere	25
Figure 2-3. Disused Somatomotor Cortex Dissociates from the Remainder of the Somatomotor Network.....	26
Figure 2-4: Spectral Analysis of rs-fMRI Signals from L-SM1 _{ue} and R-SM1 _{ue} during the Pre, Cast and Post Periods.....	28
Figure 2-5: Disuse Pulses in Somatomotor Cortex.....	29
Figure 2-6. Disuse Pulses Propagate through the Disused Somatomotor Sub-Circuit.....	31
Figure 2-S1: Casting Induced Disuse and Decreased Fine Motor Skill of the Dominant Upper Extremity and Increased Use of the Non-Dominant Upper Extremity	53
Figure 2-S2: Disused Cerebellum (R-Cblm _{ue}) Disconnected from the Opposite Hemisphere (L-Cblm _{ue}).....	55
Figure 2-S3: Example Pulses in all Participants	57
Figure 2-S4: Whole-Brain Maps and Pulse Propagation in All Participants.....	58
Figure 2-S5: Pulses in L-SM1 _{ue} Occur in the Absence of Hand Movements.....	60
Figure 2-S6: Wearing a Cast During Scanning Does Not Recreate the Effects of Prolonged Casting	62
Figure 3-1. Experimental Design and Spontaneous Activity Pulses	72
Figure 3-2. Cast-driven Changes in Functional Connectivity (FC) of Disused Somatomotor Cortex (L-SM1 _{ue}).....	74
Figure 3-3. Disused Somatomotor Cortex (L-SM1 _{ue}) Functional Connectivity (FC) Changes in Network Space.....	76
Figure 3-4: Whole-brain Analyses of Disuse-driven Functional Connectivity (FC) Changes	78
Figure 3-5: Connectivity between Disused Somatomotor Cortex and Cingulo-opercular Network during Disuse and Temporary Casting	80
Figure 3-6. Relationship of Spontaneous Activity Pulses to Functional Connectivity (FC) Changes.....	82
Figure 3-7: Censoring Pulses from Functional Connectivity (FC) Measurements.....	84
Figure 3-8. Addition of Simulated Pulses.....	86
Figure 3-S1: Functional Connectivity (FC) Changes Involving the Disused Somatomotor Cortex (L-SM1 _{ue}) in Anatomical Space (All Participants).....	105
Figure 3-S2: Functional Connectivity (FC) Changes Involving the Disused Somatomotor Cortex (L-SM1 _{ue}) in Anatomical and Network Space in Nico and Omar	107
Figure 3-S3: Whole-brain Patterns of Disuse-driven Plasticity.....	109
Figure 3-S4: Functional Connectivity (FC) Changes Explained by Spontaneous Activity Pulses	111
Figure 3-S5: Alternative Distributions for Pulse Magnitudes	113
Figure 3-S6: Functional Connectivity (FC) Changes Caused by Simulated Spontaneous Activity Pulses (All Participants).....	114
Figure 3-S6: Functional Connectivity (FC) Decreases Were Not Explained by Spontaneous Activity Pulses	116
Figure 4-1: Wave-like Propagation of Spontaneous Activity Pulses.....	131

List of Tables

Table 2-S1. MRI Acquisition and Processing Parameters.....	64
--	----

Acknowledgements

I want to start by thanking my mentors, my collaborators, my family, and all the others who have contributed to this thesis and to my education as a neuroscientist. I'm infinitely grateful for the support you have given me that has culminated in this work.

My path into neuroscience dates back to my childhood and there have been many teachers and instructors who helped to train me as a student, a scientist, a physician and a neuroscientist. My first ever clinical role model was Scott Thiel, MD. Dr. Thiel delivered me as a baby and served as my primary physician into early adulthood. He showed me that medicine requires a combination of knowledge and genuine concern for patients' overall wellbeing. Years later, after I had started my own medical training, I had the unique opportunity to shadow Dr. Thiel in the same clinic where I had received care for so many years.

Jeffrey Denburg, PhD, taught me neurobiology at the University of Iowa and was the first to inspire me to ask how my brain produces the incredible, beautiful consciousness I experience every day. Dr. Denburg's teaching led me to pursue an undergraduate research project in neuroscience and he pointed me to Josh Weiner, PhD as a well-suited mentor.

Dr. Weiner was indeed an excellent mentor. He taught me to generate and test hypotheses, and his developmental neurobiology lab gave me numerous hands-on opportunities to apply the molecular and genetic concepts that I was learning in my biology coursework. Dr. Weiner helped me present my first scientific poster, write multiple successful fellowship applications, and produce an honors thesis on trans-synaptic protein interactions regulating synapse development.

He was also a wonderful role model as an academic scientist, demonstrating caring mentorship of all his students and a well-tuned work-life balance. I am also grateful to Michael Molumby, PhD, a graduate student in Dr. Weiner's lab who later extended and published my project (Molumby et al., 2017). Another student in Dr. Weiner's lab, Austin Keeler, PhD, was like an older brother and taught me almost all of my lab skills. Dr. Keeler was also a TA in Dr. Denburg's neurobiology course. He taught me to read scientific literature and frequently engaged in stimulating discussions at the boundaries of philosophy and neuroscience.

My time at Iowa was further enriched by Nandakumar Narayanan, M.D., Ph.D., whom I initially sought out for shadowing opportunities in neurology. I loved seeing how Dr. Narayanan guided his patients in caring for their neurological disorders and how he applied recent medical science to treat them effectively. I still remember my sense of fascination when Dr. Narayanan asked me to ponder the inner experience of a patient we saw with severe anterograde amnesia. Dr. Narayanan took immediate interest in my medical and scientific ambitions and encouraged me to apply to MSTP programs. Drs. Narayanan, Denburg and Weiner were all critical mentors during my application to medical and graduate school.

Michael Bruchas, PhD, was my first scientific mentor at Washington University. During a summer rotation after my first year of medical school, I got the opportunity to manipulate neural activity in a newly discovered GABAergic projection from the amygdala to the ventromedial prefrontal cortex during reward learning. This project was my first opportunity to independently synthesize scientific literature, generate a novel hypothesis and design an experiment to test it. Based on previous descriptions of circuitry within the amygdala and ventromedial prefrontal

cortex and prior fear conditioning experiments, I predicted that optogenetic stimulation of the novel projection would enhance reward extinction in mice, which turned out to be true. This finding later contributed to a manuscript on the projection, which was published by Dong-oh Seo, PhD (Seo et al., 2016). I'd also like to thank Jordan McCall, PhD and Ream Al-Hasani, PhD, who taught me many laboratory techniques and served as excellent role models.

My second year of medical school introduced me to new clinical mentors in psychiatry and neurology. I shadowed Anne Glowinski, MD, MPE, and Timothy Spiegel, MD, in the Child and Adolescent Psychiatry clinic and St. Louis Children's Hospital. While watching Dr. Glowinski manage a teenager progressing toward schizophrenia, I was impressed by the high stakes of psychiatric care. Observing Dr. Spiegel's discussion with the parents of a teenager who recently attempted suicide—and afterwards discussing how the personality disorders visible in the parents likely affected the patient's health—gave me an appreciation for the many layers of complexity that psychiatrists must disentangle in order to effectively manage mental illnesses. Bradley Schlaggar, MD, PhD, provided a wonderful example of compassion and empathy in neurology. I distinctly remember how carefully he communicated with a young mother whose child had experienced a devastating stroke. He took several minutes to ensure that the mother understood the child's prognosis and felt supported by her care team despite a language barrier.

After spending my second year of medical school studying human disease, I strongly wanted to investigate brain disorders in humans. Deanna Barch, PhD could not have been a more perfect mentor to introduce me to the field of human neuroscience. During a summer rotation in her lab, I examined diffusion tensor imaging (DTI) data collected longitudinally in children with very

early-onset depression. These data allowed us to ask how depression influenced the development of the white-matter connections between brain regions. Weekly meetings with Dr. Barch were always incredibly productive and she quickly led me to a hypothesis regarding development of the cingulum bundle. It was very exciting to test clinically relevant questions in actual patients.

My project with Dr. Barch also required a skillset that was completely new to me: computer programming. The process of learning multiple new computer languages and executing a complex DTI processing pipeline was very exciting and challenging, but it could have become overwhelming without the help of Michael Harms, PhD and Sridhar Kandala. Dr. Barch was also critical later in my training in helping me to prepare my first training grant. Dr. Barch runs an annual course on grant writing that was the most useful course I have taken in graduate school. She taught me nearly everything I know about grant strategy and gave detailed feedback on several key sections of my F31 application.

Dr. Barch introduced me to several human neuroscience methodologies. One method I found particularly exciting was the recording of spontaneous brain activity using resting-state functional MRI (rs-fMRI). This method non-invasively tracks patterns of brain activity while participants lie quietly awake in an MRI scanner. Many studies have linked atypical patterns of spontaneous activity to neurological and psychiatric diseases, but to date, the clinical utility of rs-fMRI is limited to pre-surgical mapping. Advancing clinical application of rs-fMRI would be an incredibly exciting and fulfilling outcome for my career. I decided to pursue a project examining spontaneous brain activity and I soon discovered that I was at the world's top institution for this exact topic. Some of the earliest application of human imaging methods to study brain activity

were performed by Marcus Raichle, MD, and Steven Petersen, PhD, at Washington University. Together with others, they built the Neuroimaging Laboratories (NIL), an expansive but tight-knit network of dozens of faculty members, post-docs and graduate students. This uniquely collaborative environment is where I began my career as a neuroscientist.

My final rotation was with Nico Dosenbach, MD, PhD. Dr. Dosenbach was early in his career and provided a great demonstration of how to build a lab. When I joined the lab, it consisted of one post-doc, Mario Ortega, PhD, one graduate student, Catherine Hoyt, PhD, OTD, OTR/L, and one research assistant, Jacqueline Hampton. Each of my original lab-mates contributed greatly to the work described here. Dr. Dosenbach, in addition to advising me throughout my PhD training, also volunteered as the first participant in our casting study. Dr. Ortega came in every morning for 38 consecutive days at 5 a.m. to scan Dr. Dosenbach, and he helped teach me to work with rs-fMRI data. Dr. Hoyt, a practicing occupational therapist, was critical in constructing safe and effective casts and quantifying changes in behavior. Ms. Hampton organized and managed much of the data collection for this project. Her organizational skill made the entire experiment run smoothly, despite its extensive data collection.

The Dosenbach Lab closely adjoins the labs of Drs. Petersen and Schlaggar and Deanna Greene, PhD, who all provided helpful intellectual feedback. The students, post-docs and research assistants in these adjoining labs also became valuable colleagues. Timothy Laumann, MD, PhD, taught me a great deal about processing MRI data and offered exciting and inspiring tales of his early clinical experiences in psychiatry. Ashley Nielsen, PhD, volunteered as a participant in our study. A frequent study participant, Dr. Nielsen had honed an impressive ability to hold still

during extended (30+ min) rs-fMRI scans. She went to painstaking efforts to provide reliable data and avoid confounding lifestyle changes. Caterina Gratton, PhD, worked as a post-doc with Dr. Petersen during most of my training and provided an outstanding example of how to apply an existing skill set to new problems and launch a new career. Evan Gordon, PhD, was a former post-doc of Dr. Petersen. He was actually at the VA in Waco, TX the during most of my training, but we frequently collaborated on multiple projects. Dr. Gordon was a crucial resource for generating individual-specific network parcellations and his well-organized code served as an example for my own analysis scripts. Ben Seitzman, PhD, a graduate student and later post-doc of Dr. Petersen, was a wonderful source of information, conversation, and frozen candy bars. Babatunde Adeyemo worked as a laboratory technician for Dr. Petersen and provided valuable assistance with data quality control, as well as frequent conversation.

Dr. Dosenbach is always hustling, and our lab has grown steadily over the past several years. We have added three new graduate students, Andrew Van, Annie Zheng and Nicole Seider; two new post-docs, Scott Marek, PhD, and David Montez, PhD; two engineers, Ryland Miller and Amy Mirro; a neurology fellow, Ben Kay, MD, PhD; a masters student, Derek Miller; and a new research assistant, Kristen Scheidter. Many of these lab-mates have helped to collect and analyze the data in this project or have put these data to use in their own lines of work. Together with the students, post-docs and research assistants of our adjoining labs, these people have also created a fun and wonderful lab environment for me to enjoy throughout my PhD.

I also enjoyed the company and collaboration of many other members of the NIL. I could not have completed any of this project without the guidance of Abraham Snyder, MD, PhD. Dr.

Snyder in many ways served as second research advisor throughout my PhD training. He was involved in every aspect of this thesis work. Dr. Snyder taught me crucial data processing skills, guided me through literature reviews, provided advise on data collection, discussed complex neural mechanisms at length, and provided extensive edits on all of my writing. I also got to enjoy Dr. Snyder's company during late-night jigsaw puzzle sessions, Korean barbecue dinners and classical music performances. Working with Marcus Raichle, MD, was one of the most exciting honors of my PhD. It was a recording of Dr. Raichle's Kavli Prize lecture that inspired me to pursue the study of spontaneous neural activity. My first meeting with Dr. Raichle brought the nervousness of meeting a favorite celebrity. Dr. Raichle's contributions to this thesis work have been invaluable. He, along with his graduate student Ryan Raut, suggested the connection between disuse-driven spontaneous activity pulses and developmental slow activity transients, which, for me, has been the most fascinating idea to come from this project. I am also very grateful to Joshua Shimony, MD, PhD, who taught me everything I know about the fundamental physics underlying magnetic resonance imaging. Dr. Shimony volunteers to teach an annual summer seminar on the topic, which is very well attended, even by senior faculty members. This is just one example of Dr. Shimony's kind and generous nature. Alexandre Carter, MD, PhD, is another member of the NIL who has helped to guide me though my PhD training. His expertise in stroke, neurorehabilitation, neural stimulation, and behavioral monitoring have made him an important collaborator. Last but not least, I must thank my friend Aaron Tanenbaum, a laboratory technician in the NIL. Mr. Tanenbaum's programming skill made him a useful colleague for overcoming technical challenges. I'm also grateful for his refined palette, which make him an excellent chef and a natural cicerone.

Washington University has an excellent Neuroscience program beyond the NIL. I benefitted greatly from the collaboration of Dr. Jin-Moo Lee. Dr. Lee, as well as Zachary Rosenthal, an MD/PhD candidate training with Dr. Lee, were vital sources of information regarding the role of intracortical inhibition on spontaneous neural activity. They provided useful recommendations of existing literature and shared their own cutting-edge results, both of which were highly influential on my interpretations of the phenomena revealed by my experiments.

This work has also relied on several organizations that have provided financial and administrative support. The Medical Scientist Training Program (MSTP) at Washington University admitted me for MD/PhD training and provided stipend and tuition support during medical school and the first year of my PhD training. Additionally, the MSTP's Program Director, Wayne Yokoyama, MD, as well as its senior administrators, Brian Sullivan, Christy Durbin, and Linda Perniciaro, have provided key guidance and administrative support to assist with all aspects of my clinical and scientific training. Some of my financial support has also come from the Division of Biology and Biomedical Sciences (DBBS), and I frequently relied on two of its administrators, Sally Vogt and Dana Kharibian, for advice and administrative support. I also received a full year of financial support, as well as advanced multidisciplinary training, from the Cognitive Computational and Systems Neuroscience (CCSN) pathway and the McDonnell Center for Systems Neuroscience, with additional administrative support from Carmen Horn and Laura Williams, MBA. Finally, a large portion of the research funding that has been awarded to me, both directly and indirectly, came from the National Institutes of Health (NIH), especially the National Institute of Neurological Disorders and Stroke (NINDS). I thank my Program Officer, Daofen Chen, PhD, for overseeing the evaluation and funding of my own

training fellowship (F31-NS110332) and a career development grant awarded to Dr. Dosenbach (K23-NS088590), which both supported this thesis work.

I am immensely grateful to my family and friends, who have supported me throughout my education and made my work feel worthwhile. My parents, Michele and Andrew, praised my intelligence from a very young age and encouraged me to pursue a career in medicine. Their love, sacrifice, and guidance were crucial in shaping my path through my early education and into college. My grandparents, Bill, Jody, Ron, and Mary, always ask for updates on my research progress and remind me of the unique value of what I am doing. My brother, Lucas, shares my interest in pharmacology and we have had many discussions on the topic. My sister, Ella, is constantly reminding me of my early academic achievements, as she models her own educational path off of mine. My parents-in-law, Steve, Rachel, Jean, and Ken, and my new sisters, Rebekah, Annah, Mallory, and Colleen, have always kept close tabs on my progress through PhD training and asked extraordinarily insightful questions about my thesis work.

Some of my closest friends, Doug Baker, Patrick Sprecher, and Cole Wigert, have known me since high school. Their cooperation and friendly competition were key to my success in high school. We all continue to have deep and meaningful conversations about the inner workings of the mind and other fundamental mysteries of the universe. Kalyan Tripathy, Lindsey Brier, Chuner Guo, Ethan Trifari, Chris Mejias, and several others mentioned earlier in these acknowledgements, have made my time in St. Louis wonderful and exciting and will remain close friends and colleagues throughout my career.

Most of all, I thank my wife, Sarah Gross. Her love and support have made all of this worthwhile. We were first attracted to each other, in part, because of our intelligence and shared interest in medicine. Sarah is always the first to hear about my key findings, and she reads all of my writing. Along with our dog, Otto, and our two cats, Coffee and Africa, she is my constant companion and the source of my sanity. Next year, Sarah and I will apply together for our residency training, and we will continue to build and support one another throughout our careers.

Dillan Newbold

Washington University in St. Louis

May 2022

ABSTRACT OF THE DISSERTATION

Disuse-Driven Plasticity in the Human Brain

by

Dillan Newbold

Doctor of Philosophy in Biology and Biomedical Sciences

Neurosciences

Washington University, 2022

Professor Nico Dosenbach, Chair

Brain circuits are shaped and maintained by active use. We blocked use of motor circuits in three adult participants by constraining the dominant upper extremity in a cast for two weeks, causing loss of strength and fine motor function. Daily resting-state functional magnetic resonance imaging (rs-fMRI) collected for 42-64 days before, during and after casting revealed two sets of changes in brain function. First, large, spontaneous pulses of activity occurred in the disused motor circuits. Pulses showed a consistent pattern of propagation through the disused circuits—occurring earliest in the dorsal anterior cingulate cortex (dACC) and supplementary motor area (SMA), then propagating to the primary motor cortex, and finally occurring in motor regions of the cerebellum. Second, participants exhibited anatomically focal changes in functional connectivity (FC), i.e., synchrony of spontaneous activity. The disused motor cortex lost typical FC with the remainder of the somatomotor system. Additionally, disused regions of the primary motor cortex and cerebellum became more connected to an executive control system known as the cingulo-opercular network (CON). Spontaneous activity pulses, which occurred in disused

motor regions and the CON, accounted for observed increases in FC. Loss of FC between the disused motor circuits and the somatomotor network was not explained by pulses and may have resulted from decreased co-use of the affected circuits with the remainder of the somatomotor system, which is typically thought to maintain FC in a Hebbian-like manner. Together, these two forms of plasticity, Hebbian disconnection from the somatomotor system and pulse-mediated connection to the CON, may form a protective “standby mode” that isolates disused circuits and prevents premature functional degradation.

Chapter 1: Introduction

This thesis concerns plasticity, the process that shapes brain circuits during development and continually refines them throughout life. A crucial part of normal developmental plasticity is active use of brain circuits (Blumberg et al., 2013; Buzsáki, 2019). Regular use may also be required to maintain circuits throughout life. Motor circuits deprived use receive no feedback by which to maintain an accurate representation of the body or the outside world. Such deprivation, referred to here as disuse, causes systematic reorganization of affected circuits and leads to deterioration of function (Clark et al., 2008; Milliken et al., 2013).

What mechanisms does the brain have to protect circuits from disuse-driven functional deterioration? One possibility is that circuits are maintained by internally generated spontaneous activity. Spontaneous activity helps to shape circuits early in development, before they have had any contact with the outside world. We suggest that related mechanisms may act in the adult brain to maintain the organization of large-scale circuits during disuse.

1.1 Disuse-Driven Neural Plasticity

1.1.1 Remapping the Cerebral Cortex

A great deal of progress in neuroscience has come from experiments that blocked the normal interactions between brain circuits and the outside world, i.e. experiments that induced disuse. The most famous example of this approach is the Nobel Prize-winning work of David Hubel and Torsten Wiesel. Neurons in the primary visual cortex (V1) respond to visual stimuli at specific

positions in visual space, termed receptive fields (Hubel and Wiesel, 1959). V1 is retinotopically organized, such that adjacent points in visual space (adjacent receptive fields) are represented by adjacent columns of cortical neurons (Drager, 1975). For portions of the visual field visible to both eyes, V1 receives overlapping binocular inputs (Hubel and Wiesel, 1959). Binocularly innervated regions of V1 organize into alternating stripes of neurons that respond to inputs from one of the two eyes (Grafstein, 1971; Hubel and Wiesel, 1972; LeVay et al., 1975). Hubel and Wiesel showed that these alternating representations are shaped by use-driven plasticity, as afferents from the two eyes compete with one another for representational territory in V1 (Wiesel and Hubel, 1963, 1965). Monocular deprivation, i.e., suturing shut one eye, causes afferents from the deprived eye to lose territory in V1, with neurons previously responsive to the sutured eye instead responding to the un-sutured eye.

A related form of plasticity can be seen in the primary somatosensory cortex (S1). S1 forms a somatotopic map of the body, with adjacent regions of the body represented by nearby neurons in S1 (Penfield and Boldrey, 1937). The trigeminal nerve territory of the face and neck is represented in the ventrolateral portion of S1 and the spinal nerves provide inputs to the dorsal portion, with the most caudal afferents (e.g., those from the lower extremities and perineum) innervating the dorsomedial portion of S1 along the interhemispheric fissure. Even in the fully developed adult brain, this somatotopic organization can be remapped by disuse. Severing the median nerve of one upper limb (Merzenich et al., 1983a) or amputating one digit (Merzenich et al., 1984) causes S1 neurons that previously responded to tactile stimulation of the deafferented or amputated skin to instead respond to stimulation of neighboring skin. In the case of amputation of an entire limb, the deafferented cortex can even respond to stimulation of the face,

forming a “phantom map” of the amputated limb on the skin of the face (Ramachandran et al., 1992). Similar somatotopic reorganization is also seen in rodents after whisker trimming (Van der Loos and Woolsey, 1973; Diamond et al., 1993).

Topographic remapping is not limited to sensory areas. Another somatotopic map exists in the primary motor cortex (M1). Representations of distal upper extremity movements are adjacent in M1 to more proximal representations. These neighboring response fields can be mapped out in non-human primates by applying focalized electrical stimulation and documenting subsequent motor responses. Casting one upper extremity for several months causes distal representations to lose territory in M1 (Milliken et al., 2013). After casting, stimulating regions that once elicited finger or wrist movements now caused movements at the elbow and shoulder joints. This motor plasticity lasted several weeks after casting but eventually reversed after casts were removed and regular limb use resumed.

Most studies to date of topographic plasticity have used focalized recording techniques, usually focusing on a single brain region. Thus, little is known about how use and disuse reorganize large-scale circuits spanning multiple cortical and subcortical regions. However, these single-region studies have revealed a great deal concerning the molecular and cellular mechanisms of disuse-driven plasticity.

1.1.2 Disinhibition of Disused Circuits

Experiments examining the time course of plasticity following peripheral nerve deafferentation revealed that map plasticity proceeds through two phases (Merzenich et al., 1983b). Immediately

after deafferentation, some neurons in the deafferented cortical area begin to respond to previously silent afferent inputs, a phenomenon termed “unmasking”. Then, over the course of several weeks, new sensory representations fill the entire deafferented cortex and are gradually refined into a smooth somatotopic map. Because “new” representations were observed immediately after deafferentation, the authors speculated that these inputs must have been present prior to deafferentation and that deafferentation removed some mechanism that previously suppressed their responses, hence the term “unmasking”. Later work revealed that unmasking is mediated, at least in part, by focal disinhibition of disused cortex, evident as local reductions in gamma amino butyric acid (GABA) (Garrahy et al., 1991), a key inhibitory neurotransmitter, and GABA receptor expression (Wellman et al., 2002). The gradual remapping process that occurs after unmasking appears to be driven by activity-dependent plasticity, as this gradual remapping, but not the initial unmasking, is blocked by chronic administration of an NMDA-receptor antagonist (Garrahy and Muja, 1996).

Other animal models of disuse provided additional insights into the physiological mechanisms supporting map plasticity. Studies of barrel cortex plasticity following whisker trimming found additional evidence of disinhibition in disused cortex (Welker et al., 1989; Fuchs and Salazar, 1998; Kelly et al., 1999). Although disuse-driven disinhibition appears to be mediated by multiple mechanisms, later work found that an especially rapid mechanism of disinhibition following whisker trimming is reduced intrinsic excitability of parvalbumin-positive inhibitory interneurons (Gainey et al., 2018).

Altered physiology of inhibitory interneurons is not only important for acute unmasking during disuse but may be crucial for permitting disuse-driven plasticity more broadly. A point that has so far been ignored in this introduction is the effect of developmental age on disuse-

driven plasticity. Early experiments focused on disuse-driven plasticity in neonatal animals (Wiesel and Hubel, 1963, 1965; Van der Loos and Woolsey, 1973). It turned out that plasticity of a given brain region is always greatest during a specific period of early development, known as a critical period (Hubel and Wiesel, 1970). Later investigations into critical period physiology pointed to changes in inhibitory interneurons, especially the maturation of parvalbumin-positive interneurons, as a key factor permitting critical period plasticity (Hensch, 2004). Mice lacking one isoform of glutamic acid decarboxylase (GAD65), an enzyme responsible for the synthesis of GABA, never enter a critical period (Hensch et al., 1998). This deficit can be reversed by infusion of diazepam, a GABA agonist (Fagiolini and Hensch, 2000). Additionally, transplantation of immature inhibitory interneurons permits critical period-like plasticity in the adult cortex (Southwell et al., 2010; Tang et al., 2014). Disinhibition following disuse may represent a form of developmental regression that “reopens” a critical period-like physiological state and enhances adult plasticity (Harauzov et al., 2010; Letzkus et al., 2015).

1.2 Spontaneous Activity and Plasticity

1.2.1 Spontaneous Waves of Activity and Early Brain Development

Although early visual experience greatly influences the development of retinotopic maps in V1 (Wiesel and Hubel, 1963, 1965), retinotopy is present even prior to visual experience (Wiesel and Hubel, 1974). Development of retinotopic maps before visual experience depends on a combination of genetically encoded axon guidance cues and spontaneous neural activity (Espinosa and Stryker, 2012). Neurons in prenatal V1 express ephrin-A signaling molecules in a gradient, such that neurons located more posteriorly in V1 express greater levels of ephrin-A

(Feldheim and O'Leary, 2010). Similarly, neurons in the developing lateral geniculate nucleus (LGN), which project to V1, express a gradient of EphA receptors. As axon growth cones navigate from the LGN to V1, axons expressing high levels of EphA receptors tend to terminate in regions of V1 with high ephrin-A concentrations and axons with low EphA receptor expression terminate in regions with low ephrin-A concentrations. Additional families of signaling molecules and receptors establish a ventral-dorsal axis of V1 topography (Feldheim and O'Leary, 2010). Together, these various signaling molecules guide the formation of a crude retinotopic map in V1.

Once a retinotopic map is roughly established in V1 by molecular guidance cues, retinotopy is further refined by waves of spontaneous activity that originate in the retina. Early evidence of activity-dependent prenatal visual development came from experiments showing that silencing LGN neurons of fetal cats with tetrodotoxin, a sodium channel blocker, prevented segregation of inputs from the left and right eyes within the LGN (Shatz and Stryker, 1988). Because cats lack photoreceptors prior to birth (Greiner and Weidman, 1980), it was assumed that the activity that supported retinogeniculate segregation must be generated spontaneously. Spontaneous activity in retinal ganglion cells, which project to the LGN, was directly observed soon afterwards (Galli and Maffei, 1988). Closer examination of this spontaneous activity revealed that it propagated as waves across the retina (Meister et al., 1991). Two decades later, the advent of *in vivo* calcium imaging made it possible to demonstrate that these retinal waves triggered similar waves of activity in higher visual structures, including the superior colliculus and primary and secondary visual cortex (Ackman et al., 2012). It was suggested that co-activation of neighboring retinal ganglion cells during spontaneous retinal waves could instruct refinement of retinotopic maps in

downstream structures (Meister et al., 1991; Wong, 1999), a theory later formalized using computational modeling (Butts et al., 2007; Kim et al., 2020). The importance of retinal waves in retinotopic refinement was also confirmed experimentally. Both genetic and pharmacologic blockage of retinal waves during development disrupts normal retinotopy in the LGN (Cang et al., 2005).

A similar form of spontaneous activity helps to shape the somatomotor maps in the cerebellum, cerebral cortex and other brain regions (Blumberg et al., 2013; Buzsáki, 2019). Spontaneous embryonic movements have been studied for over 150 years (Preyer, 1885) and have long been thought to support development of the somatomotor system (Hamburger, 1963). Embryological movements are triggered by waves of spontaneous activity that propagate between motor neurons in the spinal cord (Provine, 1972; Blankenship and Feller, 2010). Patterned somatosensory feedback resulting from spontaneous movements is thought to promote self-organization of pattern-generating circuits in the spinal cord (Petersson et al., 2003).

Patterned afferent inputs resulting from retinal waves or spontaneous embryological movements are relayed by the thalamus to the cortex. Excitatory feedback between the thalamus and cortex is thought to amplify afferent inputs, producing a characteristic long-lasting (1-10 s) cortical depolarization crested by higher frequency (~14 Hz) cortico-thalamic oscillations (Khazipov et al., 2004). Interestingly, these oscillations continue to occur even if the spinal cord is severed, although they occur less frequently, indicating that they can also be triggered by mechanisms within the brain, possibly involving thalamus and cortex (Khazipov et al., 2004). Similar oscillatory patterns, referred to as either slow activity transients, spindle bursts or delta brushes,

also occur in the visual cortex, where they are triggered by retinal waves (Hanganu et al., 2006; Colonnese and Khazipov, 2010). In both the visual and somatomotor systems, repeated reactivation caused by thalamo-cortical oscillations may promote activity-dependent plasticity and thus enhance topological refinement by spontaneous activity waves (Khazipov et al., 2004; Buzsáki, 2019). Delta brushes have also been observed in preterm human infants using scalp electroencephalography (Khazipov and Luhmann, 2006; Milh et al., 2007; Tolonen et al., 2007).

1.2.2 Spontaneous Activity During Developmental Critical Periods and Adulthood

As development progresses, the dynamics of spontaneous neural activity gradually transform into a continuous pattern of Gaussian fluctuations. Early prenatal brain activity shows a discontinuous pattern, in which brief neural activations are separated by long periods of silence (Tolonen et al., 2007). The brief activations are slow activity transients that depolarize nearly all of the neurons in a given brain region and the long period of silence represent refractory periods (Blankenship and Feller, 2010). Later in development, the mechanisms that generate slow activity transients change and so do the overall dynamics of spontaneous activity (Blankenship and Feller, 2010). As GABAergic inhibition begins to dampen slow activity transients, the interleaved refractory periods also become shorter (Tolonen et al., 2007). This inhibition of spontaneous activity is thought to promote responses to external stimuli that drive plasticity during developmental critical periods (Toyoizumi et al., 2013). Perhaps because of this elevated inhibitory tone, spontaneous activity in the adult brain is typically characterized by stationary, ongoing fluctuations without transients (Laumann et al., 2017).

1.3 Tracking Plasticity in the Human Brain

1.3.1 Recoding of Human Brain Activity

Historically, neuroscience has mostly relied on animal models. The electrophysiological, histological and biochemical techniques classically used to study the brain are generally far too invasive to use in humans. One of the earliest non-invasive methods for recording brain activity was electroencephalography (EEG). Hans Berger showed in 1924 that wires mounted on the scalp could record activity that occurs persistently in the human brain (Berger, 1929). EEG has been incredibly informative, revealing unique forms of spontaneous activity that occur in sleep (Davis et al., 1937), early development (Dreyfus-Brisac and Larroche, 1971), and neurological diseases (Jasper and Kershman, 1941). Even today, EEG is still the most widely used tool for clinical recordings of the human brain (Tatum et al., 2018). However, EEG is severely limited in its spatial resolution (Hedrich et al., 2017). More localized electrophysiological techniques can only be applied to patients undergoing neurosurgery (Penfield and Boldrey, 1937).

A major advance in human neuroscience was the application of radiological imaging techniques to record human brain activity. Marcus Raichle and others in the Neuroimaging Labs (NIL) at Washington University showed that positron emission tomography (PET), which allows quantitative mapping of tissue radiography (Raichle, 1979), could be used to monitor cerebral blood flow (Herscovitch et al., 1983; Raichle et al., 1983). Soon, Dr. Raichle, along with Steven Petersen, Peter Fox, Michael Posner, and Mark Mintun, showed that this approach could be used to study the human brain in action, revealing brain regions with increased blood flow during specific cognitive operations (Petersen et al., 1988).

Neural recordings became even less invasive with the discovery that deoxygenated hemoglobin provides a naturally occurring MRI contrast agent, sensitive to changes in cerebral blood flow (Ogawa et al., 1990). This permitted recording of neural activity without the need for radioactive tracers. In addition to dramatically improving the practicality of collecting human neuroimaging data, blood oxygen level-dependent (BOLD) functional MRI (fMRI) provided superior anatomical localization, allowing distinction of activity in neuronal populations separated by as little as 1.4mm (Engel et al., 1994). The discovery of the BOLD signal led the widespread use of fMRI to examine brain function during uniquely human cognitive operations, such as social processing (Eisenberger et al., 2003), moral judgements (Greene et al., 2001), and placebo responses (Wager et al., 2004), and enabled *in vivo* examinations of the patients with neurological and psychiatric diseases (Bush et al., 1999; Sheline et al., 2001).

1.3.2 Large-Scale Functional Networks

Brain regions do not function in isolation but instead cooperate with other brain regions to perform specific cognitive operations. The concepts of brain networks—sets of cooperating brain regions—has existed for at least several decades (Posner and Petersen, 1990). Non-invasive, whole-brain imaging has made it possible to study brain networks directly in the human brain. Early studies identified networks based on shared activation patterns during task performance (Raichle et al., 2001; Shulman et al., 2001; Dosenbach et al., 2006). However, this approach is challenging for at least two reasons: 1) a given network is only activated during specific tasks, meaning that many tasks must be studied in order to comprehensively map the functions of all brain regions, and 2) many tasks activate multiple networks, meaning that a group of regions

labeled as a network based on one task may be divided into multiple networks based on other tasks.

Another approach for identifying brain networks is the analysis of spontaneous activity, i.e., activity not directly related to external stimuli or overt behaviors, recorded while participants lie at rest. The vast majority of the brain's energy is expended on spontaneous activity (Raichle, 2006). The largest fluctuations in spontaneous activity occur at an infra-slow time scale (< 0.1 Hz) (He et al., 2010), which means that they can be monitored using fMRI. Among the first to realize that spontaneous fluctuations in adult brain activity recorded with fMRI were of functional importance was Bharat Biswal. He showed in 1995 that spontaneous fluctuations in the BOLD signal recorded in the left motor cortex were not noise, but were in fact tightly correlated with fluctuations in other regions of the motor system (Biswal et al., 1995). Biswal termed this synchrony in spontaneous activity “functional connectivity,” a name that remains widely used today.

Functional connectivity (FC) does not only exist within the motor system. FC was also observed in the visual and auditory cortex (Lowe et al., 1998; Cordes et al., 2001). Several brain networks previously identified by task activations were also shown to exhibit FC (Greicius et al., 2003; Fox et al., 2006; Dosenbach et al., 2007). In 2005, Mike Fox, Avi Snyder, Justin Vincent, Maurizio Corbetta, David Van Essen, and Marc Raichle showed that the entire cerebral cortex could be divided into two diametrically opposed systems based on FC (Fox et al., 2005). This comprehensive analysis of FC was expanded in 2011 by Jonathan Power and others working with Steve Petersen, who used a graph theoretic community detection algorithm (Rosvall and

Bergstrom, 2008) to identify over a dozen functional networks in the cerebral cortex (Power et al., 2011). Almost simultaneously, B. T. Thomas Yeo and others published another FC-based cortical parcellation using alternative methods (Yeo et al., 2011).

Although different studies have divided the brain into differing numbers of functional networks, some key brain networks include the visual, auditor and somatomotor networks; (Lowe et al., 1998; Cordes et al., 2001); the ventral and dorsal attention networks (Shulman et al., 2001; Fox et al., 2006); the default mode network with roles in internally directed cognition and episodic memory (Raichle et al., 2001; Greicius et al., 2003); the salience network thought to assess the homeostatic relevance of external stimuli (Seeley et al., 2007); the frontoparietal control network supporting error-processing and moment-to-moment adjustments in behavior (Dosenbach et al., 2007; Dosenbach et al., 2008; Marek and Dosenbach, 2019); and the cingulo-opercular control network (CON), which maintains executive control during goal-directed behavior (Dosenbach et al., 2006; Dosenbach et al., 2007; Dosenbach et al., 2008).

1.3.3 Precision Functional Mapping

FC measurements include substantial variance, which results from a combination of measurement noise, differences in behavioral state, and inter-individual variability (Gratton et al., 2018). The classic approach to overcoming measurement variability was to pool data from many individuals into a group-average measurement (Power et al., 2011; Yeo et al., 2011). This approach is problematic because individuals differ in their anatomy. Sophisticated registration algorithms have enabled near-perfect alignment of individuals based on cortical folding and myelination (Robinson et al., 2014). However, even with near-perfect anatomical registration,

individuals still differ in their functional anatomy; a brain region that is part of one network in one individual may align with a region with an entirely distinct function in another individual (Seitzman et al., 2019). A more recent approach to dealing with measurement variability is to collect extensive rs-fMRI data (>30 minutes) in each participant and carry out analyses separately in each individual, an approach termed Precision Functional Mapping (PFM).

PFM was initially inspired by Russ Poldrack, who scanned himself twice per week for an entire year as part of an experiment he termed the MyConnectome Project (Poldrack et al., 2015). He shared this extensive dataset with Steve Petersen's lab, where Tim Laumann and others applied the lab's network parcellation methods to generate a high-fidelity map showing the functional organization of Dr. Poldrack's brain (Laumann et al., 2015). Dr. Laumann also analyzed how the reliability of this functional map changed with the amount of data collected, revealing that at least 30 minutes of data were required to achieve a test-retest correlation of 0.9. This study also revealed several regions of Dr. Poldrack's brain that functionally differed from a previously published, group-averaged parcellation. PFM was further advanced by Dr. Nico Dosenbach, another trainee of Dr. Petersen, and others, who collected 10 additional highly sampled individual-specific rs-fMRI datasets (Gordon et al., 2017). This study, termed the Midnight Scan Club (MSC) experiment, confirmed many of the findings from MyConnectome Project and also revealed new individual differences in functional network organization. The MSC dataset has since been used to generate individual-specific maps of several deeper brain structures, which are classically challenging to map using rs-fMRI because of their poor signal-to-noise ratios, including the cerebellum (Marek et al., 2018), basal ganglia (Greene et al., 2020), amygdala (Sylvester et al., 2020), and hippocampus (Zheng et al., *in preparation*). In addition to identifying

individual differences, PFM also allow for finer-scale network parcellation (Braga and Buckner, 2017; Gordon et al., 2020) and tracking of FC changes across time (Poldrack et al., 2015; Pritschet et al., 2020).

Another key finding of PFM is that functional network organization is highly stable across time (Laumann et al., 2015) and across behavioral states (Gratton et al., 2018). The highly reliable measurement provided by PFM lead to an obvious scientific question: Can a person's functional network organization be modified by experiment manipulations?

1.3.4 Plasticity of Human Brain Networks

Several prior studies have induced changes in human behavior or experience in hopes of measuring plasticity with rs-fMRI. Perhaps the first of these studies was by Dhond *et al.*, who reported strengthened FC in the somatomotor and default mode networks following 2.5 minutes of acupuncture (Dhond et al., 2008). A year later, Lewis *et al.* used a visual discrimination task to train participants to focus their attention on one visual quadrant (Lewis et al., 2009). They reported many different changes in FC throughout the brain, but the most compelling of these effects was a decrease in FC between the dorsal attention network and the trained quadrant of V1. They also found increased FC between the untrained regions of V1 and the default mode network. At least two separate studies have scanned participants before and after training on a visuomotor adaptation task (Albert et al., 2009; Shannon et al., 2016). This task requires participants to use a joystick to move a cursor from a center point on a screen to surrounding targets. As trials progress, the relationship between joystick movement and cursor movement is gradually rotated, so that the cursor moves up to 60 degrees away from the direction of joystick

movement. Participants can learn to compensate for this rotation quickly, even if they are unaware of the rotation. Albert *et al.* reported increased FC in a fronto-parietal network and in some cerebellar regions following motor adaptation training (Albert et al., 2009). Shannon *et al.* found reduced FC between a ventrolateral premotor region (Brodmann Area 44) and the primary visual cortex (Shannon et al., 2016). The Shannon study also reported other functional changes in BA44, including reduced activation during task performance and increased aerobic glycolysis (measured using PET) after training.

Many other studies have attempted to induce changes in FC using various training paradigms. Some additional examples include serial reaction time tasks (Sami et al., 2014), force field adaptation (Vahdat et al., 2011), and real-time neurofeedback (Harmelech et al., 2013). Several other studies are reviewed by Guerra-Carrillo *et al.* (Guerra-Carrillo et al., 2014). Although these studies, and those mentioned in the previous paragraph, used a wide variety of training paradigms, they have at least one unifying feature: they all reported very small changes in FC ($\Delta r \sim 0.1$) following training. This fits with a more recent finding that whole-brain patterns of FC are highly stable across months of scanning (Laumann et al., 2015). In aggregate, these works suggest that FC can be modified slightly by experience, but that functional connections appear to be roughly the same despite a person's recent experiences.

There have been some observations that show FC can be modified drastically under extreme circumstances. Patients that have suffered strokes of the corticospinal tract (CST) can show markedly reduced FC ($\Delta r \sim 0.5$) between the left and right motor cortex (Carter et al., 2012). For patients with mild CST damage, reductions in FC predict residual strength and fine motor

function, such that higher FC (more similar to control participants) predicted greater strength and fine motor function (Carter et al., 2012). A related finding is reduced FC in patients missing one hand, either due to a congenital malformation or an amputation (Hahamy et al., 2015). In these patients, FC between the left and right motor cortex strongly predicted the amount of use of the residual upper extremity, such that individuals with greater FC showed greater use of the residual arm. Both of these studies reveal a close link between motor function and FC, at least under extreme circumstances. However, it is not clear what, if any, causal relationship exists between FC and limb use. Does retained somatomotor FC in stroke and one-handed patients support residual motor function? Does reduced limb use in patients drive loss of FC?

Observational studies of naturally occurring abnormalities in motor function cannot address questions of causality. Such questions can only be answered by experimental interventions that modify limb use and test for resulting changes in FC. However, prior attempts to change patterns of behavior and experience have produced only minute changes in FC. One reason that prior training studies have failed to produce the effect sizes seen in patient populations may be the limited duration of training. The most extensive training paradigm was the visual discrimination task used by Lewis *et al.* Participants completed thousands of trials (mean = 5,600 trials) in order to reach a performance threshold (Lewis et al., 2009). This required hours of training spaced over several days. However, even this intensive training paradigm is nothing like the duration of behavioral modification that results from limb amputation or stroke, which impact participants during all hours of the day. In order to achieve large changes in FC ($\Delta r > 0.2$), a persistent behavioral manipulation may be necessary.

Chapter 2: Plasticity and Spontaneous Activity

Pulses in Disused Human Brain Circuits

This chapter has been published as a journal article. The citation is:

Newbold, D.J., Laumann, T.O., Hoyt, C.R., Hampton, J.M., Montez, D.F., Raut, R.V., Ortega, M., Mitra, A., Nielsen, A.N., Miller, D.B., Adeyemo, B., Nguyen, A.L., Scheidter, K.M., Tanenbaum, A.B., Van, A.N., Marek, S., Schlaggar B.L., Carter, A.R., Greene, D.J., Gordon, E.M., Raichle, M.E., Petersen, S.E., Snyder, A.Z., Dosenbach, N.U.F., Plasticity and spontaneous activity pulses in disused human brain circuits. *Neuron* (2020), <https://doi.org/10.1016/j.neuron.2020.05.007>

Nico Dosenbach, Abraham Snyder, Timothy Laumann, Catherine Hoyt, and I designed the study. Ashley Nielsen and Nico Dosenbach volunteered as participants. Catherine Hoyt, Jacqueline Hampton, Kristen Scheidter, and I collected the behavioral data. Jacqueline Hampton, Mario Ortega, Nico Dosenbach, Annie Nguyen, Kristen Scheidter, and I collected the MRI data. Timothy Laumann, Abraham Snyder, Evan Gordon, Derek Miller, Mario Ortega, David Montez, Andrew Van, Catherine Hoyt, Aaron Tanenbaum, Babatunde Adeyemo, and I analyzed the data. Nico Dosenbach, Abraham Snyder, Tim Laumann, Ryan Raut, Marcus Raichle, Steven Petersen, Evan Gordon, Anish Mitra, Alexandre Carter, Catherine Hoyt, Ashley Nielsen, David Montez, Mario Ortega, Babatunde Adeyemo, Scott Marek, Deanna Greene, Bradley Schlaggar, and I interpreted the results. Nico Dosenbach, Abraham Snyder, Tim Laumann, Marcus Raichle, and I wrote the manuscript with input from all other authors.

2.1 Preface

Executing and interpreting the experiments described in this chapter have been the greatest challenges of my academic career and creating this manuscript has taken up the vast majority of my time as a PhD candidate. This has been a long journey with contributions from many brilliant and skilled individuals. Over 5 years ago, my advisor, Nico Dosenbach, along with Avi Snyder

and Tim Laumann, wanted a powerful experimental manipulation that would drive measurable plasticity in human participants. They had recently finished another experiment that precisely mapped the individual functional organizations of ten human brains using 5 hours of rs-fMRI recording per participant. The dense sampling approach, termed Precision Functional Mapping (PFM), yielded unprecedentedly reliable estimates of functional connectivity (FC) in each participant, as well as reproducible individual differences in brain organization. Moreover, FC measurements and individual differences were highly stable across 10 days of scanning. With this novel approach to making precise, stable measurements of FC, the next logical question was, “Can FC be manipulated experimentally?”

Many prior experiments had attempted to measure changes in FC by scanning participants before and after training on some behavioral task. However, all of these experiments produced miniscule changes in FC ($\Delta r \sim 0.1$) that were often poorly localized to anatomical circuits. Two limitations that likely contributed to the small effects seen in prior studies were under-sampling of rs-fMRI measurements (often <10 minutes data per participant) and the use of temporally limited training paradigms (at most ~1 hour of training per day). Nico, Avi and Tim believed that a more drastic and sustained behavioral intervention, combined with PFM may reveal stronger plasticity effects. Within a month, Nico was fit with a fiberglass cast covering his entire dominant arm. He wore the cast 24/7 for two weeks and scanned himself for 30 minutes every day for 38 consecutive days.

When I joined the Dosenbach Lab in 2016, Nico had already finished the first run of the experiment, and Tim and Avi had processed the resting-state functional MRI data and found

strong preliminary results. Nico showed a large decrease in FC ($\Delta r = -0.23$) that progressed throughout the cast period and reversed after cast removal. The obvious promise of these early findings was a major part of my motivation to join the lab. I and several other contributors spent the next two years replicating this initial finding in two additional participants, Ashley Nielsen and “Omar Little” (pseudonym). Thanks in part to several improvements to our methodology and experimental design, these additional participants showed even stronger effects than we saw in Nico (Ashley: $\Delta r = -0.86$, Omar: $\Delta r = -0.61$). We were all surprised with the rapid time course of the changes we measured. 30 minutes of casting while lying in the scanner drove no large FC changes, but as little as 12 hours of casting can nearly eliminate homotopic FC. We had found that rs-fMRI measurements can be strongly influenced a person’s recent experiences and behaviors.

The improved methods applied to our second two participants also made it possible to discover a new phenomenon in the casted rs-fMRI data: large, paroxysmal pulses of spontaneous activity in the disused motor circuits. It took multiple years of analysis, literature review, and discussions with Nico, Avi and Tim—as well as Marc Raichle, Steve Petersen, Ryan Raut and several others—to form a solid understanding of this novel physiological phenomenon. The work that follows is the consensus view of these authors, reached over hundreds of hours of discussion and editing.

2.2 Abstract

To induce brain plasticity in humans, we casted the dominant upper extremity for two weeks and tracked changes in functional connectivity using daily 30-minute scans of resting-state functional MRI (rs-fMRI). Casting caused cortical and cerebellar regions controlling the disused extremity to functionally disconnect from the rest of the somatomotor system, while internal connectivity within the disused sub-circuit was maintained. Functional disconnection was evident within 48 hours, progressed throughout the cast period, and reversed after cast removal. During the cast period, large, spontaneous pulses of activity propagated through the disused somatomotor sub-circuit. The adult brain seems to rely on regular use to maintain its functional architecture. Disuse-driven spontaneous activity pulses may help preserve functionally disconnected sub-circuits.

2.3 Introduction

Use-driven plasticity is critical for shaping neural circuits during development, learning, and recovery from injury (Wiesel and Hubel, 1965; Reynolds et al., 2001; Murphy and Corbett, 2009). Yet, the large-scale functional organization of the human brain is remarkably stable from day to day and largely robust to changes in behavioral state (Laumann et al., 2015; Gratton et al., 2018). Resting-state functional magnetic resonance imaging (rs-fMRI) provides a powerful means of examining human brain organization by recording spontaneous neural activity, i.e., activity not related to external stimuli or overt behaviors. Spontaneous activity consumes the vast majority of the brain's metabolic energy (Raichle, 2006) and is synchronized within functionally related regions, a phenomenon known as functional connectivity (FC) (Biswal et al., 1995). FC is

characteristically strong between corresponding regions of the left and right hemispheres (homotopic regions) and within large-scale functional systems with distinct cognitive functions (Power et al., 2011; Yeo et al., 2011).

It has been hypothesized that FC is modulated through Hebbian-like processes, such that FC is strengthened through coactivation of brain regions (Dosenbach et al., 2008; Lewis et al., 2009; Harmelech and Malach, 2013; Guerra-Carrillo et al., 2014; Shannon et al., 2016). Previous attempts to induce changes in brain organization using training paradigms have shown only subtle changes in FC ($\Delta r \sim 0.1$) (Lewis et al., 2009; Harmelech and Malach, 2013; Guerra-Carrillo et al., 2014; Shannon et al., 2016). In addition, prior studies relied on endpoint measurements and were therefore unable to describe the time courses of FC alterations. Developmental FC changes (Dosenbach et al., 2010; Smyser et al., 2010; Grayson and Fair, 2017; Nielsen et al., 2019) suggest that patterns of coactivation could be accumulated over years, but little is known about the effects of behavioral changes on brain organization over shorter time frames.

To induce FC changes in human participants, we adopted an approach used in classic animal plasticity studies, which impose sensory or motor deprivation (e.g., monocular deprivation, deafferentation, limb constraint) in a small number of intensively studied individuals (Wiesel and Hubel, 1965; Merzenich et al., 1983a; Milliken et al., 2013). We casted the dominant upper extremity of three adult participants ('Nico', 'Ashley' and 'Omar') for two weeks and tracked changes in FC over 6-9 weeks using daily 30-minute rs-fMRI scans (21-32 hours of rs-fMRI/participant, 152 scans total; Figures 1A and S1). This highly sampled, longitudinal

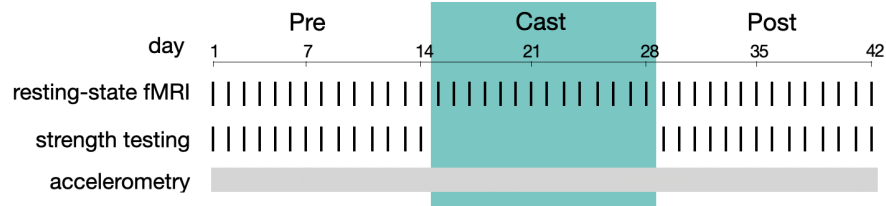
approach allowed us to measure disuse-driven plasticity in each individual and replicate results across all participants.

2.4 Results

2.4.1 Casting Caused Disuse and Reduced Strength of the Dominant Upper Extremity

Casts constrained movement of the elbow, wrist and fingers (Figure 1B). Accelerometers worn continuously on both wrists documented greatly reduced use of the casted upper extremity (Figures 1C and S1; use counts; Nico: -41%, Ashley: -55%, Omar: -46%). Immediately after cast removal, participants showed reduced grip strength (Figure 1D; dynamometry; Nico: -27%, Ashley: -42%, Omar: -39%) and reduced fine motor skill (Figure S1; Purdue Pegboard; Nico: -24%, Ashley: -29%, Omar: -12%). Participants showed increased use of the un-casted upper extremity (Figure S1; Nico: +24%, Ashley: +15%, Omar: +23%) and reported subjective improvement in the use of this extremity during activities of daily living (Video S1), but they did not consistently show improvements in strength or fine motor skill (Figures 1D and S1).

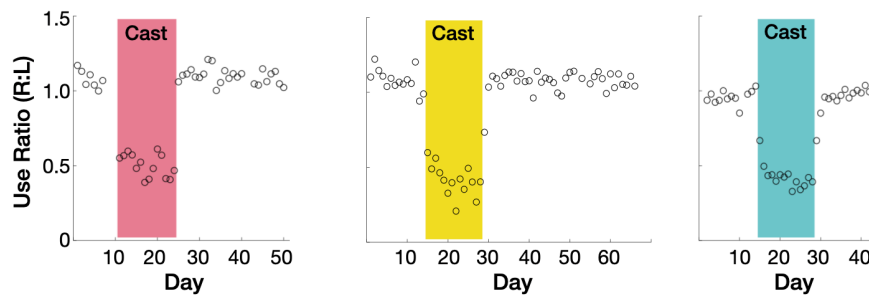
A Experimental design



B Casts



C Accelerometry



D Strength testing

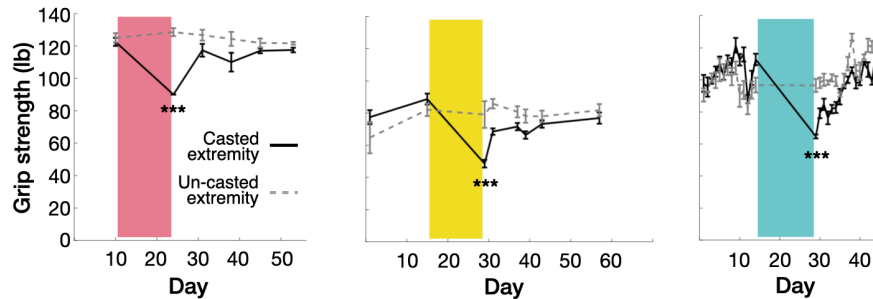
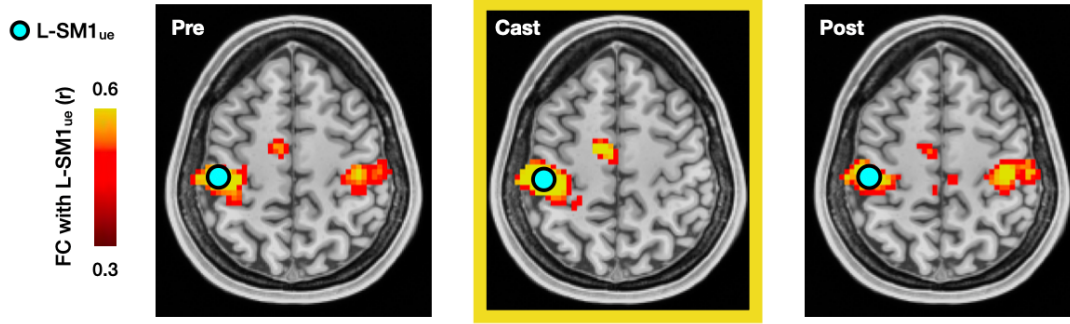


Figure 2-1. Casting caused disuse and reduced strength of the dominant upper extremity. (A) Experimental design for an example participant (Omar). (B) Casts covered the entire dominant upper extremity. Cast colors are used in subsequent figures to identify participants: pink (Nico), yellow (Ashley), green (Omar). (C) Daily accelerometry data from both wrists, plotted as use ratios (R/L use counts). Use count = seconds each day when RMS acceleration > 0.16 m/s². (D) Grip strength before and after casting (***) $P < 0.001$). Error bars indicate s.e.m. across three repeated measurements.

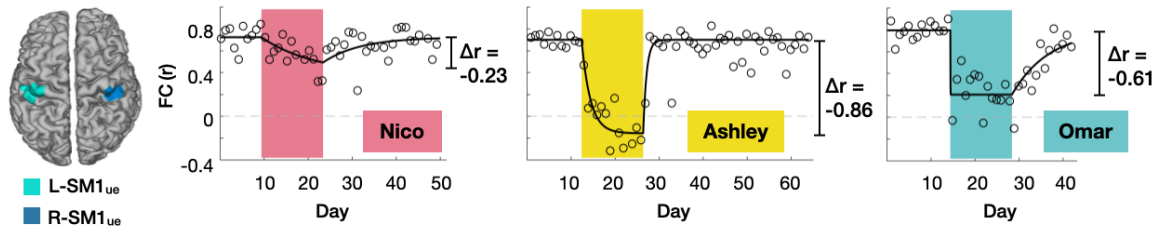
2.4.2 Disused Somatomotor Regions Became Functionally Uncoupled from the Remainder of the Somatomotor System

FC was originally discovered by Biswal *et al.* between the right upper-extremity primary somatomotor cortex (L-SM1_{ue}) and the homotopic region of the opposite hemisphere (R-SM1_{ue}) (Biswal *et al.*, 1995). Prior to casting, all participants showed strong homotopic FC between L-SM1_{ue} and R-SM1_{ue} (Figures 2A and 2B). Casting led to a large reduction in FC between L-SM1_{ue} and R-SM1_{ue} in all participants (Figure 2B; Nico: $\Delta r = -0.23$, Ashley: $\Delta r = -0.86$, Omar: $\Delta r = -0.61$). We also found significantly decreased FC between the disused upper-extremity region of the cerebellum (R-Cblm_{ue}) and its homotopic counterpart (L-Cblm_{ue}; Figure S2; Nico: $\Delta r = -0.16$, Ashley: $\Delta r = -0.07$, Omar: $\Delta r = -0.33$). Decreased homotopic FC was somatotopically specific to the disused upper-extremity somatomotor cortex and cerebellum (L-SM1_{ue}:R-SM1_{ue}, R-Cblm_{ue}:L-Cblm_{ue}) and did not occur in lower-extremity (L-SM1_{le}:R-SM1_{le}, R-Cblm_{le}:L-Cblm_{le}) or face regions (L-SM1_{face}:R-SM1_{face}, R-Cblm_{face}:L-Cblm_{face}; Figures 2C, 2D and S2). In all participants, FC decreases became significant within 48 hours of casting (Nico: Cast day 2 $\Delta r = -0.22$, $P < 0.001$; Ashley: Cast day 1 $\Delta r = -0.23$, $P < 0.001$; Omar: Cast day 1 $\Delta r = -0.83$, $P < 0.001$). While disused regions in the somatomotor cortex and cerebellum (L-SM1_{ue} and R-Cblm_{ue}) were functionally disconnected from the opposite hemisphere, these same regions became more connected to each other (Figure S2). The net effect was that disused brain regions dissociated from the remainder of the somatomotor system (Figure 3). All effects returned to baseline within days after cast removal (Figures 2, 3, and S2).

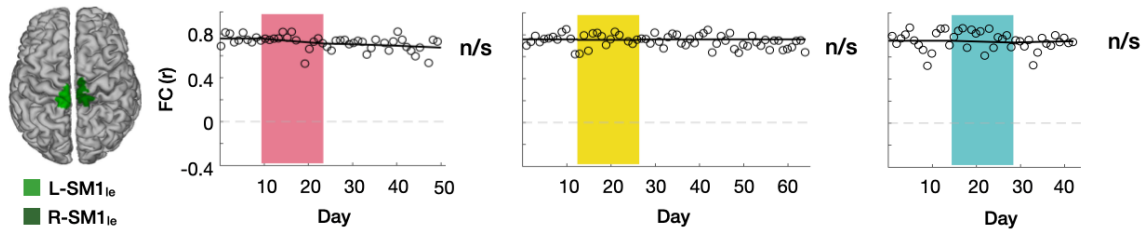
A Functional connectivity (FC) seed maps



B Daily time course of FC: upper extremity



C Daily time course of FC: lower extremity (negative control)



D Daily time course of FC: face (negative control)

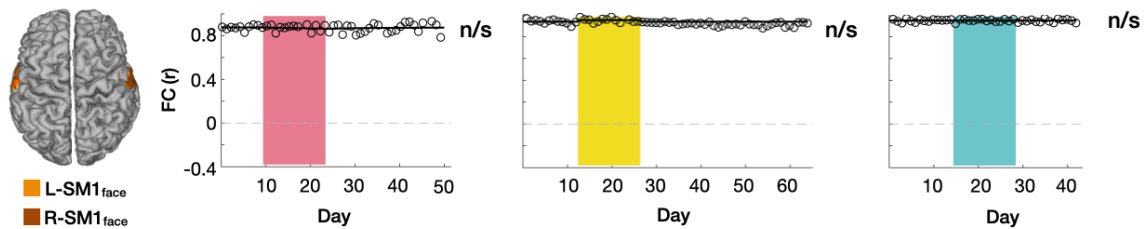
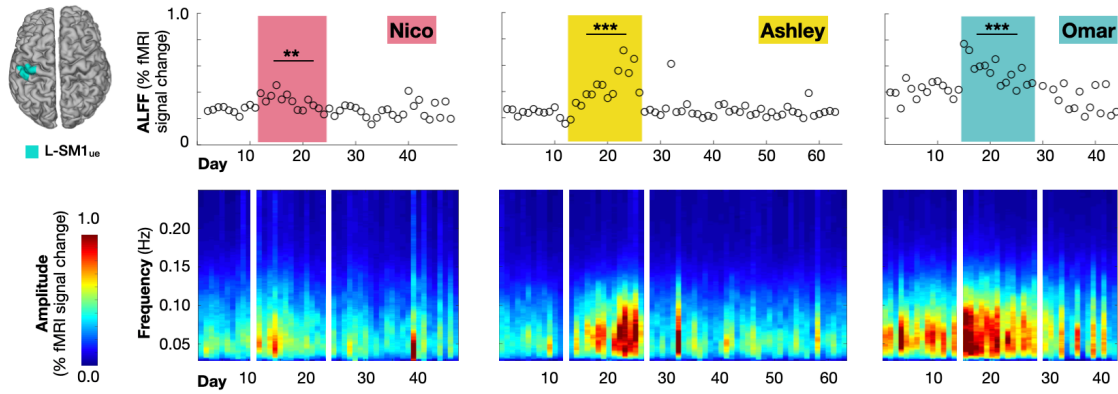


Figure 2-2. Disused Somatomotor Cortex Became Functionally Uncoupled from the Remainder of the Somatomotor Cortex. (A) Seed maps showing functional connectivity (FC) of each voxel with the left primary somatomotor cortex (L-SM1_{UE}) during scans acquired before, during and after casting (Pre, Cast, Post) in an example participant (Ashley). The L-SM1_{UE} region of interest (ROI) was defined using task functional MRI. (B) Daily time course of FC between L-SM1_{UE} and R-SM1_{UE} for each participant. Δr values are based on a time-varying exponential decay model (black lines, $dr/dt = \alpha(r_{\infty} - r)$; Nico: $P = 0.002$, Ashley: $P < 0.001$, Omar: $P < 0.001$). (C and D) Daily time course of FC in lower extremity (C) and face (D) regions of the left and right somatomotor cortex.

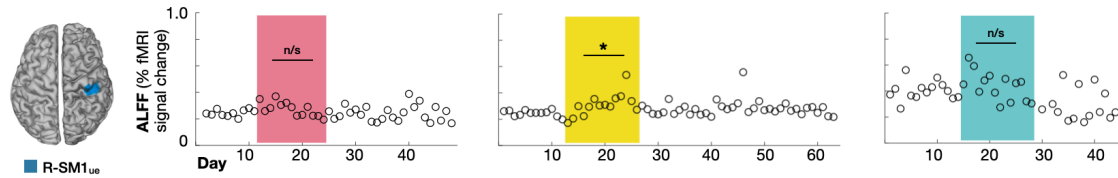
2.4.3 Spontaneous Activity Pulses Emerged in the Disused Somatomotor Cortex During Casting

To further characterize the changes in spontaneous activity caused by casting, we closely examined rs-fMRI signals in L-SM1_{ue} and R-SM1_{ue}. During the cast period, all participants showed significantly increased amplitude of low-frequency fluctuations (ALFF) in L-SM1_{ue} (Figure 4A; Nico: +22%, Ashley: +81%, Omar: +36%), and one participant showed increased ALFF in R-SM1_{ue} (Figure 4B; Ashley: +26%). Increased ALFF was specific to the upper-extremity somatomotor cortex and did not occur in adjacent regions (L-SM1_{le} and L-SM1_{face}; Figures 4C and 4D). Unexpectedly, inspection of the rs-fMRI timeseries revealed large, spontaneous pulses of activity during the cast period (Figures 5A and S3). We termed these events “disuse pulses”. The shape of disuse pulses (Figures 5B and S3) resembled the canonical hemodynamic response to a brief stimulus (Lindquist et al., 2009). Disuse pulses had a large amplitude (up to 1.5% signal change) and were easily distinguished from ongoing spontaneous fluctuations in L-SM1_{ue} (<0.5% signal change; Figures 5A and S3). Pulses were essentially absent prior to casting (Nico: 1.1 pulses/scan; Ashley: 0.2; Omar: 1.0), occurred frequently during the cast period (Nico: 4.2; Ashley: 11.4; Omar: 12.3), and were infrequent after cast removal (Nico: 0.9; Ashley: 0.8; Omar: 1.9; Figure 5C).

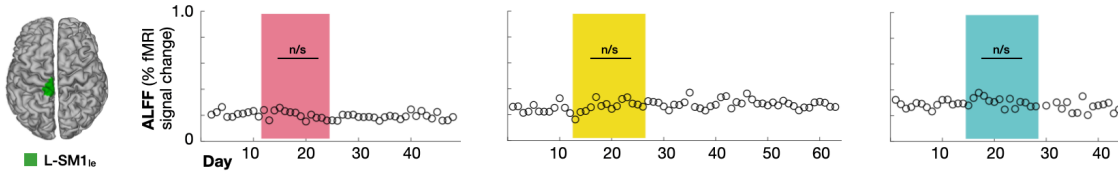
A L-SM1_{ue} amplitude



B R-SM1_{ue} amplitude



C L-SM1_{le} amplitude (negative control)



D L-SM1_{face} amplitude (negative control)

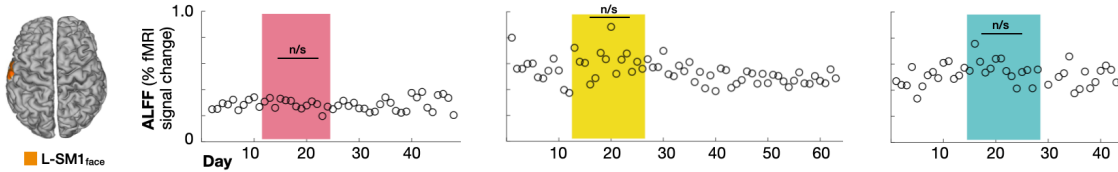


Figure 2-4: Spectral analysis of rs-fMRI signals from L-SM1_{ue} and R-SM1_{ue} during the pre, cast and post periods. (A) *Top*: Amplitude of low-frequency fluctuations (ALFF) in rs-fMRI signals recorded from L-SM1_{ue} during each 30-minute session. All participants showed significantly increased L-SM1_{ue} ALFF during the cast period, relative to the pre period (Nico: +22%, $P < 0.01$; Ashley: +81%, $P < 0.001$; Omar: +36%, $P < 0.001$). *Bottom*: Amplitude spectra of L-SM1_{ue} rs-fMRI signals during each 30-minute session. (B) ALFF in rs-fMRI signals recorded from R-SM1_{ue} during each 30-minute session. One participant showed slightly increased R-SM1_{ue} ALFF during the cast period (Ashley: +26%, $P = 0.02$). Two participants showed non-significant changes in the same direction (Nico: +12%, $P = 0.13$; Omar: +9%, $P = 0.33$). (C and D) As a negative control, we plotted ALFF in during each session in two un-affected somatomotor regions (L-SM1_{le} and L-SM1_{face}). None of the participants showed significant changes in L-SM1_{le} or L-SM1_{face} ALFF in during the cast period.

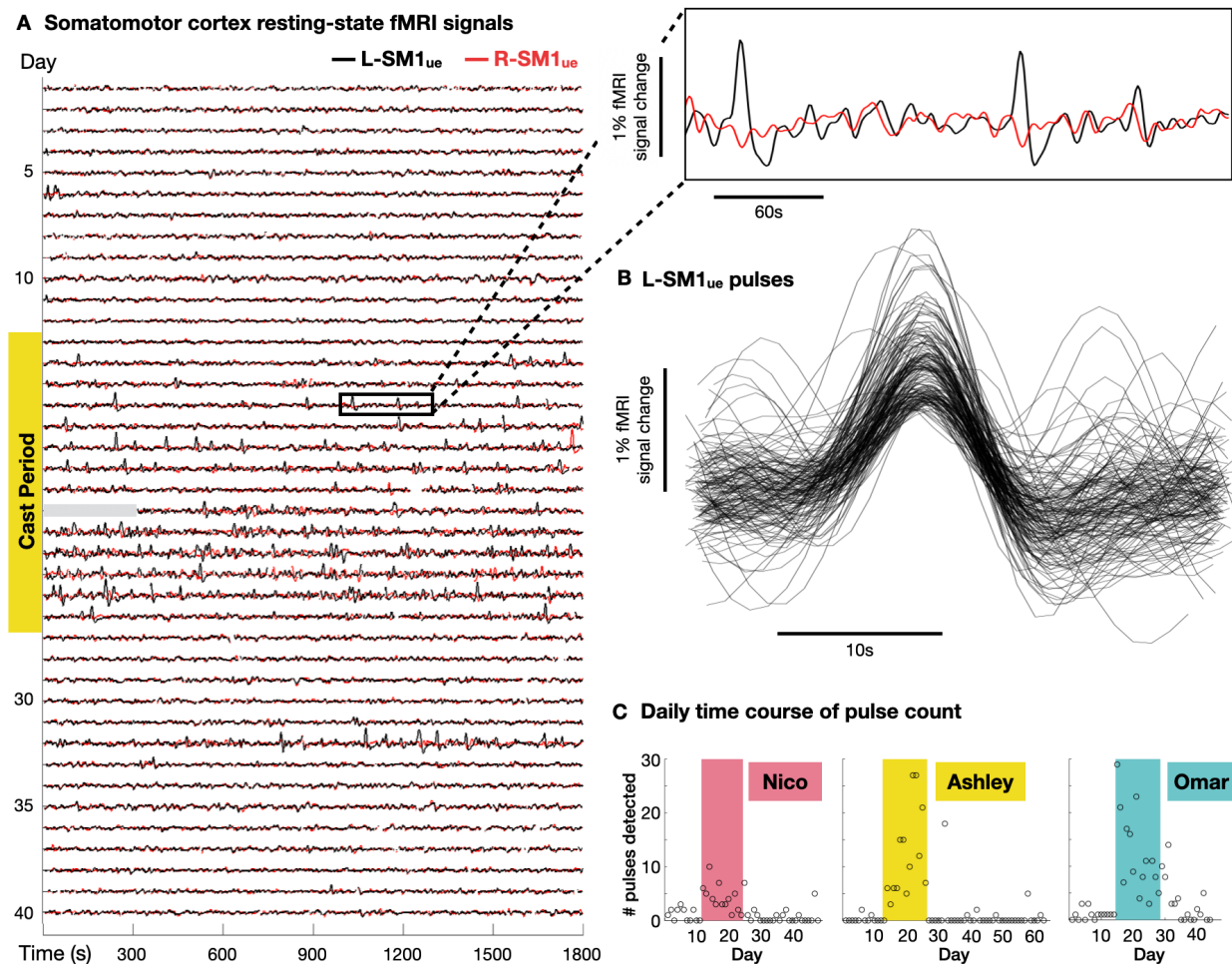


Figure 2-5: Disuse pulses in somatomotor cortex. (A) Resting-state functional MRI (rs-fMRI) signals from left and right primary somatomotor cortex (L-SM1_{ue} and R-SM1_{ue}) before, during and after casting in an example participant (Ashley; all participants Figure S3). During the cast period, large pulses occur in L-SM1_{ue} (see inset at top-right). Data for first five minutes of scan 21 are unavailable (gray bar). (B) Recordings of 144 disuse pulses detected in an example participant (Ashley). (C) Number of pulses detected during each day of the experiment. All participants showed significantly more pulses per session during the cast period than during the pre period. (Nico: $P = 0.002$; Ashley: $P < 0.001$; Omar: $P < 0.001$)

2.4.4 Disuse Pulses Propagated through the Disused Somatomotor Sub-circuit

Disuse pulses were not only present in L-SM1_{ue} but propagated throughout the disused upper-extremity sub-circuit, i.e., L-SM1_{ue}, L-SMA_{ue}, and R-Cblm_{ue} (Figures 6A and S4). A consistent pattern of pulse propagation was observed in all participants. Pulses sequentially occurred in L-SMA_{ue}, L-SM1_{ue} and then R-Cblm_{ue}, with mean time delays of ~200ms and ~600ms, respectively (Figures 6B, 6C and S4). This sequence of temporal lags is similar to that found in ongoing spontaneous activity (Mitra et al., 2014; Marek et al., 2018; Raut et al., 2020).

Monitoring of upper extremity movements in one participant (Omar), using a highly sensitive pressure bladder placed inside the cast, showed that most pulses occurred in the absence of movements (Figure S5). To verify that spontaneous activity changes observed during the cast period were due to disuse during daily life rather than the presence of casts during scanning, we conducted a control experiment in which participants wore removable casts only during 30-minute scans. We found only minimal changes in FC and almost no pulse-like events, indicating that the large decreases in FC and numerous disuse pulses observed during the cast period were not driven by wearing a cast during scans (Figure S6).

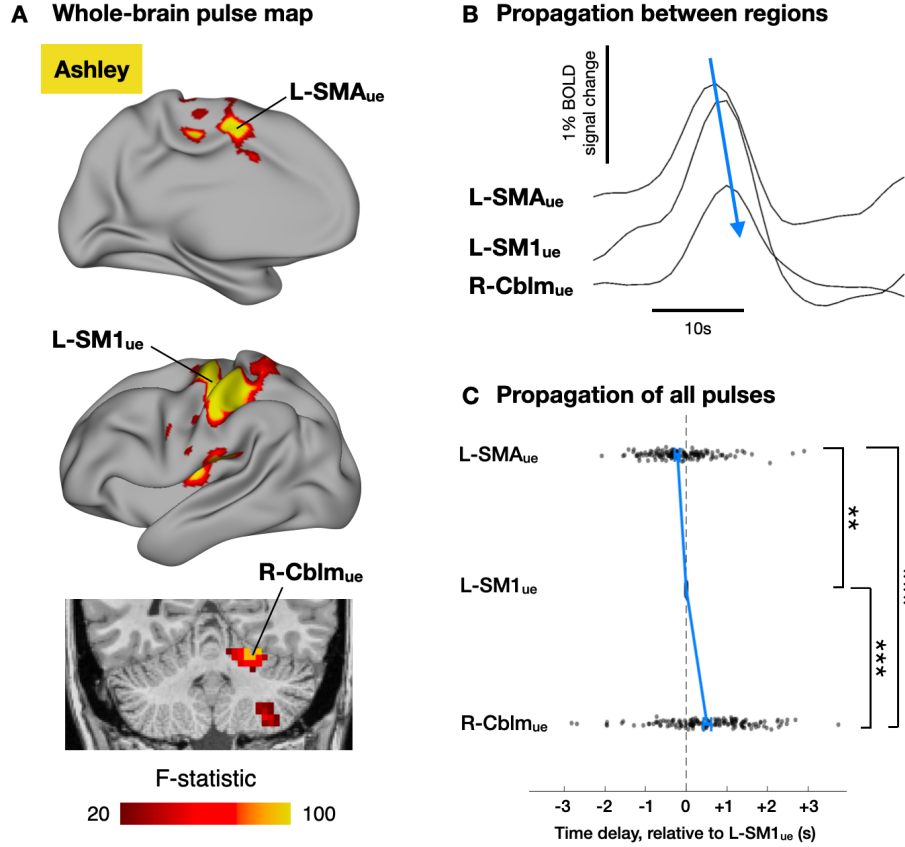


Figure 2-6. Disuse Pulses Propagate through the Disused Somatomotor Sub-circuit. (A) Whole-brain analysis of variance (ANOVA) of disuse pulses in an example participant (Ashley; all participants shown in Figure S4). In addition to L-SM1_{ue}, pulses also occur in left supplementary motor area (L-SMA_{ue}) and right cerebellum (R-Cblm_{ue}). (B) Example pulse in L-SMA_{ue}, L-SM1_{ue} and R-Cblm_{ue}. Note the temporal offset of peaks in each region. (C) Time delays (relative to L-SM1_{ue}) of all pulses in each region for an example participant (Ashley; all participant Figure S4). Blue lines indicate median delay \pm s.e.m. in each region. Pulses occurred first in L-SMA_{ue}, then L-SM1_{ue}, and finally in R-Cblm_{ue}. Pulse times were determined by parabolic interpolation of cross-correlations with the mean pulse time series. **P<0.01. ***P<0.001.

2.5 Discussion

2.5.1 Disuse Drives Large Decreases in Functional Connectivity

The magnitude of FC changes induced by casting ($\Delta r = -0.23, -0.86, -0.61$) is noteworthy because FC is typically highly stable from day to day (Laumann et al., 2015; Gratton et al., 2018). By the end of the two-week cast period, FC in all participants was as low as has been observed after motor stroke (Carter et al., 2012) or limb amputation (Makin et al., 2013). Animal studies that pharmacogenetically manipulated specific brain regions were able to drive large changes in FC ($\Delta r > 0.3$) (Grayson et al., 2016; Rosenthal et al., 2019). Yet, prior human studies of experimentally induced plasticity found much smaller effects ($\Delta r \sim 0.1$) (Lewis et al., 2009; Guerra-Carrillo et al., 2014; Shannon et al., 2016). Key differences between the current experiment and previous studies are: 1) use of a sustained behavioral intervention, 2) inducing disuse as opposed to training a skill, 3) measuring daily time courses (Wenger et al., 2017) rather than comparing only pre/post, 4) overcoming sampling variable with longer (30-minute) scans (Laumann et al., 2015; Gordon et al., 2017), and 5) conducting analyses at the level of individual participants, enabling three-fold replication of all major findings.

2.5.2 Functional Connectivity Can Change Rapidly Over a Span of Days

The observed loss of homotopic FC during disuse, corroborated by animal models of visual deprivation and deafferentation (Pawela et al., 2010; Kraft et al., 2017), supports the hypothesis that FC can be strengthened by coactivation of brain regions (Lewis et al., 2009; Harmelech and Malach, 2013; Guerra-Carrillo et al., 2014; Shannon et al., 2016). The interval over which the

effects of coactivation are accumulated was previously unknown (Lewis et al., 2009; Harmelech and Malach, 2013; Guerra-Carrillo et al., 2014). Some have suggested that patterns of coactivation are accumulated over many years (Shannon et al., 2016). However, the current results demonstrate that FC can be significantly altered within 12-48 hours when a sufficiently strong behavioral constraint is imposed, suggesting that FC is determined, at least in part, by a person's recent behaviors and experiences. The close relationship between FC and recent behavior raises the fascinating possibility that group differences in FC found in certain neuropsychiatric conditions, e.g., stroke (Carter et al., 2012; Siegel et al., 2018), limb amputation (Makin et al., 2013), Parkinson's disease (Gratton et al., 2019), Tourette syndrome (Nielsen et al., 2020), may in part reflect disease-specific differences in day-to-day behavior.

2.5.3 Disused Sub-circuits Maintain Internal Connectivity

In addition to disconnecting from the opposite hemisphere, disused regions (L-SM1_{uc} and R-Cblm_{uc}) became more strongly connected to each other. Increased FC amongst disused regions has also been observed in mice during binocular deprivation (Kraft et al., 2017). Disuse-driven increases in FC were not predicted by the Hebbian FC hypothesis. A straightforward Hebbian account would have predicted that disused regions should disconnect from all other regions. Rather, FC amongst disused regions (L-SM1_{uc} and R-Cblm_{uc}) seems to have increased because disused regions showed synchronized pulses of activity during the cast period.

2.5.4 Spontaneous Activity Shapes Neural Circuits during Development

The presence of spontaneous pulses in the disused somatomotor sub-circuit may reflect processes that help maintain the functional organization of the adult brain. Simultaneously, pulses may also have contributed to reductions in FC between the disused sub-circuit and the remainder of the somatomotor system. Spontaneous activity serves several known roles in shaping neural circuits (Buzsáki, 2019). Hippocampal sharp-wave ripples and thalamic sleep spindles are thought to facilitate transfer of newly formed memories to the cortex (Buzsaki, 2015; Klinzing et al., 2019). Moreover, large-amplitude transients at low frequencies, similar to the disuse pulses described here, are a hallmark feature of developing brains and help to shape brain-wide circuits *in utero* (Tolonen et al., 2007). In the developing visual system, spontaneous waves of activity originate in the retina and propagate through the entire visual system, helping to link circuits across several cortical and subcortical regions (Katz and Shatz, 1996; Ackman et al., 2012). Similar activity-dependent refinement of the somatomotor system is triggered by spontaneous activation of spinal motor neurons (Khazipov et al., 2004). The finding of disuse pulses in our participants suggests that adult brain circuits may retain a latent potential to self-organize through spontaneous activity. Slow activity transients show a characteristic pattern of electrical activity, known as delta-brushes (Khazipov et al., 2004; Tolonen et al., 2007). Future experiments utilizing electroencephalography (EEG) in humans or microelectrode recording in animals will allow closer comparison of disuse pulses to slow activity transients seen in development.

2.5.5 Focal Disinhibition May Allow for the Emergence of Spontaneous Activity Pulses

The disuse pulses observed in our participants were larger (up to 1.5% signal change) than the spontaneous activity fluctuations typically observed in the adult brain and may have resulted from disinhibition of disused circuits. During postnatal critical periods, inhibitory interneurons begin to suppress spontaneous activity, shifting the primary driver of activity-dependent plasticity from internal to external sources (Toyoizumi et al., 2013). Perhaps as a result of increased inhibitory tone, spontaneous activity in the adult brain does not typically include transients and is instead characterized by ongoing, stationary fluctuations (Laumann et al., 2017). Disused circuits exhibit characteristic changes in local physiology: principal cells begin responding to previously silent inputs (Wiesel and Hubel, 1965; Merzenich et al., 1983a), inhibitory interneurons become less active (Gainey et al., 2018), and the synapses between inhibitory interneurons and principal cells are weakened (Wellman et al., 2002). Disuse-driven disinhibition may permit the reemergence of spontaneous pulses of activity in the adult brain. Indeed, pharmacogenetic suppression of inhibitory interneurons in the somatosensory cortex of adult mice produces spontaneous bursts of activity that propagate to functionally connected regions (Rosenthal et al., 2019). Focal disinhibition is also thought to occur after stroke (Liepert et al., 2000), another condition in which circuits are disused (van der Pas et al., 2011). An important question is whether spontaneous pulses of activity arise during stroke recovery and how they impact clinical outcomes.

2.5.6 The human brain – plastic yet stable

In the absence of regular use, our participants showed rapid loss of homotopic somatomotor FC. Thus, the human brain retains a surprising capacity for use-driven plasticity into adulthood. Simultaneously, large pulses of spontaneous activity began propagating through the disused somatomotor sub-circuit, helping to maintain its internal functional connectivity. Since somatomotor connectivity and motor performance returned to the baseline quickly after cast removal, disuse pulses may have protected the integrity of the disused sub-circuit. Functional disconnection of disused sub-circuits, stabilized by spontaneous activity pulses, may allow the brain to reorganize itself rapidly without compromising its overall stability. Disuse pulses, analogous to waves of spontaneous activity seen during development, may allow the adult brain to bridge the seeming chasm between plasticity and stability.

2.6 Methods

2.6.1 Human participants

Participants were three healthy, adult volunteers. All denied recent injuries of the dominant upper extremity and any contraindications to MRI (e.g., metallic implants, claustrophobia). Because of the large amount of data collected, we were able to analyze each participant individually, allowing us to test all hypotheses in triplicate. The first participant was a 35-year-old male who was a participant in the Midnight Scan Club experiment (MSC02) (Gordon et al., 2017; Marek et al., 2018; Greene et al., 2020; Sylvester et al., 2020) and the senior investigator of this study (N.U.F.D., ‘Nico’). The second participant was a 25-year-old female, also drawn from the Midnight Scan Club cohort (MSC06) and was a member of the research team (A.N.N., ‘Ashley’). The third participant was a 27-year-old male (‘Omar’). All participants were right handed, as assessed by the Edinburgh Handedness Inventory (Oldfield, 1971) (Nico: +100, right-handed; Ashley: +91, right-handed; Omar: +60, right-handed). The Washington University School of Medicine Institutional Review Board approved the study protocol and provided experimental oversight. Participants provided informed consent for all aspects of the study and were paid for their participation. Participants also consented to be identified in publications, presentations and media releases by inclusion of their photographs and names.

2.6.2 Experimental intervention

Constraint of the dominant upper extremity was achieved by fitting each participant with a fiberglass cast that extended from just below the shoulder to past the fingertips. Casts contained an inner layer of Delta-Dry water-resistant padding (BSN Medical, Luxembourg) that provided a

comfortable layer of cushioning permitting airflow; thus, participants could bathe without developing skin irritation. Extra padding was applied around the ulnar styloid process, olecranon and antecubital fossa. A strong outer shell was constructed from Delta-Lite Plus fiberglass casting tape. Tape was applied with the elbow bent at a natural angle (approximately 95°), the wrist slightly extended, the fingers slightly flexed, and the thumb extended. Casts were constructed by an Occupational Therapist (C.R.H.) specially trained in therapy involving casting. All participants were fit with a temporary cast several days before the two-week casting period to practice achieving a comfortable position; practice casts were removed after about 10 minutes. In one participant (Omar), the cast was remade after one day to correct uncomfortable finger position. All casts were removed using a specialized, oscillating blade saw that cuts fiberglass without harming the underlying skin.

In order to test for any effects of wearing casts during scans, we cut the casts from the original experiment in half along their long axes, applied felt to the inside surfaces and all cut edges, and added Velcro fasteners to create casts that could be easily applied and removed at the start and end of scanning. Participants wore removable casts during half of the rs-fMRI sessions acquired during a control experiment but did not wear these casts during daily activities.

2.6.3 Activity monitoring

Behavior during normal daily life was assessed using accelerometers worn on each wrist. All participants wore a wGT3X-BT accelerometer (Actigraph, Pensacola) on each wrist throughout the day and night for the full duration of the experiment. The only times participants removed

their accelerometers were during daily MRI scans. The accelerometers recorded acceleration along three orthogonal dimensions with a sampling rate of 30Hz.

2.6.4 Strength testing

Grip strength was measured with a Jamar Smart Hand Digital Dynamometer (Patterson Medical, Warrenville). Participants were instructed to form a closed fist around a handle on the dynamometer, keeping the arm at the side with the elbow bent at 90°, and squeeze as tightly as possible. Maximal force was recorded in pounds. This was repeated for each hand in triplicate at each measurement time point (Figure 1D).

2.6.5 Fine motor testing

Fine motor function of each upper extremity was assessed using the Purdue pegboard task (Tiffin and Asher, 1948). Participants were instructed to use one hand to pick up small (~1 inch) metal pegs one at a time from a bin and insert them into a row of small holes on a pegboard. Participants were given 30 seconds to insert as many pegs as possible. The task was then repeated with the other hand. This task was repeated in triplicate at each assessment (Figure S2B).

2.6.6 MRI acquisition

Participants were scanned every day of the experiment, for 42-64 consecutive days, except for rare days when the scanner or the participant was unavailable (Figure S1). Imaging was performed at a consistent hour of the day (Supplementary Table 1) to minimize diurnal effects in

functional connectivity (Shannon et al., 2013). Sequence details are listed in Supplementary Table 1. Every session included a 30-minute resting-state blood oxygen level-dependent (BOLD) fMRI scan, during which participants were instructed to hold still and look at a white fixation crosshair presented on a black background. During one scan (Ashley, scan 21), the fixation crosshair was not presented until 5 minutes into the scan, so these 5 minutes of data were excluded from further processing. Head motion was tracked in real time using Framewise Integrated Real-time MRI Monitoring software (FIRMM) (Dosenbach et al., 2017). An eye-tracking camera (EyeLink, Ottawa) was used to monitor participants for drowsiness. Some sessions prior to casting (Figure S1) included motor tasks, during which participants were instructed to move their left hand, right hand, left foot, right foot, or tongue in a block design cued by visual stimuli (Barch et al., 2013). Two 4-minute runs of this task were completed during each task session.

2.6.7 Hand movement monitoring

Hand movements during rs-fMRI scans were tracked using a highly sensitive pneumatic bladder (Siemens, Munich), originally designed for tracking respiratory movements. This bladder was inserted into the end of the cast, along the palmar surface of the fingers during rs-fMRI scans (see Figure S10 for a photo showing the bladder position). Instructing the participant to make very small hand movements during a test run confirmed that the bladder was extremely sensitive to movements at the finger joints, wrist, elbow and shoulder. Additionally, although the bladder was inserted inside the cast, we were still able to detect respiration.

2.6.8 Analysis of accelerometry data

Data from wrist-based accelerometers were transferred off of the devices during MRI scans and down sampled to 1Hz. All analyses were based on a root mean square (RMS) of the three acceleration directions. Use counts were calculated as the number of seconds per day when the RMS acceleration exceeded a noise threshold of 10 accelerometer units (Hoyt et al., 2019) (1 accelerometer unit = 0.016 m/s^2). Periods of sleep were detected as blocks of 15 minutes or more with a use count below 100. “% Time Moving” reported in Figure S2 was calculated as the daily use count normalized by the total number of waking seconds recorded each day. Use ratios reported in Figure 1C were calculated as the ratio of use counts for the left and right upper extremities.

2.6.9 MR image processing

Structural images (T1- and T2-weighted) were corrected for gain field inhomogeneity using FSL Fast (Zhang et al., 2001), and aligned to the 711-2B implementation of Talairach atlas space using the 4dfp MRI processing software package (<https://readthedocs.org/projects/4dfp/>). The 711-2B template conforms to the 1988 Talairach atlas (Talairach and Tournoux, 1988) according to the method of Lancaster *et. al.* (Lancaster et al., 1995). Relative to MNI152, 711-2B space is about 5% smaller and 2° anteriorly rotated about the ear-to-ear axis. Mean T1- and T2-weighted images (T1w and T2w) were computed by coregistration and averaging multiple acquisitions. The mean T1w for each participant was run through the FreeSurfer pipeline (version 5.3) (Fischl, 2012) to generate an anatomical segmentation and 3D surface models of the cerebral cortex.

fMRI processing followed a previously published pipeline (Raut et al., 2019). Briefly, preprocessing included temporal interpolation to correct for slice time differences, correction of intensity differences between odd and even slices and rigid-body correction for head movement. Atlas transformation of the functional data was computed as a composition of transforms: native space mean functional image \rightarrow T2w \rightarrow T1w \rightarrow atlas representative template. The functional data were resampled in atlas space in one step including correction for susceptibility inhomogeneity-related distortion (Jenkinson et al., 2012).

Denoising was accomplished by regression of nuisance time series following a CompCor-like strategy (Behzadi et al., 2007; Raut et al., 2019). Regressors included the 6 rigid parameters derived by retrospective motion correction, the global signal averaged over the brain, and orthogonalized waveforms extracted from the ventricles, white matter and extra-cranial tissues (excluding the eyes). Frame censoring (scrubbing) was computed on the basis of both frame-wise displacement (FD) and variance of derivatives (DVARS) measures (Power et al., 2012) with thresholds set individually for each participant (Supplementary Table 1). Rigid-body motion parameters were low-pass filtered (< 0.1 Hz) prior to FD computation to remove respiratory artifacts in head-motion estimates (Fair et al., 2020). Grayordinate image intensity plots (Power, 2017) were visually checked to confirm artifact reduction. The data then were temporally bandpass filtered prior to nuisance regression, retaining frequencies between 0.005 Hz and 0.1 Hz. Censored frames were replaced by linearly interpolated values prior to filtering and re-censored afterwards.

Preprocessed functional data (BOLD time series) were extracted from the cerebral cortex and cerebellum using FreeSurfer-based segmentations and cortical surface models. Cortical data were projected onto a 2D surface (generated by FreeSurfer) using tools distributed as part of the Human Connectome Workbench software package (Marcus et al., 2011). As previously described (Gordon et al., 2017), cortical projection involves selecting voxels that fall between two surface models fit to the inner and outer surfaces of the cortex and interpolating between these voxels to project BOLD data from each cortical hemisphere to a ~164,000-vertex 2D surface. Surface projected data are then downsampled to ~32,000-vertices and geodesically smoothed using a 2-dimensional 6-mm full-width half max (FWHM) smoothing kernel. Cerebellar voxels were kept in volume space and smoothed using a 3-dimensional 4.7mm FWHM kernel.

2.6.10 ROI selection

Most analyses utilized individual-specific task-defined regions of interest (ROIs). Task-defined ROIs were selected using an automated analysis of task fMRI data, as previously described (Marek et al., 2018). For each movement in the motor task (hand, tongue or foot movement), we selected ROIs inside of two anatomical regions, which were automatically labeled by FreeSurfer: the primary somatomotor cortex (pre- and post-central gyri) and the superior half of the cerebellum. To select ROIs within each anatomical region, we first located the vertex/voxel showing maximal task synchrony (Marek et al., 2018) during the motor task and then grew the ROI to a preset size (400 vertices in the somatomotor cortex, 40 voxels in the cerebellum) by selecting neighboring vertices/voxels in descending order of task synchrony. ROIs for an example participant (Omar) are shown in Figure 2.

The graph-theoretic analyses shown in Figures 2E and S4 required multiple ROIs per somatomotor region in order to showcase connectivity both within and between regions. To select ROIs for graph analyses, a set of parcels spanning the entire cerebral cortex was generated for each participant, and each parcel was assigned to one of 17 canonical functional networks using a graph theory-based community detection algorithm (Rosvall and Bergstrom, 2008). Parcels and network assignments for our first two participants (Nico and Ashley) were previously generated and published (Gordon et al., 2017). We used identical methods for our third participant (Omar).

2.6.11 Functional connectivity measurement

Mean BOLD time series were extracted from each ROI by averaging the time series of all vertices within the ROI. Functional connectivity between ROIs was then measured for each session by computing the Pearson correlation between mean ROI BOLD time series, excluding high-motion frames (Supplementary Table 1). Daily time series of functional connectivity between ROIs are shown in Figure 2. Functional connectivity seed maps were computed for the left-hemisphere somatomotor cortex (L-SM1_{ue}) ROI for each session by correlating the mean time series from the ROI with the time series from every voxel. Seed maps are shown in Figure 2.

2.6.12 Exponential decay model

The daily time course of functional connectivity between regions of interest (ROIs) was modeled using the following differential equation:

$$\frac{dr}{dt} = \alpha(r_{\infty} - r) \quad (1)$$

$$r_{\infty} = \begin{cases} r_c & \text{if casted} \\ r_0 & \text{if not casted} \end{cases} \quad \alpha = \begin{cases} \alpha_1 & \text{during casting} \\ \alpha_2 & \text{after casting} \end{cases}$$

where r is the current functional connectivity between two ROIs, r_0 is the baseline functional connectivity, r_c is the equilibrium functional connectivity in the casted state, α_1 describes the rate of change during the cast period and α_2 describes the rate of change during the post period. r_0 was set to the mean functional connectivity in the pre period. The other three parameters (r_c , α_1 and α_2) were fit to the data using a least squares approach.

Total change in functional connectivity (Δr) reported in Figures 2 and S3, was computed as the difference between the modeled functional connectivity (r) at the end of the cast period minus baseline functional connectivity (r_0). The significance of Δr was evaluated via permutation resampling (see *Statistical analyses*, below).

2.6.13 Graph-theoretic analyses

Graph analyses were based on a set of cortical parcels (see *ROI selection*, above) that were assigned to the face, lower-extremity and upper-extremity somatomotor networks (SMN). We excluded any parcels that were located outside of the pre- and post-central gyri. The resulting set of ROIs for each participant are shown in Figure S4A. Functional connectivity was computed for all pairs of somatomotor parcels and then averaged across sessions to produce a weighted graph of the SMN for each experimental period (Pre, Cast, Post; Figure S4B, *top*). Thresholded graphs ($FC > 0.3$) were displayed as spring-embedded plots (Figures 2E and S4B, *bottom*), as previously

described (Gordon et al., 2017). Next, we computed modularity (Newman, 2004; Bullmore and Sporns, 2009) for each graph. Modularity quantifies the extent to which different communities in a graph segregate away from one another. We defined two communities for computing modularity: 1) the casted upper extremity parcels (left-hemisphere parcels assigned to the upper-extremity SMN) and 2) the remainder of the SMN (bilateral lower-extremity and face SMN parcels and right-hemisphere upper-extremity SMN parcels). Thus, modularity reflects the degree of separation between the casted-extremity representation and the remainder of the SMN. Modularity (Q) is computed as:

$$Q = \frac{1}{2m} \sum_{ij} \left[A_{ij} - \frac{k_i k_j}{2m} \right] \delta(c_i, c_j) \quad (2)$$

where i and j are nodes in the graph, A_{ij} is the connection strength between nodes i and j , k_i and k_j the sums of all connection weights involving node i and node j , respectively, m is the sum of all connection weights in the graph, c_i and c_j are the community assignments of node i and node j , respectively, and δ is the Kronecker delta function (1 if c_i and c_j are identical and zero otherwise). Statistical significance of changes in modularity were evaluated using permutation resampling (see *Statistical analysis*, below).

2.6.14 Spectral analyses

rs-fMRI signals from L-SM1_{ue} and R-SM1_{ue} were Fourier transformed to obtain amplitude density spectra. Spectra from all 30-minute scans in each participant are shown in Figure S5. Amplitude of low-frequency fluctuations (Zang et al., 2007) (ALFF) for L-SM1_{ue} and R-SM1_{ue} was calculated as the root mean square of amplitude across low frequencies (0.05 – 0.1 Hz). A daily time course of L-SM1_{ue} and R-SM1_{ue} ALFF for each participant is shown in Figure S5.

ALFF during the cast period was compared to ALFF during the pre period using an unpaired t-test (see *Statistical Analyses*, below).

2.6.15 Pulse detection

Example pulses were initially selected by visual inspection of L-SM1_{ue} and R-SM1_{ue} rs-fMRI signals. Based on these examples, threshold criteria were set to define pulses as large ($>0.4\%$ rs-fMRI signal change in L-SM1_{ue}), unilateral (L-SM1_{ue} minus R-SM1_{ue} $> 0.3\%$ rs-fMRI signal change) peaks in the L-SM1_{ue} rs-fMRI signal. The number of pulses detected during each 30-minute rs-fMRI scan is shown in Figure 3C. To ensure that results did not depend on specific thresholds, we repeated all analyses using a range of thresholds (L-SM1_{ue} $> 0.2\%$ to 1.2% signal change; (L-SM1_{ue} – R-SM1_{ue}) $> 0.0\%$ to 0.4% signal change). All thresholds yielded qualitatively similar results. Once pulses were detected in L-SM1_{ue}, we used an analysis of variance (Clare et al., 1999) (ANOVA) of whole-brain rs-fMRI signals surrounding each L-SM1_{ue} pulse (13.2 seconds before to 17.6 seconds after each pulse peak) to determine if other brain regions showed consistent patterns of activity during pulses. Because the ANOVA F-statistic increases with increasing sample sizes, we divided by the square root of n (the number of pulses) to normalize maps across participants. The resulting maps are shown in Figures 4 and S8.

2.6.16 Pulse timing analyses

The exact timing of each pulse was estimated by temporally aligning each pulse event with the mean L-SM1_{ue} pulse waveform. This alignment was implemented by parabolic optimization of the cross-correlation between each pulse event in each region of interest (L-SM1_{ue}, L-SMA_{ue},

and R-Cblm_{uc}) and the mean pulse waveform. See Figure S9 for graphic explanation of the alignment procedure. A similar approach was recently shown to provide reliable estimates of sub-TR time delays between rs-fMRI time series (Raut et al., 2019). Figures 4C and S8 show the relative time delays of pulse waveforms extracted from L-SM1_{uc}, L-SMA_{uc}, and R-Cblm_{uc}. Pulse times between regions were then compared using Wilcoxon signed rank tests (see *Statistical analyses*, below).

2.6.17 Hand movement analyses

Pressure readings were acquired at 400 Hz. Pressure traces were low-pass filtered (<2 Hz) to remove high-frequency noise and differentiated to remove occasional shifts in baseline. The amplitude of pressure traces was normalized across recordings by dividing by the median deviation from the mean. Fully processed traces from the pressure bladder during 30-minute rs-fMRI scans are shown in Figure S10. Movements were detected by squaring the processed pressure trace, smoothing with a kernel of 1 second, and applying a threshold of 0.6. Disuse pulses detected in the rs-fMRI signals (see *Pulse detection*, above) were classified as spontaneous if no movements were detected within 8 seconds preceding the pulse peak. The percentage of pulses classified as spontaneous during each session is shown in Figure S10.

2.6.18 Statistical analyses

All statistical tests were performed identically for each participant. Whenever appropriate, we used simple parametric statistical tests:

- Accelerometry use counts measured during each day of the cast period (Nico: n = 13 days; Ashley: n = 14; Omar: n = 14) were compared to use counts during the pre period

(Nico: $n = 7$; Ashley: $n = 14$; Omar: $n = 14$) using a two-sided, unpaired t-test (Nico: d.f. = 18; Ashley: d.f. = 26; Omar: d.f. = 26). This test was performed separately for each upper extremity (Figure S2).

- Grip strength immediately after cast removal, measured in triplicate for each hand (all participants: $n = 3$ measurements), was compared to all strength measurements acquired prior to casting (Nico: $n=3$; Ashley: $n=6$; Omar: $n=42$) using a two-sided, un-paired t-test (Nico: d.f. = 4, Ashley: d.f. = 7, Omar: d.f. = 43). This test was performed separately for each upper extremity (Figure 1D)
- Performance on the Purdue pegboard task (# pegs inserted in 30 seconds) immediately after cast removal (all participants: $n = 3$ trials), was compared to all trials conducted prior to casting (Nico: $n=3$; Ashley: $n=6$; Omar: $n=9$) using a two-sided, un-paired t-test (Nico: d.f. = 4, Ashley: d.f. = 7, Omar: d.f. = 10). This test was performed separately for each upper extremity (Figure S2)
- To determine how quickly functional connectivity (FC) between the left and right somatomotor cortex (L-SM1_{ue} and R-SM1_{ue}) became significantly decreased in each participant, FC measured during each session of the cast period was compared to all sessions of the pre period (Nico: $n = 10$ sessions; Ashley: $n = 12$; Omar: $n = 14$) using two-sided, one-sample t-tests (Nico: d.f. = 9; Ashley: d.f. = 11; Omar: d.f. = 13) conducted separately for each Cast session. We reported the time required for FC during a Cast session to become significantly lower ($P < 0.05$) than FC during the pre period
- FC between L-SM1_{ue} and R-Cblm_{ue} measured during each session of the cast period (Nico: $n = 13$ sessions; Ashley: $n = 13$; Omar: $n = 14$) was compared to FC during the pre

period (Nico: $n = 10$; Ashley: $n = 12$; Omar: $n = 14$) using a two-sided, unpaired t-test (Nico: d.f. = 21, Ashley: d.f. = 23, Omar: d.f. = 26; Figure S4)

- Amplitude of low frequency fluctuations (ALFF) in $L-SM1_{ue}$ measured during each session of the cast period (Nico: $n = 13$ sessions; Ashley: $n = 13$; Omar: $n = 14$) was compared to ALFF measured during each session of the pre period (Nico: $n = 10$; Ashley: $n = 12$; Omar: $n = 14$) using a two-sided, unpaired t-test (Nico: d.f. = 21, Ashley: d.f. = 23, Omar: d.f. = 26). This test was repeated for $R-SM1_{ue}$, $L-SM1_{le}$, and $L-SM1_{face}$ (Figure S5)
- The number of disuse pulses detected in $L-SM1_{ue}$ during each session of the cast period (Nico: $n = 13$ sessions; Ashley: $n = 13$; Omar: $n = 14$) was compared to the number of pulses detected during each session of the pre period (Nico: $n = 10$; Ashley: $n = 12$; Omar: $n = 14$) using a two-sided, unpaired t-test (Nico: d.f. = 21, Ashley: d.f. = 23, Omar: d.f. = 26).
- The relative timing of disuse pulses in $L-SMA_{ue}$ and $L-SM1_{ue}$ was compared using a Wilcoxon signed rank test (Nico: d.f. = 64, Ashley: d.f. = 143, Omar: d.f. = 156). This test was repeated to compare the relative timing of disuse pulses in $L-SMA_{ue}$ and $R-Cblm_{ue}$ and the relative timing of disuse pulses in $L-SM1_{ue}$ and $R-Cblm_{ue}$ (Figures 4C and S8).
- To evaluate the effects of wearing a removable cast during scanning, FC between $L-SM1_{ue}:R-SM1_{ue}$ and $L-Cblm_{ue}:R-Cblm_{ue}$ measured while participants wore removable casts (“On” sessions; Nico: $n = 6$ sessions; Ashley: $n = 12$; Omar: $n = 6$) was compared to sessions acquired without casts (“Off” sessions; Nico: $n = 6$ sessions; Ashley: $n = 12$; Omar: $n = 6$) using a two-sided un-paired t-test (Nico: d.f. = 10; Ashley: d.f. = 22; Omar:

d.f. = 10). The same test was used to compare the number of pulse-like events detected during On sessions to the number of events detected in Off sessions (Figure S11).

When parametric statistical tests were not appropriate to test a specific hypothesis, we tested results against a null distribution generated via permutation resampling. In each case, our null hypothesis was that no changes occurred due to casting and any observed differences were due to measurement error. We modeled this null hypothesis by permuting the order of MRI sessions 10,000 times, eliminating any temporal relationship between sessions and the casting intervention. Each permuted sample was treated exactly as the actual data in order to compute a null distribution for the value of interest. The P-value reported for each test represents the two-sided probability that a value in the null distribution has a greater magnitude than the observed value. Permutation resampling was used to generate null distributions for the following values:

- Change in functional connectivity (Δr) during casting, based on the exponential decay model (Figures 2B-D and S3)
- Change in modularity of the somatomotor network (ΔQ) during casting (Figures 2E and S4)

All analyses were hypothesis driven and tested in a small number of regions of interest (ROIs), defined using independent data (task activations or baseline FC gradients). Correction for multiple comparisons was not necessary for most analyses. In cases where tests were applied to multiple ROIs, a Benjamini-Hochberg procedure was applied to correct for multiple comparisons, maintaining false discovery rates < 0.05 . This correction was applied to the following tests:

- Decreases in homotopic FC, tested in three pairs of ROIs: L-SM1_{uc}:R-SM1_{uc}, R-Cblm_{uc}:L-Cblm_{uc}, and L-SMA_{uc}:R-SMA_{uc} (Figures 2 and S3)
- Delays in pulse timing, tested between three pairs of ROIs: L-SM1_{uc}→R-Cblm_{uc}, L-SMA_{uc}→L-SM1_{uc}, and L-SMA_{uc}→R-Cblm_{uc} (Figures 4 and S9)

Each of the three participants constituted a separate replication of the experiment, rather than multiple comparisons, so no correction was necessary for tests repeated in each participant.

2.6.19 Data visualization

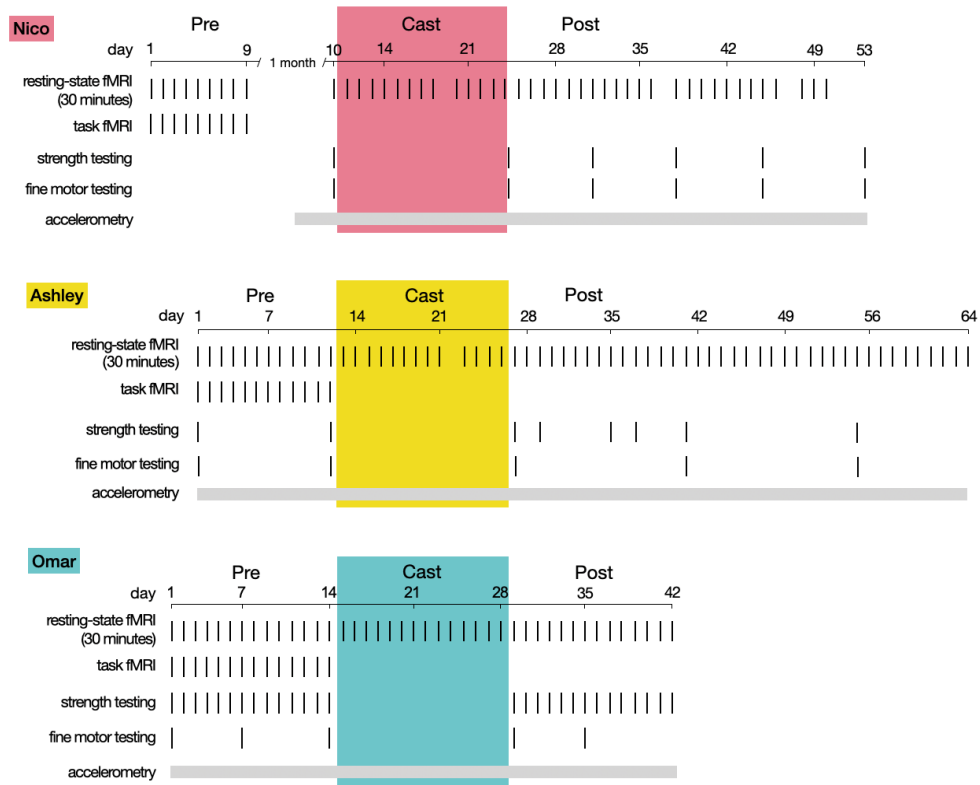
Regions of interest and whole-brain pulse maps were shown on cortical surfaces generated by FreeSurfer (Fischl, 2012) and Human Connectome Project (HCP) Workbench software packages (Marcus et al., 2011). These images were rendered using HCP Workbench (Marcus et al., 2011). All other figures were produced using Matlab (www.mathworks.com).

2.6.20 Data and code availability

The neuroimaging data generated during this study are available at OpenNeuro.org with the identifier ds002766. All code needed to reproduce our analyses is available on Gitlab (<https://gitlab.com/DosenbachGreene/cast-induced-plasticity>).

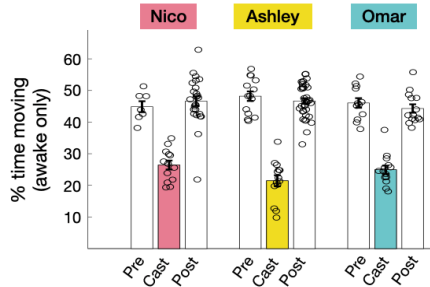
2.7 Supplemental figures

A Experimental designs

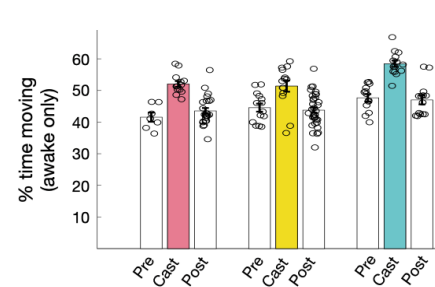


B Upper extremity movements (accelerometry)

Casted upper extremity



Un-casted upper extremity



C Pegboard task performance

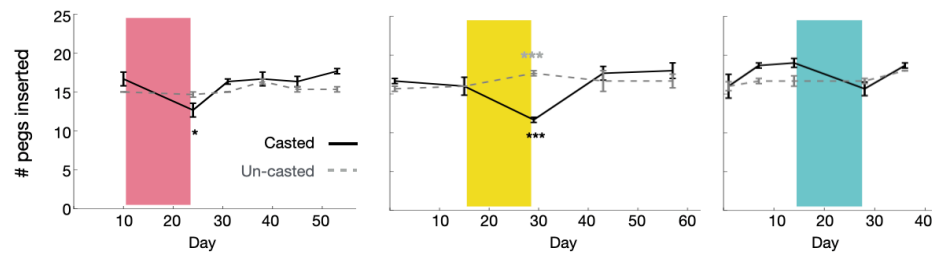
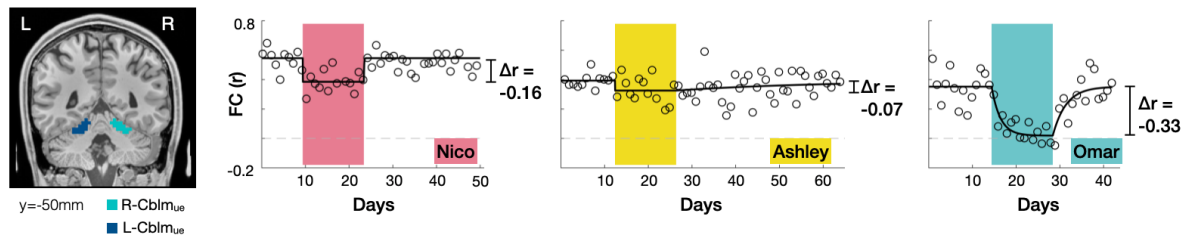


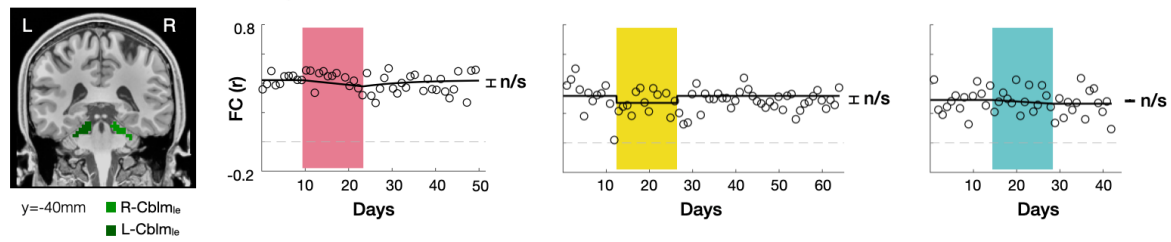
Figure 2-S1: See next page for caption.

Figure 2-S1: Casting induced disuse and decreased fine motor skill of the dominant upper extremity and increased use of the non-dominant upper extremity. (A) Experimental design for all participants. Data acquisition included resting-state functional MRI (rs-fMRI), task-based functional MRI (fMRI), strength testing, fine motor testing, and constant behavioral monitoring using wearable accelerometers. MRI sessions were missed only for unresolvable technical reasons, e.g., scanner not available. The principal investigator on the study, a 35-year-old male ('Nico'), served as a pilot participant. He was scanned 35 out of 38 consecutive mornings at 5:00 a.m. using a Siemens Trio 3T MRI scanner. Baseline data consisted of 1 session acquired immediately before casting and 9 sessions acquired using an identical protocol one month before casting. Our second participant, a 25-year-old female ('Ashley'), was scanned 63 out of 64 consecutive nights at 9:00 p.m. using a Siemens Prisma 3T MRI scanner. Baseline data consisted of 12 sessions acquired immediately prior to casting. Our third participant, a 27-year-old male ('Omar'), was scanned 42 out of 42 consecutive nights at 9:00 p.m. using the same scanner and MRI acquisition sequences that were used for Ashley (Supplementary Table 1). Baseline data consisted of 14 scans acquired immediately prior to casting. (B) *Left*: Upper extremity movements during daily activity were monitored using accelerometers worn on each wrist for the full duration of the experiment. Daily use counts were computed as the number of seconds during each day during which movement was detected. Use counts were normalized by the total time awake each day to yield % time in movement. Bars show average use counts during each experimental period (Pre, Cast, Post) \pm s.e.m. All participants used the casted upper extremity significantly less during the cast period (Nico: -41%, $P < 0.001$; Ashley: -55%, $P < 0.001$; Omar: -46%, $P < 0.001$). *Right*: All participants used the un-casted upper extremity significantly more during the cast period (Nico: +25%, $P < 0.001$; Ashley: +15%, $P = 0.004$; Omar: +23%, $P < 0.001$). (C) Fine motor skill was assessed using the Purdue pegboard task. Error bars indicate \pm s.e.m. across three task runs. Immediately after cast removal, two participants showed significantly reduced performance of the casted extremity (# pegs inserted in 30 seconds) and one participant showed a trend in the same direction (Nico: -24%, $P = 0.033$; Ashley: -29%, $P < 0.001$; Omar: -12%, $P = 0.12$). One participant showed significantly increased performance of the un-casted extremity and two participants did not show any significant change (Nico: -2%, $P = 0.37$; Ashley: +11%, $P < 0.001$; Omar: +1%, $P = 0.70$).

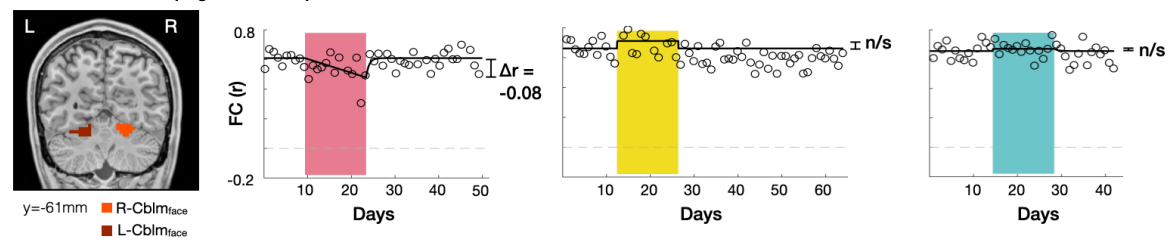
A Cerebellar FC: upper extremity



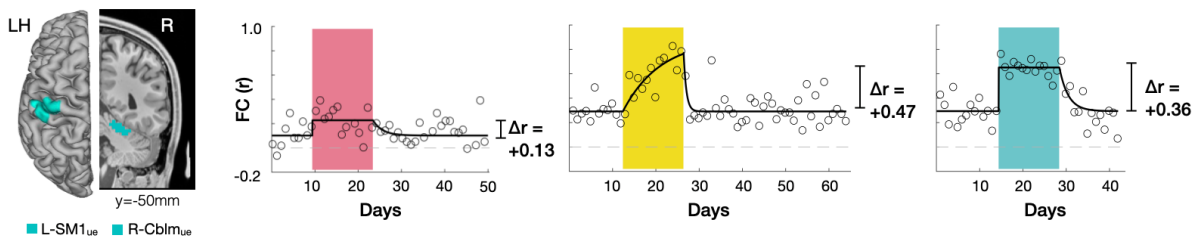
B Cerebellar FC: lower extremity (negative control)



C Cerebellar FC: face (negative control)



D FC between somatomotor cortex and cerebellum: upper extremity



E Supplementary motor area (SMA) FC: upper extremity

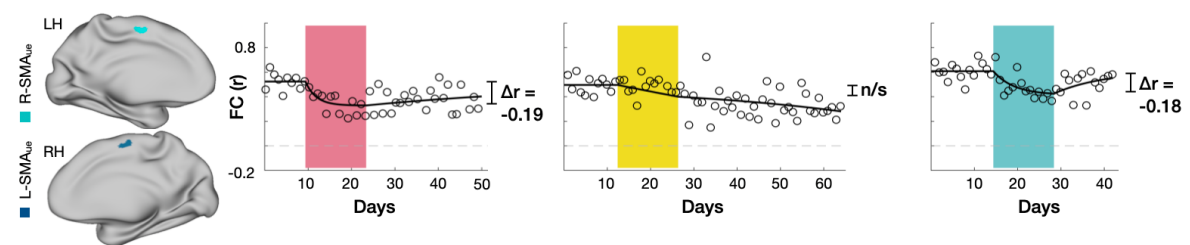
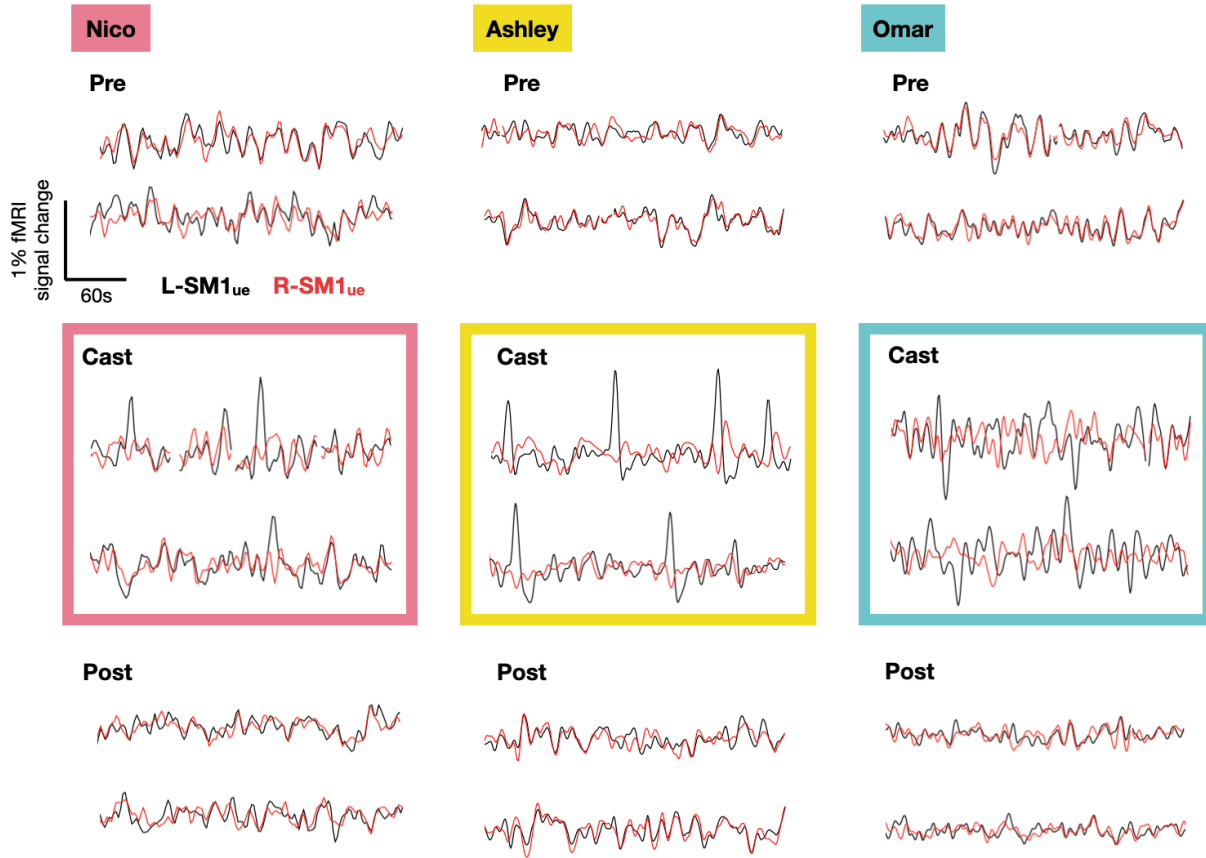


Figure 2-S2: See next page for caption.

Figure 2-S2: Disused cerebellum (R-Cblm_{ue}) disconnected from the opposite hemisphere (L-Cblm_{ue}), related to Figure 2. (A) *Left*: L-Cblm_{ue} and R-Cblm_{ue} regions of interest (ROIs), located by a hand-movement task. *Right*: Daily time course of FC between L-Cblm_{ue} and R-Cblm_{ue} for each participant. Δr values based on a time-varying exponential decay model (black lines, $dr/dt = \alpha(r_{\infty} - r)$). All participants showed significantly decreased FC during the cast period (Nico: $\Delta r = -0.16$, $P = 0.002$; Ashley: $\Delta r = -0.07$, $P = 0.035$; Omar: $\Delta r = -0.33$, $P < 0.001$). (B) *Left*: L-Cblm_{le} and R-Cblm_{le} ROIs, located by a foot-movement task. *Right*: Daily time course of FC between L-Cblm_{le} and R-Cblm_{le} for each participant. No participants showed significantly decreased FC during the cast period (Nico: $\Delta r = -0.01$, $P = 0.92$; Ashley: $\Delta r = -0.05$, $P = 0.24$; Omar: $\Delta r = -0.00$, $P = 1.0$). (C) *Left*: L-Cblm_{face} and R-Cblm_{face} ROIs, located by a tongue-movement task. *Right*: Daily time course of FC between L-Cblm_{face} and R-Cblm_{face} for each participant. One participant showed significantly decreased FC during the cast period (Nico: $\Delta r = -0.08$, $P = 0.027$; Ashley: $\Delta r = +0.05$, $P = 0.28$; Omar: $\Delta r = +0.02$, $P = 0.73$). (D) *Left*: L-SM1_{ue} and R-Cblm_{ue} ROIs. *Right*: Daily time course of FC between L-SM1_{ue} and R-Cblm_{ue} for each participant. All participants showed significantly increased FC during the cast period (Nico: $\Delta r = +0.13$, $P = 0.019$; Ashley: $\Delta r = +0.47$, $P < 0.001$; Omar: $\Delta r = +0.36$, $P < 0.001$). (E) *Left*: L-SMA_{ue} and R-SMA_{ue} ROIs. *Right*: Daily time course of FC between L-SMA_{ue} and R-SMA_{ue} for each participant. Two participants showed significantly decreased FC during the cast period (Nico: $\Delta r = -0.19$, $P < 0.001$; Ashley: $\Delta r = -0.09$, $P = 0.17$; Omar: $\Delta r = -0.18$, $P < 0.001$). In total, three sets of regions were tested for FC decreases (SM1, Cblm and SMA), so a Benjamini-Hochberg correction was used to maintain a false discovery rate < 0.05 . All effects survived correction except for the decrease in FC between L-Cblm_{ue} and R-Cblm_{ue} observed in one participant (Ashley).

A Example rs-fMRI signals



B L-SM1_{ue} pulses

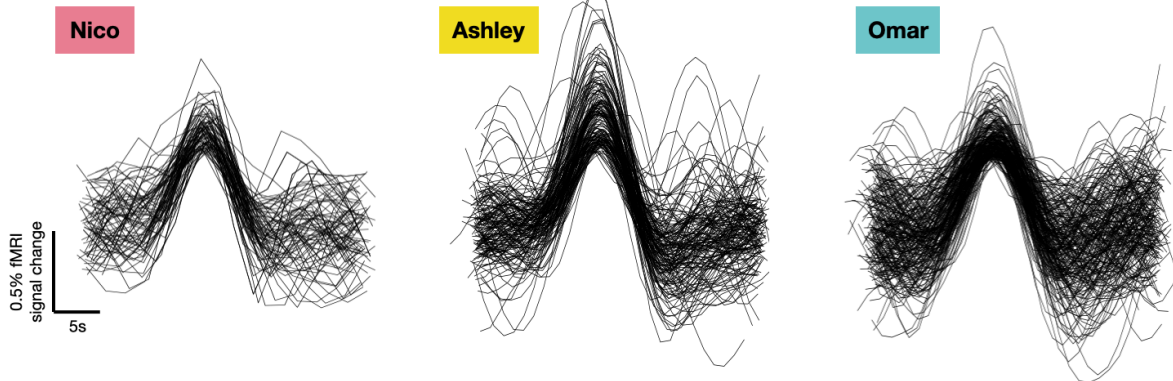
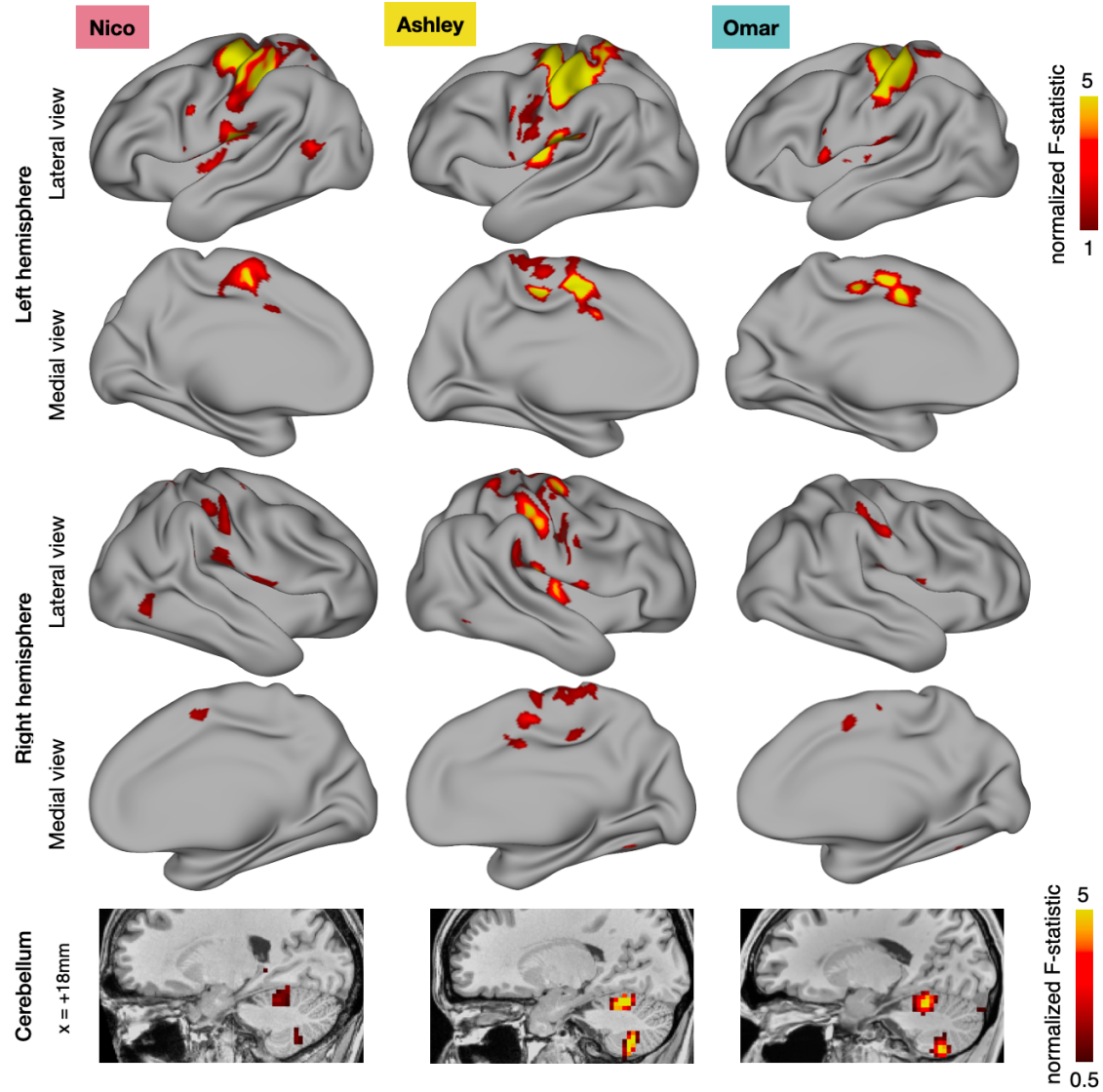


Figure 2-S3: Disused somatomotor cortex (L-SM1_{ue}) pulses in all participants. (A) Example resting-state fMRI signals from L-SM1_{ue} and R-SM1_{ue} during the Pre, Cast and Post periods. (B) All detected pulses superimposed on one another for each participant (Nico: n = 65; Ashley: n=144; Omar: n = 157)

A Whole-brain pulse maps



B Pulse propagation

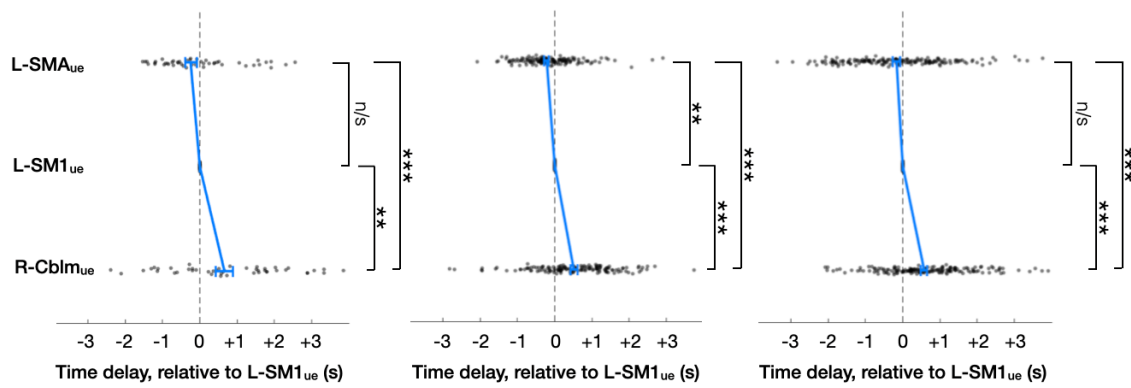


Figure 2-S4: See next page for caption.

Figure 2-S4: Whole-brain maps and pulse propagation in all participants. (A) All participants showed consistent activations in the left supplementary motor area, bilateral insula, right post-central sulcus and right cerebellum. Activations were detected using an analysis of variance (ANOVA). Because the ANOVA F-statistic increases with increasing sample sizes, we divided by the square root of n (# of pulses) to normalize maps across participants. (B) Timing of all pulses in L-SM1_{ue}, L-SMA_{ue}, and R-Cblm_{ue} relative to the L-SM1_{ue}. Blue lines indicate median \pm s.e.m. timing in each region. Time delays between regions were tested using a Wilcoxon signed rank test. $**P < 0.01$; $***P < 0.001$. All participants showed significant time delays between L-SMA_{ue} and R-Cblm_{ue} (Nico: 1.1s, $P < 0.001$; Ashley: 0.7s, $P < 0.001$; Omar: 0.7s, $P < 0.001$) and between L-SM1_{ue} and R-Cblm_{ue} (Nico: 0.7s, $P < 0.01$; Ashley: 0.5s, $P < 0.001$; Omar: 0.6s, $P < 0.001$). One participant showed a significant time delay between L-SMA_{ue} and L-SM1_{ue} (Ashley: 0.2s, $P < 0.01$), and two participants showed non-significant time delays in the same direction (Nico: 0.2s, $P = 0.63$; Omar: 0.2s, $P = 0.07$). Because three time delays were tested (L-SM1_{ue} \rightarrow R-Cblm_{ue}, L-SMA_{ue} \rightarrow L-SM1_{ue} and L-SMA_{ue} \rightarrow R-Cblm_{ue}), a Benjamini-Hochberg correction was used to maintain a false discovery rate < 0.05 . All effects survived correction.

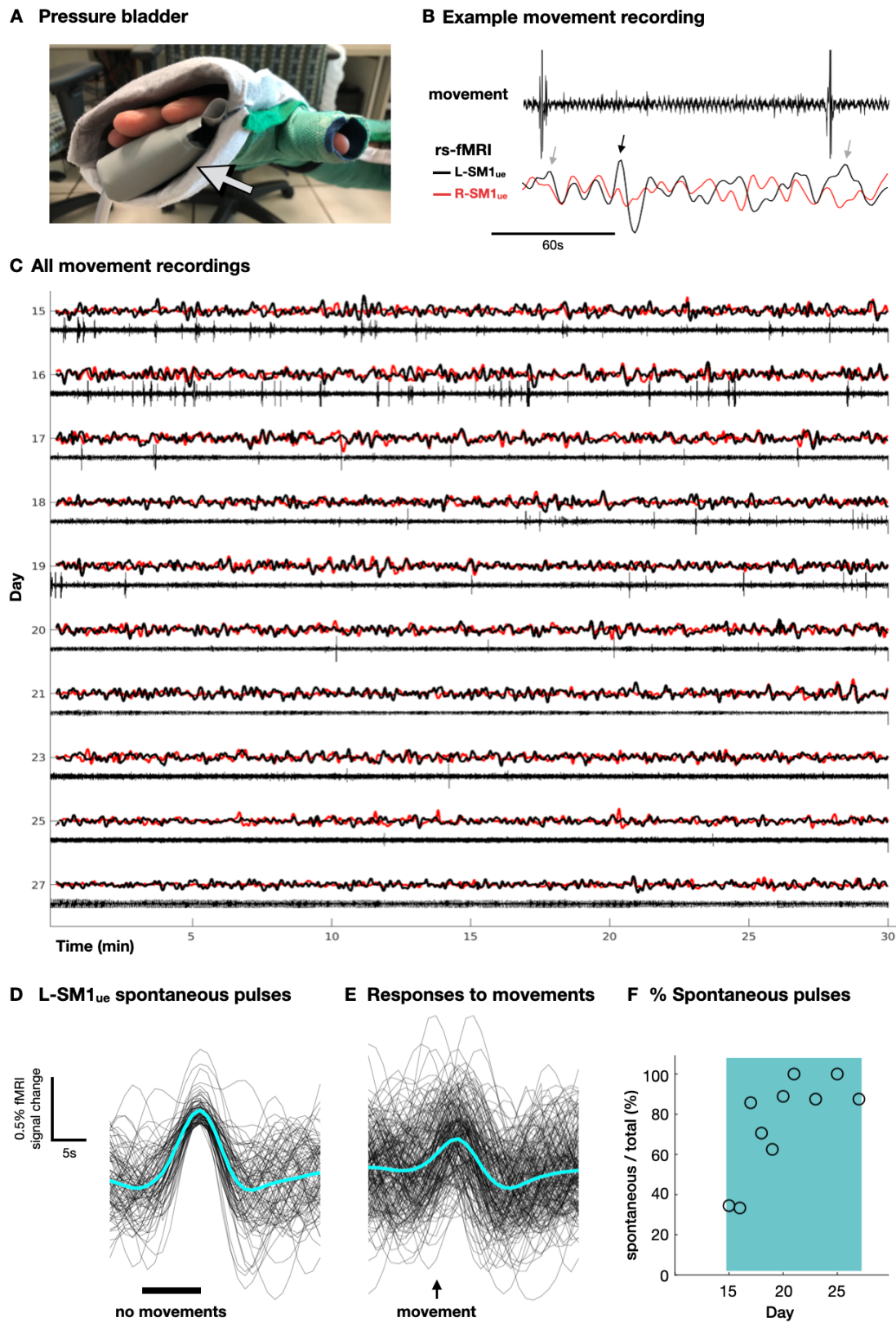


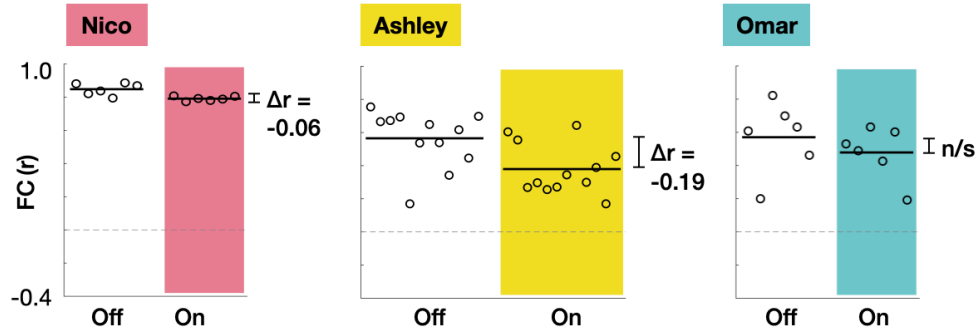
Figure 2-S5: See next page for caption.

Figure 2-S5: Pulses in L-SM1_{ue} occur in the absence of hand movements. (A) Hand movements in one participant (Omar) were monitored using a highly sensitive pressure bladder (gray arrow) inserted into the end of the cast. (B) Example recording from pressure bladder, plotted with rs-fMRI signals from L-SM1_{ue} and R-SM1_{ue}. Small positive deflections in the L-SM1_{ue} signal peak ~5 seconds after two hand movements (gray arrows). One spontaneous pulse in L-SM1_{ue} is also shown, which occurs in the absence of hand movement (black arrow). (C) Full 30-minute recordings from 10 sessions acquired during the cast period. (D) L-SM1_{ue} fMRI traces during all spontaneous pulses (pulses for which no movements were detected within 8 seconds prior to the pulse peak; n = 94). Mean pulse shown in cyan. (E) L-SM1_{ue} fMRI traces surrounding each detected movement (n = 202). Peak responses occur an average of ~3 seconds after each movement. (F) Percent of all pulses detected that occurred spontaneously during each session. In total, 66% of detected pulses occurred spontaneously.

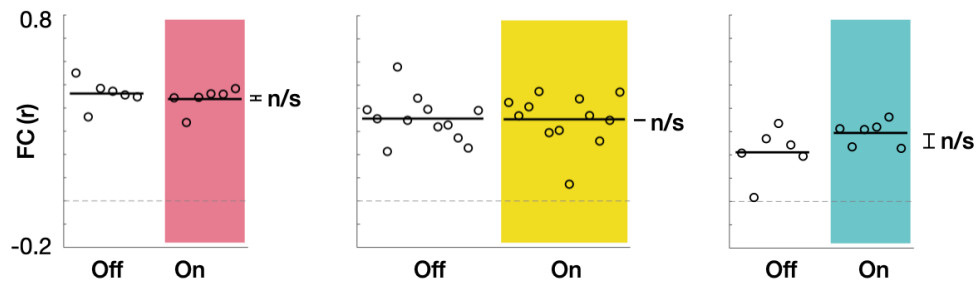
A Removable cast



B FC between L-SM1_{UE} and R-SM1_{UE}



C FC between R-Cblm_{UE} and L-Cblm_{UE}



D L-SM1_{UE} pulses

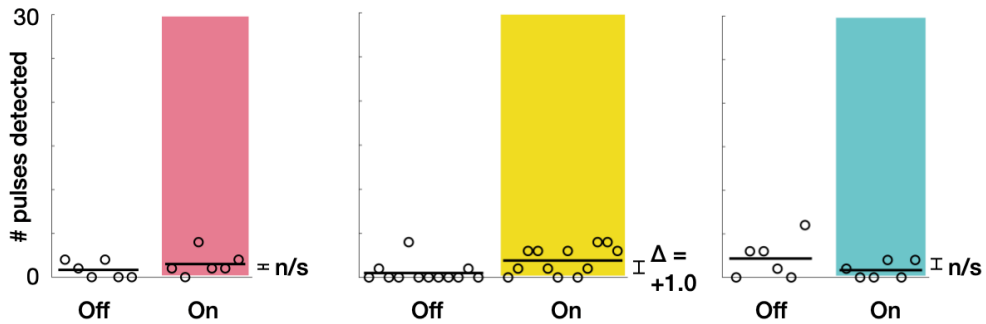


Figure 2-S6: See next page for caption.

Figure 2-S6: Wearing a cast during scanning does not recreate the effects of prolonged casting. To separate the effects of disuse from any possible effects of wearing a cast during scans, we collected 12-24 additional scans in each participant. During half of these scans, participants wore a removable cast, constructed from casts used in the original experiment. (A) Photographs of a removable cast. (B) Functional connectivity (FC) between L-SM1_{ue} and R-SM1_{ue} during each session of the control experiment. Sessions are grouped into two experimental condition: wearing a removable cast (“On”) and not wearing a cast (“Off”). Black lines indicate mean across sessions in each condition. Two participants showed a significant reduction in FC in the On condition relative to the Off condition, but these effects were much smaller than those observed during continuous casting (Nico: $\Delta r = -0.06$, $P = 0.005$; Ashley: $\Delta r = -0.19$, $P = 0.01$). The remaining participant did not show any change in FC (Omar: $\Delta r = -0.09$, $P = 0.42$). (C) FC between L-Cblm_{ue} and R-Cblm_{ue} was not significantly different during On sessions compared to Off sessions in any participant (Nico: $\Delta r = -0.02$, $P = 0.49$; Ashley: $\Delta r = 0.00$, $P = 0.94$; Omar: $\Delta r = +0.08$, $P = 0.12$). (D) Number of pulses detected during each scan of the Off and On conditions, plotted on the same axes as Figure 5C. Very few events were detected in all participants. In one participant, significantly more events were detected in the ON condition (Ashley: mean pulse count = 0.5 OFF vs. 1.5 ON, $t = +2.5$, $P = 0.02$). The remaining two participants did not show a significant difference between conditions (Nico: mean pulse count = 0.8 OFF vs. 1.5 ON, $t = +0.96$, $P = 0.36$; Omar: 2.2 OFF vs. 0.8 ON, $t = -1.3$, $P = 0.22$).

Table 2-S1: MRI acquisition and processing parameters.

	Nico	Ashley	Omar
Age (years)	35	25	27
Sex	Male	Female	Male
Handedness (Edinburgh Inventory)	Right-handed (+100)	Right-handed (+91)	Right-handed (+60)
Scan time	5:00am	9:00pm	9:00pm
Scanner	Siemens Trio 3T	Siemens Prisma 3T	Siemens Prisma 3T
T1 sequence			
Pulse sequence type	Gradient echo	Gradient echo	Gradient echo
Image type	3D MP-RAGE	3D MP-RAGE	3D MP-RAGE
Field of view (mm)	204.8x204.8x179.2	240x240x166.4	240x240x166.4
Orientation	Sagittal	Sagittal	Sagittal
TE (ms)	3.74	2.22	2.22
TR (ms)	2400	2400	2400
TI (ms)	1000	1000	1000
Flip angle (°)	8	8	8
Matrix size	256x256x224	300x320x208	300x320x208
Slice thickness (mm)	0.8	0.8	0.8
Voxel size (mm)	0.8 x 0.8 x 0.8	0.8 x 0.8 x 0.8	0.8 x 0.8 x 0.8
T2 sequence			
Pulse sequence type	Spin echo	Spin echo	Spin echo
Image type	3D T2-SPC	3D T2-SPC	3D T2-SPC
Field of view (mm)	204.8x204.8x179.2	204.8x204.8x179.2	204.8x204.8x179.2
Orientation	Sagittal	Sagittal	Sagittal
TE (ms)	479	563	563
TR (ms)	3200	3200	3200
Flip angle (°)	120	120	120
Matrix size	256x256x224	300x320x208	300x320x208
Slice thickness (mm)	0.8	0.8	0.8
Voxel size (mm)	0.8 x 0.8 x 0.8	0.8 x 0.8 x 0.8	0.8 x 0.8 x 0.8
BOLD sequence			
Pulse sequence type	2D Gradient echo	2D Gradient echo	2D Gradient echo
Image type	Echo planar	Echo planar	Echo planar
Field of view (mm)	256x256x144	234x234x145.6	234x234x145.6
Multi-band factor	1	4	4
TE (ms)	27	33	33
TR (ms)	2200	1100	1100
Flip angle (°)	90	84	84
Matrix size	64x64x36	90x90x56	90x90x56
Slice thickness (mm)	4	2.6	2.6
Voxel size (mm)	4 x 4 x 4	2.6 x 2.6 x 2.6	2.6 x 2.6 x 2.6
FD threshold (mm)	0.2	0.1	0.1
DVARS threshold (% rms)	6	6	6

2.8 Acknowledgments

We thank Deanna M. Barch and Jin-Moo Lee for their comments on this research and Scott Gericke for help with the visual presentation of the results. This work was supported by NIH grants F31NS110332 (D.J.N.), NS088590 (N.U.F.D.), TR000448 (N.U.F.D.), MH1000872 (T.O.L.), 1R25MH112473 (T.O.L.), 5T32 MH100019-02 (S.M.), MH104592 (D.J.G.), 1P30NS098577 (to the Neuroimaging Informatics and Analysis Center); the US Department of Veterans Affairs Clinical Sciences Research and Development Service grant 1IK2CX001680 (E.M.G.); Kiwanis Neuroscience Research Foundation (N.U.F.D. and B.L.S.); the Jacobs Foundation grant 2016121703 (N.U.F.D.); the Child Neurology Foundation (N.U.F.D.); the McDonnell Center for Systems Neuroscience (N.U.F.D. and B.L.S.); the Mallinckrodt Institute of Radiology grant 14-011 (N.U.F.D.); the Hope Center for Neurological Disorders (N.U.F.D., B.L.S., and S.E.P.). The views expressed in this article are those of the authors and do not necessarily reflect the position or policy of the Department of Veterans Affairs or the U.S. government.

Chapter 3: Cingulo-opercular Control Network Supports Disused Motor Circuits in Standby Mode

This chapter is under consideration as journal article. The citation is:

Newbold, D. J., Gordon, E. M., Laumann, T. O., Seider, N. A., Montez, D. F., Gross, S. J., Zheng, A., Nielsen, A. N., Hoyt, C. R., Hampton, J. M., Ortega, M., Adeyemo, B., Miller, D. B., Van, A. N., Marek, S., Schlaggar, B. L., Carter, A. R., Kay, B. P., Greene, D. J., Raichle, M. E., Petersen, S. E., Snyder, A. Z., Dosenbach, N. U. F. Cingulo-opercular Control Network Supports Disused Motor Circuits in Standby Mode. *In submission*

Tim Laumann, Catherine Hoyt, Avi Snyder, Nico Dosenbach and I designed the study. Catherine Hoyt, Jackie Hampton, Mario Ortega, Nico Dosenbach and I collected the data. Evan Gordon and I analyzed the data. Evan Gordon, Tim Laumann, Nicole Seider, David Montez, Sarah Gross, Annie Zheng, Ashley Nielsen, Tunde Adeyemo, Alex Carter, Ben Kay, Deanna Greene, Marc Raichle, Steve Petersen, Avi Snyder, Nico Dosenbach and I interpreted the results. Nico Dosenbach and I wrote the manuscript with input from all other authors.

3.1 Preface

Our first paper on cast-induced plasticity revealed surprisingly large and rapid changes in FC and a previously undescribed form of spontaneous activity: pulses of spontaneous activity that propagated through the disused somatomotor circuit. However, this first paper was limited in scope, focusing exclusively on task-defined regions of interest (ROIs) in the somatomotor system. A unique advantage of resting-state functional MRI (rs-fMRI) is the ability to record activity from all regions of the brain at once. Whole-brain analysis of functional connectivity (FC) changes presents challenging statistical hurdles. Analyzing FC changes between all pairs of brain regions means making hundreds of thousands of parallel comparisons. Given the high sampling variability of rs-fMRI, many changes occurring by chance are likely to be larger than the actual effects of interest. We overcame these hurdles through both experimental and

analytical innovations. The many hours of rs-fMRI data we collected make any one of our participants the most highly sampled individual-specific rs-fMRI dataset ever collected. Pooling rs-fMRI data over up to 14 30-minute scans before and during casting allowed us to vastly reduce the amount of sampling variability in our FC measurements. We also greatly reduced the number of comparisons needed to provide a comprehensive view of cast-induced plasticity by focusing initially on FC changes between the disused somatomotor cortex (L-SM1_{uc}) and the remainder of the brain and by grouping several hundreds of brain regions into 17 canonical functional networks identified separately in each individual. These innovations provided the statistical power necessary to carry out whole-brain analyses separately in each individual and replicate all findings across our three participants.

These analyses showed that changes in FC were strikingly specific to just two functional networks: the somatomotor and cingulo-opercular networks (SMN and CON). FC changes in the SMN matched those we described in our first paper using task-based ROIs and were consistent with our initial predictions. The FC changes in the CON were more surprising. Our lab first identified the CON over a decade ago. CON regions, including parts of the dorsal anterior cingulate cortex (dACC) and frontal operculum, show sustained activity during a wide variety of behaviors and are thought to represent task sets—abstract parameters and motor programs that govern goal-driven behavior. Understanding why executive control regions in the CON showed plasticity during casting of one extremity required many hours of discussion with Steve Petersen, Tim Laumann and Avi Snyder. In the end, we decided to present three possible roles for the CON in disuse-driven plasticity.

Another topic addressed in this manuscript is the relationship between changes in FC and the spontaneous activity pulses described in our first paper. Changes in FC, temporal correlations in rs-fMRI time series, are often interpreted as an abstract reflection of structural or functional modifications of brain circuits. Our observation of spontaneous activity pulses presented an opportunity to identify a concrete change in neural activity producing altered patterns of FC. Determining whether the pulses were in fact responsible for the observed changes in FC turned out to be more challenging than I had initially expected. The method we implemented for distinguishing pulses from ongoing spontaneous activity fluctuations relied on thresholds of activity, meaning that only the largest pulses could be reliably detected. Determining the impact of all pulses, some of which could not be detected, required multiple analyses that provided distinct perspectives on the problem. In the end, concluded that the pulses likely explained increases in FC between disused motor regions and the CON but did not explain decreases in FC within the SMN. Thus, whole-brain analyses of cast-induced plasticity revealed two distinct mechanisms of FC change, one produced by spontaneous activity pulses and one that occurs independently of pulses.

3.2 Abstract

Two weeks of upper extremity casting induced plasticity beyond somatomotor regions. Whole-brain resting-state functional MRI (rs-fMRI) revealed that disused motor regions became more strongly connected to the cingulo-opercular network (CON), an executive control network that includes regions of the dorsal anterior cingulate cortex (dACC) and insula. Disuse-driven increases in functional connectivity (FC) were specific to the CON and somatomotor networks and did not involve any other networks, such as the salience, frontoparietal or default mode networks. FC increases during casting were mediated by large, spontaneous activity pulses that appeared in disused motor regions and network-adjacent CON control regions. During limb constraint, disused motor circuits appear to enter a standby mode characterized by spontaneous activity pulses and strengthened connectivity to CON executive control regions.

3.3 Introduction

Disuse is a powerful paradigm for inducing plasticity that has uncovered key organizing principles of the human brain (Wiesel and Hubel, 1965; Merzenich et al., 1983a; Feldman and Brecht, 2005; Milliken et al., 2013). Monocular deprivation revealed that multiple afferent inputs can compete for representational territory in the primary visual cortex (Wiesel and Hubel, 1965). Competition between afferents also shapes the somatomotor system, and manipulations such as peripheral nerve deafferentation, whisker trimming, and limb constraint all drive plasticity in the primary somatosensory and motor cortex (Merzenich et al., 1983a; Feldman and Brecht, 2005; Milliken et al., 2013). Most plasticity studies to date have used focal techniques, such as microelectrode recordings, to study local changes in brain function. As a result, little is known about how behavior and experience shape brain-wide functional networks.

The brain is composed of networks of regions that cooperate to perform specific cognitive operations (Posner and Petersen, 1990; Raichle et al., 2001; Shulman et al., 2001). These functional networks show synchronized spontaneous activity while the brain is at rest, a phenomenon known as resting state functional connectivity (FC) (Biswal et al., 1995; Greicius et al., 2003; Fox et al., 2005). FC can be measured non-invasively in humans using resting-state functional MRI (rs-fMRI). Whole-brain rs-fMRI has been used to parse the brain into canonical functional networks (Power et al., 2011; Yeo et al., 2011), including visual, auditory and somatomotor networks (Lowe et al., 1998; Cordes et al., 2001); ventral and dorsal attention networks (Shulman et al., 2001; Fox et al., 2006); a default mode network with roles in internally directed cognition and episodic memory (Raichle et al., 2001; Greicius et al., 2003); a salience network thought to assess the homeostatic relevance of external stimuli (Seeley et al., 2007); a frontoparietal control network supporting error-processing and moment-to-moment adjustments in behavior (Dosenbach et al., 2007; Dosenbach et al., 2008; Marek and Dosenbach, 2019); and a cingulo-opercular control network (CON), which maintains executive control during goal-directed behavior (Dosenbach et al., 2006; Dosenbach et al., 2007; Dosenbach et al., 2008).

A more recent advance in human neuroscience has been the recognition of individual variability in network organization (Mueller et al., 2013; Laumann et al., 2015; Wang et al., 2015; Gordon et al., 2017). Most early rs-fMRI studies examined central tendencies in network organization using group-averaged FC measurements (Fox et al., 2005; Power et al., 2011; Yeo et al., 2011). Recent work has demonstrated that functional networks can be described in an individual-specific manner if sufficient rs-fMRI data are acquired, an approach termed Precision Functional

Mapping (PFM) (Laumann et al., 2015; Poldrack et al., 2015; Braga and Buckner, 2017; Gordon et al., 2017; Marek et al., 2018; Greene et al., 2020; Sylvester et al., 2020). PFM respects the unique functional anatomy of each person and avoids averaging together functionally distinct brain regions across individuals.

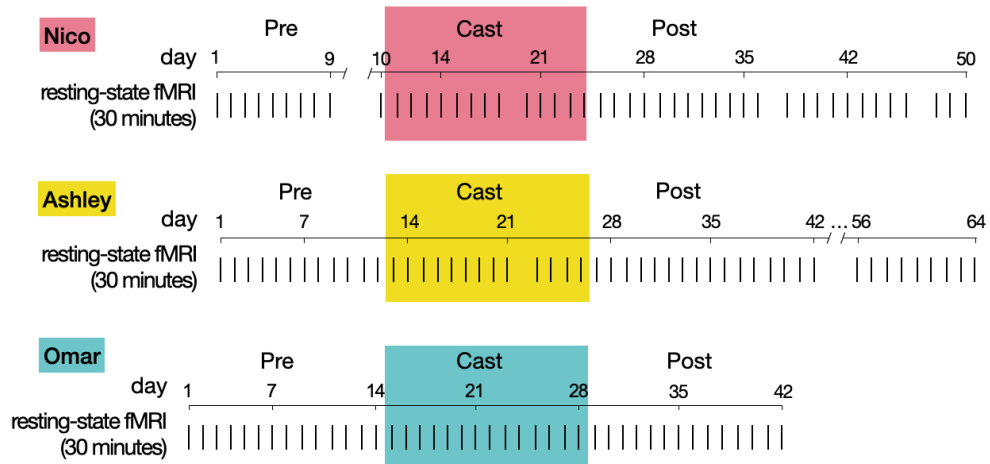
We recently demonstrated that PFM can track disuse-driven plasticity in the human brain (Newbold et al., 2020). Three adult participants (Nico, Ashley and Omar) were scanned at the same time every day for 42-64 consecutive days (30 minutes of rs-fMRI/day) before, during and after two weeks of dominant upper extremity casting (Fig. 1a-b). During casting, the upper-extremity regions of the primary somatomotor cortex (L-SM1_{ue}) and cerebellum (R-Cblm_{ue}) functionally disconnected from the remainder of the somatomotor network. Disused motor circuits also exhibited large, spontaneous pulses of activity (Fig. 1c).

Somatomotor circuits do not function in isolation. Action selection and motor control are thought to be governed by complex interactions between the somatomotor network and control networks, including the CON (Dosenbach et al., 2007). Here, we leveraged the whole-brain coverage of rs-fMRI to examine disuse-driven plasticity beyond the somatomotor system. We first examined disuse-driven changes in FC between L-SM1_{ue} and the remainder of the cerebral cortex. We then performed comprehensive analyses of FC changes between all pairs of individual-specific cortical, subcortical and cerebellar parcels (>200,000 possible connections). Finally, we tested if observed changes in FC could be explained by the occurrence of spontaneous activity pulses during the cast period.

a Dominant upper extremity casts



b Experimental design



c Disuse-driven spontaneous activity pulses

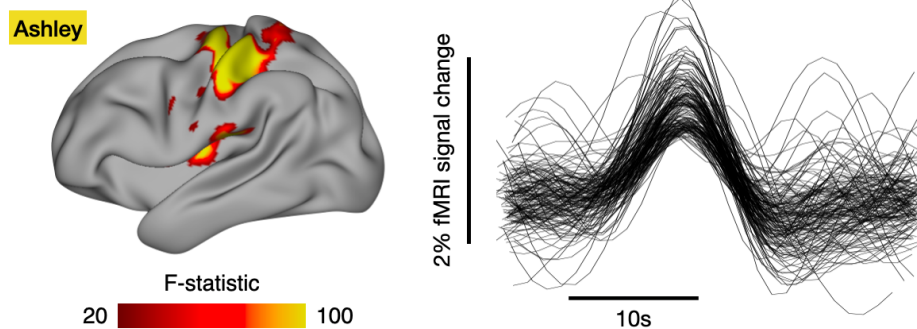


Figure 3-1: Experimental Design and Spontaneous Activity Pulses. (a) Three participants (Nico, Ashley and Omar) wore casts covering the entire dominant upper extremity for two weeks. (b) Participants were scanned every day for 42-64 consecutive days before, during and after casting. All scans included 30 minutes of resting-state functional MRI (rs-fMRI). (c) During the cast period, disused somatomotor circuits exhibited spontaneous activity pulses³⁰.

3.4 Results

3.4.1 Disuse Caused Both Increases and Decreases in Functional Connectivity

To examine disuse-driven plasticity beyond somatomotor networks, we first generated seed maps showing FC between L-SM1_{ue} and all other cortical regions before, during and after casting (Fig. 2a, Supplementary Fig. 1). Prior to casting (Pre), L-SM1_{ue} was strongly connected to the remainder of the somatomotor cortex (pre- and post-central gyri), especially homotopic R-SM1_{ue}. During the cast period (Cast), L-SM1_{ue} showed a new pattern of connectivity, with strong connections to bilateral secondary somatosensory cortex (SII), dorsal anterior cingulate cortex (dACC), and pre- and post-central sulci. After casting (Post), L-SM1_{ue} FC returned to baseline. Changes in FC during casting (Cast – Pre) and recovery (Post – Cast) were examined using sets of previously published individual-specific cortical parcels (Gordon et al., 2017; Newbold et al., 2020). Casting caused decreased L-SM1_{ue} connectivity with the remainder of the somatomotor cortex, as well as increased connectivity with the bilateral SII, dACC, and pre- and post-central sulci (Fig. 2b, Supplementary Fig. 1). FC changes after cast removal were strongly negatively correlated with changes during casting (Nico: spatial correlation, $r = -0.56$, $P < 0.001$; Ashley: $r = -0.95$, $P < 0.001$; Omar: $r = -0.32$, $P < 0.001$), indicating that most effects reversed after cast removal (Fig. 2b, Supplementary Fig. 1).

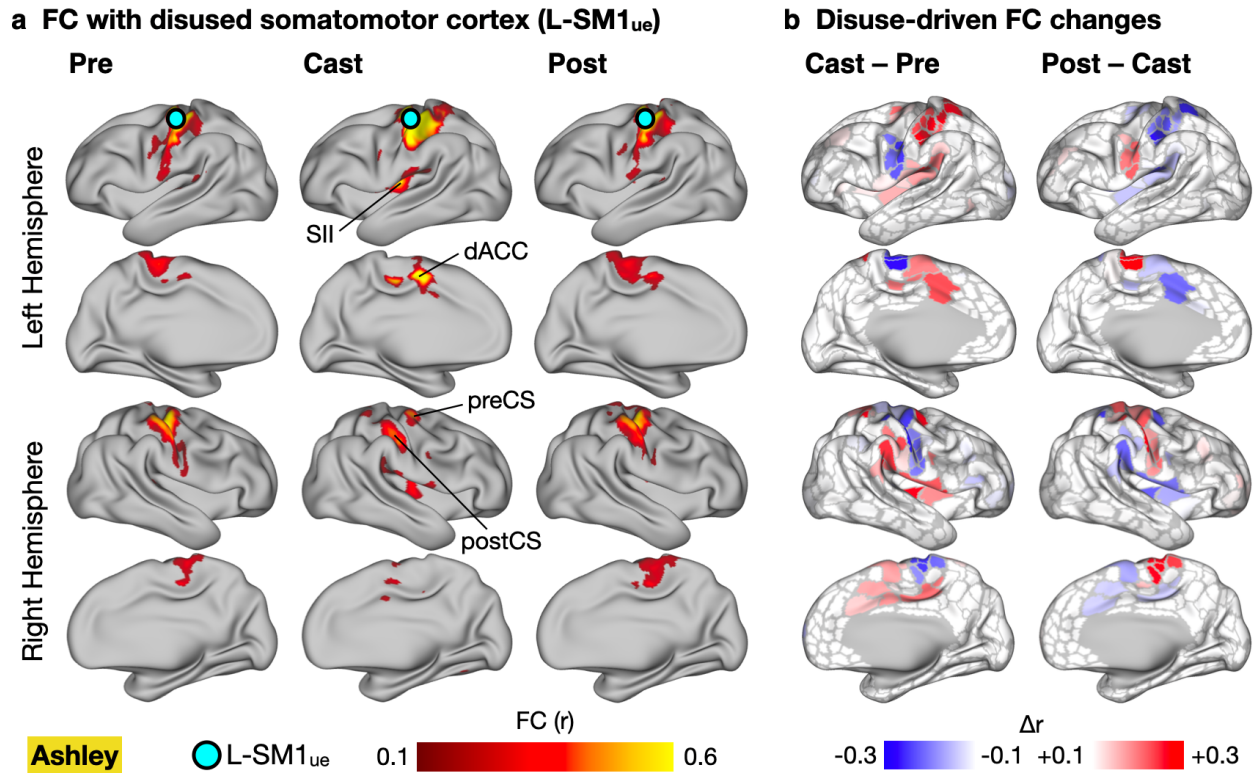


Figure 3-2: Cast-driven Changes in Functional Connectivity (FC) of Disused Somatomotor Cortex (L-SM1_{ue}). (a) Seed maps showing FC between L-SM1_{ue} and the remainder of the cerebral cortex in an example participant (Ashley; remaining participants, Supplementary Fig. 1). Seed maps were averaged across sessions before, during and after casting (Pre, Cast, Post). Labels indicate secondary somatosensory cortex (SII), dorsal anterior cingulate cortex (dACC), and pre- and post-central sulci (preCS and postCS). (b) Subtraction maps showing changes in FC during casting (Cast – Pre) and recovery (Post – Cast). Differences are shown on a set of previously published individual-specific cortical parcels²¹.

3.4.2 Disuse-driven Functional Connectivity Changes Were Highly Focal in Network Space

The brain's functional network organization can be visualized using spring-embedded graphs, which treat functional connections as spring forces, positioning more strongly connected nodes closer to one another (Fig. 3a, Supplementary Fig. 2). While L-SM1_{ue} FC increases were distributed in anatomical space, including regions on the medial and lateral surfaces of both hemispheres, nearly all of these changes mapped onto a single cluster in network space, the CON (Fig. 3b, Supplementary Fig. 2). The network focality of L-SM1_{ue} FC increases was quantified by examining the distribution of the greatest FC increases (top 5%) across the canonical functional networks (Fig. 3b). In all participants, the CON showed more FC increases than expected by chance ($P < 0.001$ for all participants). Decreases in L-SM1_{ue} FC were also localized in network space (Fig. 3c, Supplementary Fig. 2). Most of the regions showing decreased FC with L-SM1_{ue} during casting belonged to the somatomotor networks (ue-SMN, le-SMN, face-SMN and premotor). All participants showed more FC decreases than expected by chance in the upper-extremity somatomotor network (ue-SMN; $P < 0.001$ for all participants). Additionally, two participants (Ashley and Omar) showed significant FC decreases in other somatomotor networks, including the lower-extremity and face somatomotor networks (le-SMN and f-SMN) and the premotor network.

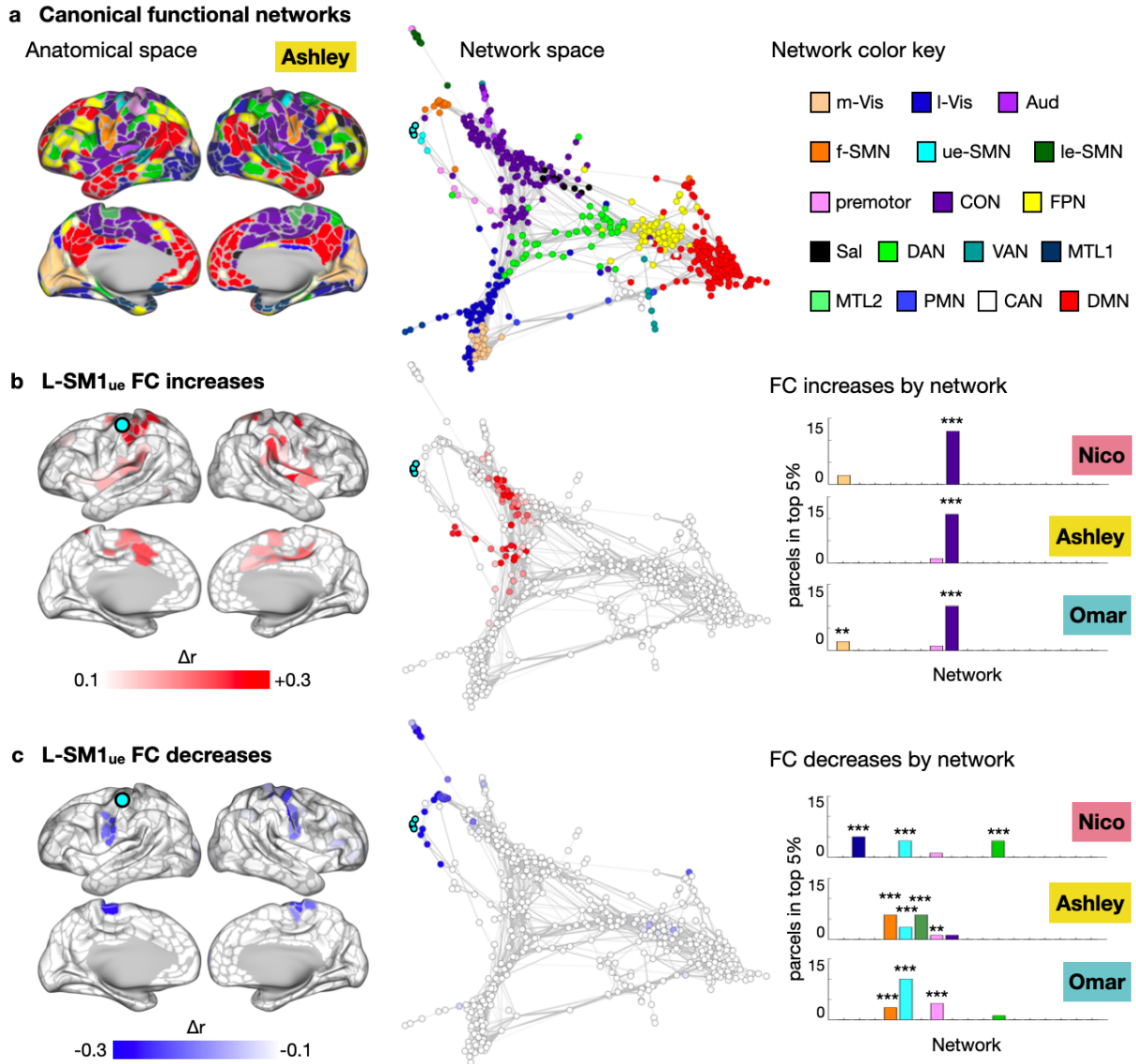


Figure 3-3: Disused Somatomotor Cortex (L-SM1_{ue}) Functional Connectivity (FC) Changes in Network Space. (a) Map of canonical functional networks in an example participant (Ashley; remaining participants, Supplementary Fig. 2). *Left*: Networks shown in anatomical space (inflated cortical surfaces). *Middle*: Same map as *Top*, shown in network space (spring-embedded graphs based on Pre scans). *Right*: Network color key: m-Vis: medial visual; l-Vis: lateral visual; Aud: auditory; f-SMN: face somatomotor; ue-SMN: upper-extremity somatomotor; le-SMN: lower-extremity somatomotor; CON: cingulo-opercular; FPN: fronto-parietal; Sal: salience; DAN: dorsal attention; VAN: ventral attention; MTL: medial temporal lobe; PMN: parietal memory; CAN: context association; DMN: default mode. (b) *Left*: Subtraction maps showing disuse-driven decreases in functional connectivity (FC) with left somatomotor cortex (L-SM1_{ue}) in anatomical space. *Middle*: Same map as *Top*, shown in network space. *Right*: Distribution of top 5% FC decreases across all networks. ** $P < 0.01$; *** $P < 0.001$; FDR < 0.05 . (c) Subtraction maps showing disuse-driven increases in FC with L-SM1_{ue} in anatomical (*Left*) and network space (*Middle*). *Right*: Distribution of top 5% FC increases across all networks.

3.4.3 Plasticity Was Restricted to the Somatomotor and Cingulo-opercular Networks

The analyses presented thus far focus on changes in connectivity between L-SM1_{ue} and the remainder of the cerebral cortex. To examine whole-brain patterns of FC changes induced by casting, we extracted rs-fMRI signals from individual-specific cortical, subcortical and cerebellar parcels (Nico: 744 parcels, Ashley: 733; Omar: 761) and examined FC changes in all possible pairwise connections (Supplementary Fig. 3). We displayed the 50 largest changes in FC (25 greatest increases and 25 greatest decreases) in anatomical space (Fig. 4a, Supplementary Fig. 3). Disuse-driven FC changes involved L-SM1_{ue} more than expected by chance (Nico: 9/50 connections, $P = 0.018$; Ashley: 37/50, $P < 0.001$; Omar: 39/50, $P < 0.001$). Figure 4b shows the total magnitude of whole-brain FC change for each vertex/voxel. The total magnitude of whole-brain FC change was significantly greater in L-SM1_{ue} than in the remainder of the brain (Fig. 4B, Supplementary Fig. 3; Nico: $P = 0.021$; Ashley: $P < 0.001$; Omar: $P = 0.005$).

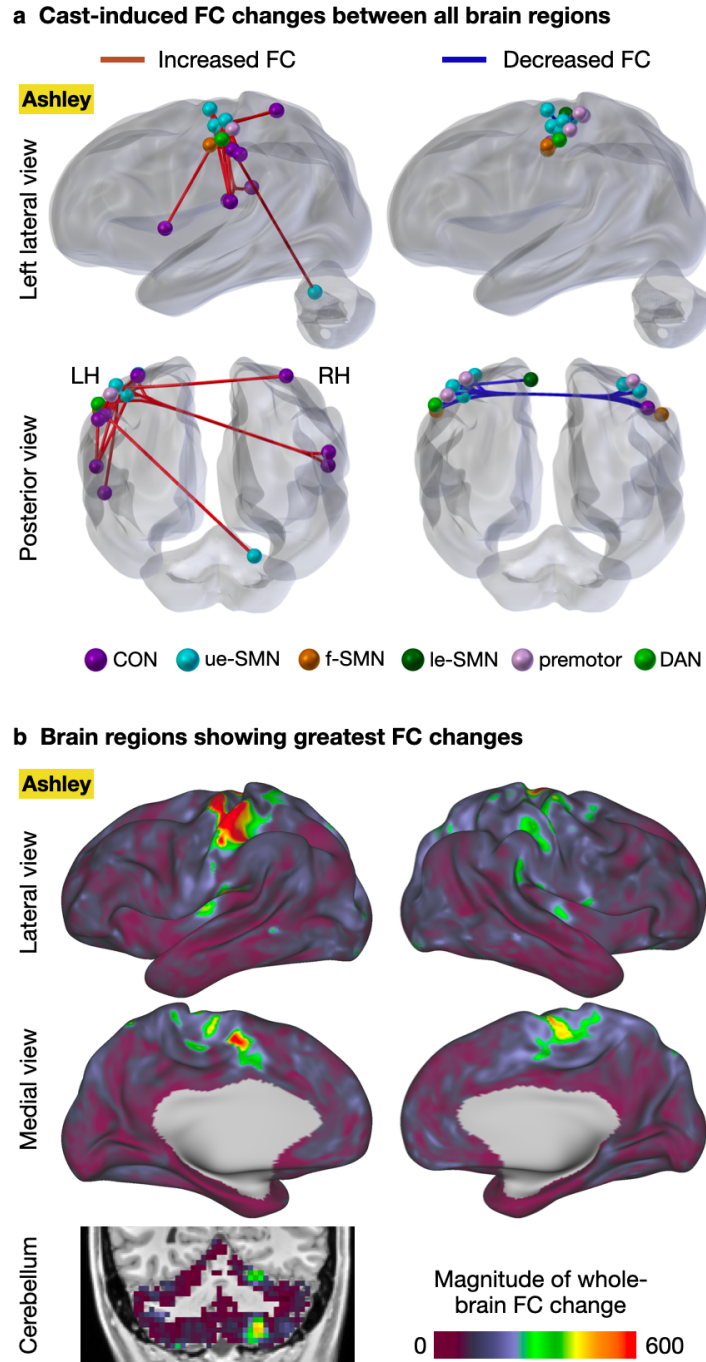
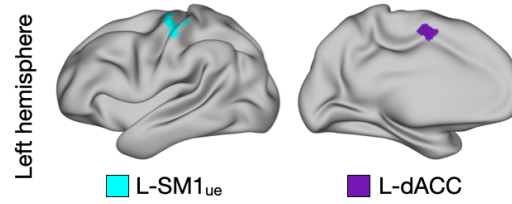


Figure 3-4: Whole-brain Analyses of Disuse-driven Functional Connectivity (FC) Changes. (a) Changes in functional connectivity (FC) were computed for all pairs of cortical, subcortical and cerebellar parcels (mean Cast FC – mean Pre FC). The 50 most altered functional connections (top 25 increases, top 25 decreases) are shown for an example participant (Ashley; all participants, Supplementary Fig. 3). (b) For each vertex/voxel, the magnitude of whole-brain FC change was computed as the sum of squared FC changes between that vertex and every other gray-matter vertex/voxel. Shown for an example participant (Ashley; all participants shown in Supplementary Fig. 4).

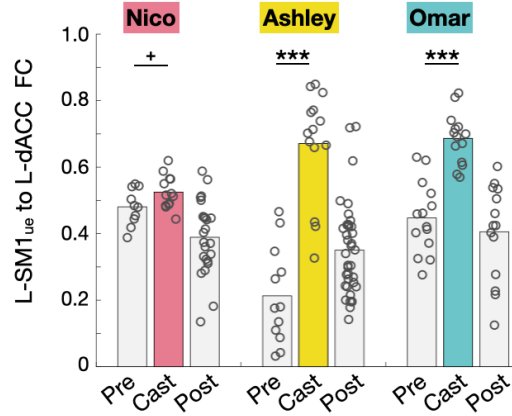
3.4.4 Increased Somatomotor Connectivity with the CON Depended on a Recent History of Disuse

To distinguish between increases in connectivity due to wearing a cast during MRI scans (i.e., an altered behavioral state) and increases in connectivity due to a history of having been casted (i.e., disuse-driven plasticity), we conducted a control experiment in which participants wore casts during 30-minute scans but were not casted during their daily lives. In both cases, we compared FC between L-SM1_{ue} and the left dorsal anterior cingulate cortex (L-dACC; Fig. 5a), a key node of the CON, in cast and no-cast conditions. As suggested by the whole-brain network analyses (Fig. 3b), FC between L-SM1_{ue} and L-dACC was significantly increased during the cast period (Fig. 5b). When participants wore casts during scans, but were not casted during their daily lives, no changes in FC were observed (Fig. 5c). This control experiment indicated that increased FC between the disused motor circuitry and the CON depended on participants' recent history of disuse, not their current state of casting.

a Motor and CON regions of interest



b Effect of disuse



c Effect of casting during scans

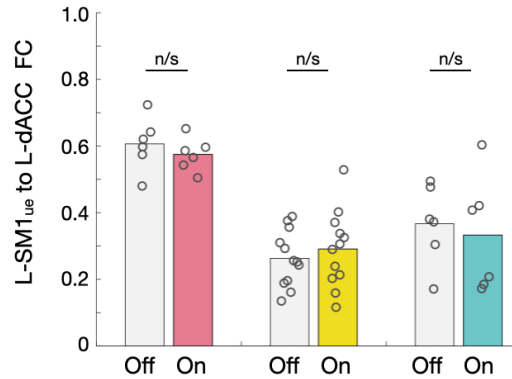
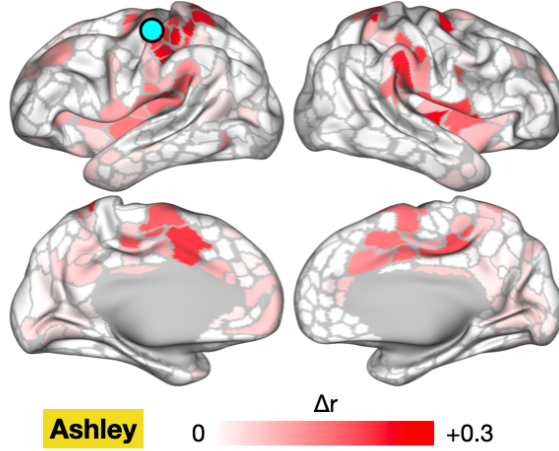


Figure 3-5: Connectivity between Disused Somatomotor Cortex and Cingulo-opercular Network during Disuse and Temporary Casting. **a**, Example regions of interest (ROIs) in the left primary somatomotor cortex (L-SM1_{ue}) and the left dorsal anterior cingulate cortex (L-dACC). **b**, Functional connectivity (FC) measured between L-SM1_{ue} and L-dACC before (Pre), during (Cast) and after casting (Post). Two participants (Ashley and Omar) show a significant increase in FC during the cast period ⁺P < 0.1, *P < 0.05, ***P < 0.001. **(C)** FC measured between L-SM1_{ue} and L-dACC during both conditions of the control experiment: without casting (Off) and with temporary casts during scans (On). No changes in FC were observed.

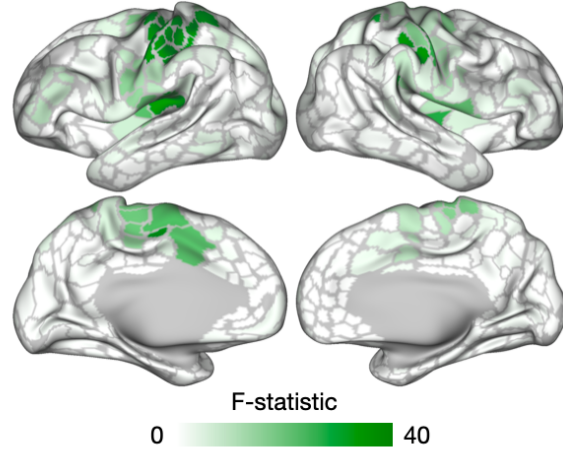
3.4.5 Network-Specific Connectivity Changes Reflect Spontaneous Activity Pulses

Increases in FC with L-SM1_{ue} showed a similar anatomical distribution to the spontaneous activity pulses we described previously (Newbold et al., 2020) (Fig. 6a-b). Additionally, FC between L-SM1_{ue} and the CON was highly correlated with the number of pulses detected in L-SM1_{ue} during each scan (Fig. 6c; Nico: $r=0.74$, $P<0.001$; Ashley: $r=0.57$, $P<0.001$; Omar: $r=0.73$, $P<0.001$). These observations led us to suspect that FC between L-SM1_{ue} and the CON was increased during the cast period because both regions showed synchronized spontaneous activity pulses.

a L-SM1_{ue} FC increases (Cast – Pre)



b Spontaneous activity pulses



c Functional connectivity vs. number of pulses detected during each scan

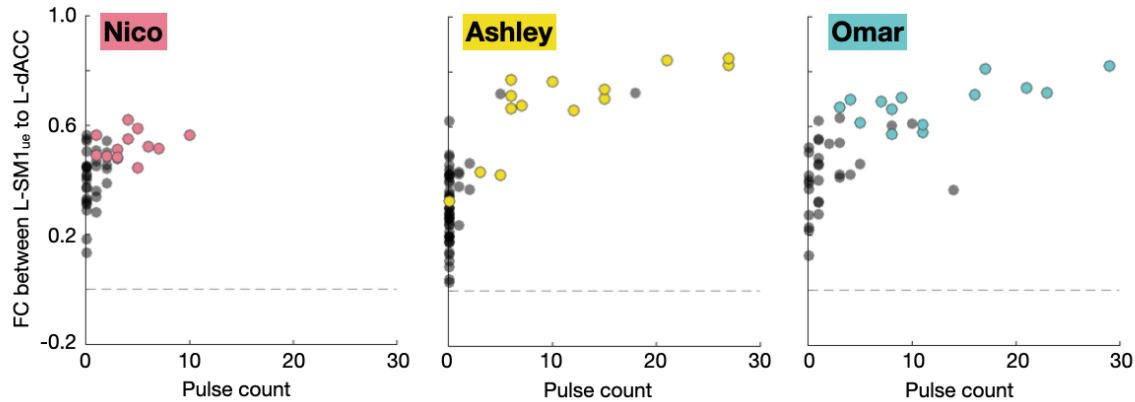


Figure 3-6: Relationship of Spontaneous Activity Pulses to Functional Connectivity (FC) Changes. (a) Increases in FC with the disused somatomotor cortex (L-SM1_{ue}) during casting, repeated from Figure 3b for reference. (b) Analysis of variance (ANOVA) showing regions with spontaneous activity pulses. ANOVA F-statistic was correlated with FC change in each parcel (Nico: $r = 0.16$, $P < 0.001$; Ashley: $r = 0.29$, $P < 0.001$; Omar: $r = 0.06$, $P = 0.12$). (c) Relationship of FC between L-SM1_{ue} and the dorsal anterior cingulate cortex (dACC; cingulo-opercular network (CON)) vs. the number of pulses detected. Each dot represents one 30-minute scan. Colored dots represent scans during the cast period. For all participants, FC between L-SM1_{ue} and dACC was significantly correlated with the number of pulses detected (Nico: $r=0.74$, $P<0.001$; Ashley: $r=0.57$, $P<0.001$; Omar: $r=0.73$, $P<0.001$).

To test if spontaneous activity pulses could explain observed increases in FC, we implemented a pulse censoring strategy, in which frames surrounding each detected pulse (13.2 s before – 17.6 s after each pulse peak) were excluded from FC calculations (Fig. 7a). This approach is similar to the censoring strategy commonly used to correct the effects of head-motion on FC (Power et al., 2012). Censoring pulses partially reduced the FC changes observed during casting (Fig. 7b; Nico: -55%, $P = 0.14$; Ashley: -28%, $P = 0.02$; Omar: -21%, $P = 0.04$; one-tailed t-test). Additionally, the spatial pattern of FC changes caused by pulse censoring (Censored – Uncensored; Fig. 7c, Supplementary Fig. 4) was negatively correlated with FC changes during casting (Nico: $r = -0.35$, $P < 0.001$; Ashley: $r = -0.90$, $P < 0.001$; Omar: $r = -0.33$, $P < 0.001$).

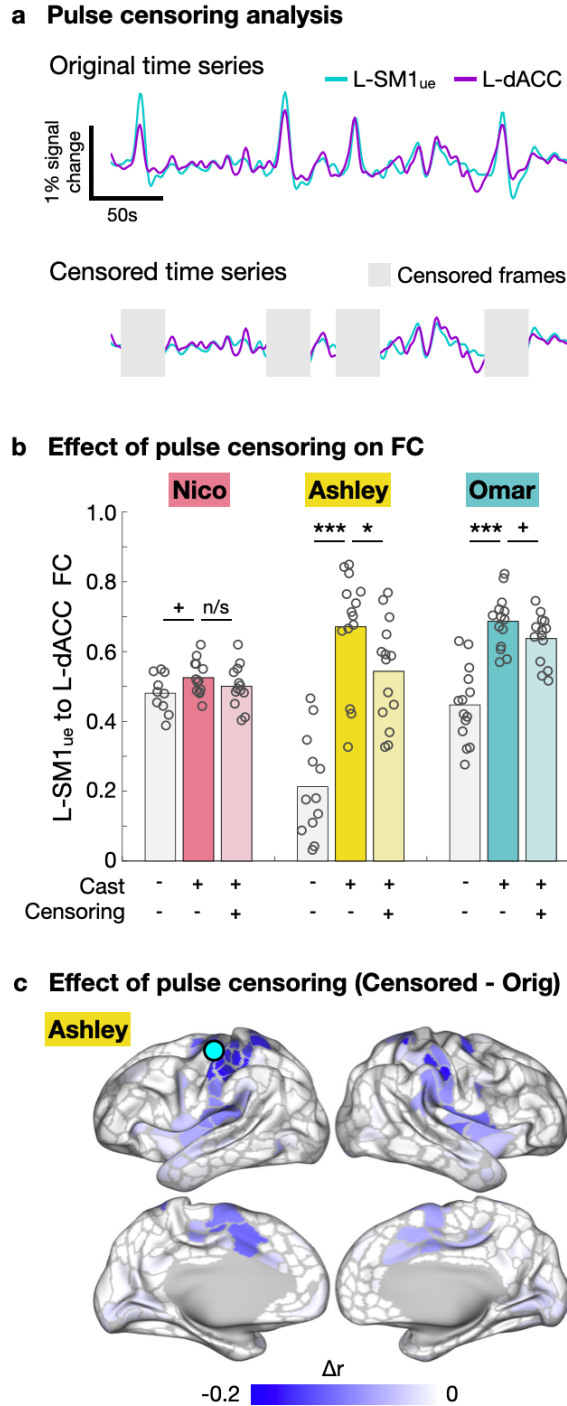


Figure 3-7: Censoring Pulses from Functional Connectivity (FC) Measurements. (a) Schematic explaining censoring approach used to remove detected pulses from FC calculation. **(b)** Censoring pulses partially reduced the difference between Pre and Cast scans. ⁺P < 0.1, *P < 0.05, ***P < 0.001. **(c)** Subtraction map showing reductions in L-SM1_{ue} FC due to pulse censoring. The spatial pattern of FC changes due to pulse censoring was significantly negatively correlated with FC changes during casting (Nico: $r = -0.35$, $P < 0.001$; Ashley: $r = -0.90$, $P < 0.001$; Omar: $r = -0.33$, $P < 0.001$)

Censoring pulses did not entirely eliminate the effect of casting on FC. The residual effect of casting after pulse censoring was negatively spatially correlated with the effects of pulse censoring (Supplementary Fig. 4; Nico: spatial correlation, $r = -0.23$, $P < 0.001$; Ashley: $r = -0.76$, $P < 0.001$; Omar: $r = -0.18$; $P < 0.001$), suggesting that the residual effect may have been driven by additional pulses that were too small to distinguish from ongoing spontaneous activity fluctuation. Pulses showed a wide distribution of magnitudes (Fig. 8a; range: 0.4 – 1.2% rs-fMRI signal change). Because pulses were detected using a threshold-based approach (Newbold et al., 2020), pulses smaller than 0.4% fMRI signal change could not be detected and censored. To test if smaller pulses that escaped detection could explain the residual increased FC between L-SM1_{ue} and L-dACC after pulse censoring, we simulated a full distribution of pulse magnitudes by adding the mean pulse time series from L-SM1_{ue} and L-dACC to the baseline rs-fMRI signals recorded from these regions prior to casting (Fig. 8b). Simulated pulse magnitudes were drawn from a log-normal distribution, fit to the magnitude distribution of detected pulses using a least-squares approach (Fig. 8a; see Supplementary Fig. 5 for triangular and exponential distributions). Adding simulated pulses caused FC increases with a similar effect size (Nico: $\Delta r = +0.07$, $P = 0.013$; Ashley: $+0.40$, $P < 0.001$; Omar: $+0.19$, $P < 0.001$) to the FC increases observed during casting (Fig. 8c). Applying the same pulse censoring strategy described above to the simulated pulses partially reduced the increases in FC (Fig. 8c; Nico: -79% , $P < 0.001$; Ashley: -58% , $P < 0.001$; Omar: -69% , $P < 0.001$), similar to the effect of pulse censoring on the actual data (Fig. 7b). Adding simulated pulses to all brain regions, using mean pulse time series specific to each region, recreated the anatomical distribution of FC changes observed during casting (Fig. 7d, Supplementary Fig. 6; Nico: $r = 0.44$, $P < 0.001$; Ashley: $r = 0.95$, $P < 0.001$; Omar: $r = 0.64$, $P <$

0.001). Thus, pulse with a full distribution of magnitudes could account for observed FC changes during casting and the partial reversal of FC changes after pulse censoring.

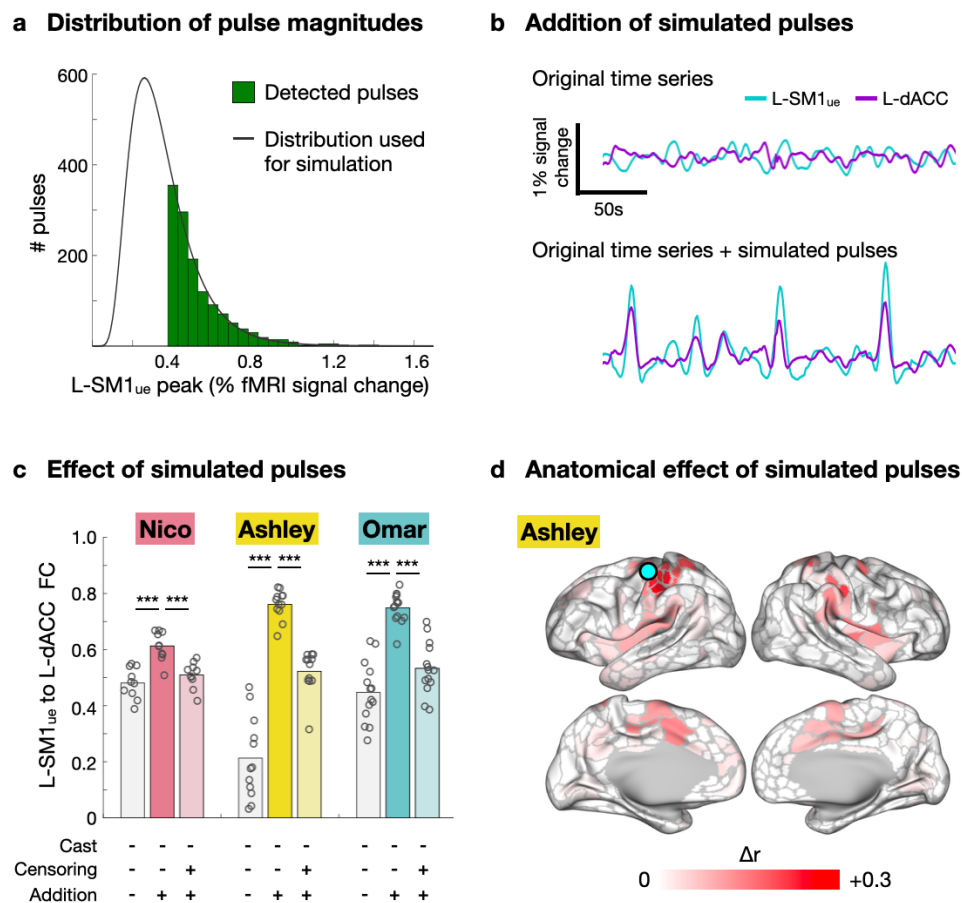


Figure 3-8: Addition of Simulated Pulses. (a) Histogram of pulse magnitudes (peak fMRI signal), pooled across participants. A log-normal distribution (black line) was fit to the data using a least-squares approach. (b) *Top*: Example resting-state functional MRI (rs-fMRI) signals from disused motor cortex (L-SM1_{ue}) and the dorsal anterior cingulate cortex (L-dACC) recorded prior to casting (Pre). *Bottom*: Same time series with simulated pulses added at random time points. Simulated pulse magnitudes were drawn from the full distribution shown in panel C. (c) Adding simulated pulses increased FC between L-SM1_{ue} and L-dACC (***P<0.001). Censoring simulated pulses partially reduced FC increases (***P<0.001). (d) Subtraction map showing increases in L-SM1_{ue} FC caused by simulated pulses in an example participant (Ashley; all participants, Supplementary Fig. 7).

We also utilized the pulse censoring and pulse addition analyses to test if pulses could explain observed decreases in FC within the somatomotor system. Pulse censoring did not significantly reverse the decrease in FC between L-SM1_{ue} and R-SM1_{ue} observed during the cast period (Supplementary Fig. 7). Adding simulated pulses to baseline time series decreased FC between L-SM1_{ue} and R-SM1_{ue}, but this effect was much smaller than that observed during casting (Supplementary Fig. 7).

3.5 Discussion

3.5.1 Disuse Drives Plasticity of Functional Networks

Daily 30-minute scans of rs-fMRI before, during, and after casting revealed that disuse not only causes plasticity within the primary motor cortex (Milliken et al., 2013; Newbold et al., 2020), but also increased functional connectivity between disused circuits and executive control regions in the CON. These increases in FC would have been difficult to observe using the focal recording techniques traditionally employed to study plasticity. Thus, understanding the total impact of disuse on brain function will require consideration of plasticity at multiple spatial scales. Future studies using positron emission tomography (PET) to monitor local metabolic changes will further strengthen the bridge between whole-brain plasticity and molecular mechanisms (Shannon et al., 2016).

The high degree of network specificity seen in disuse-driven plasticity is a powerful demonstration of the validity of individual-specific rs-fMRI network parcellations. It could have been the case that casting produced a complex pattern of FC changes involving many brain

systems. Instead, we found that virtually all of the regions showing increased connectivity with the disused motor cortex belonged to a single network, the CON. Large-scale functional networks seem to be a fundamental unit of brain organization, important not only for understanding patterns of activation during cognitive processes, but also for understanding whole-brain patterns of plasticity.

3.5.2 Spontaneous Activity Pulses Alter Functional Connectivity

The network-specific increases in FC between the disused L-SM1_{ue} and the CON likely reflect the emergence of synchronized spontaneous activity pulses in these regions during casting. FC is a measurement of the temporal correlation of spontaneous activity between brain regions. Two complementary analyses (pulse censoring and pulse addition) suggested that pulses contributed to increases in measured FC between disused motor regions and the CON. Many studies have reported increased FC in neuropsychiatric conditions, e.g., Parkinson's disease (Gratton et al., 2019) and Major Depressive Disorder (Greicius et al., 2007). Perhaps some previously reported FC increases could reflect spontaneous activity pulses, similar to those caused by limb disuse. Going forward, spontaneous activity pulses, and the network-specific FC changes they produce, could serve as a biomarker of recent disuse and states of heightened plasticity (Kucyi and Parvizi, 2020).

Decreases in connectivity within the somatomotor system were not fully explained by spontaneous activity pulses. Although the pulse addition analyses showed that spontaneous activity pulses could contribute to decreases in connectivity observed during casting, both the pulse censoring and pulse addition analyses suggested that at least part of the observed decrease

in connectivity occurred independently of pulses. Loss of typical co-activation of L-SM1_{ue} and R-SM1_{ue} during daily behavior (Newbold et al., 2020) likely contributed to casting-driven connectivity decreases, consistent with the widely held hypothesis that FC is maintained by a Hebbian-like mechanism that depends on co-activation of brain regions during behavior (Dosenbach et al., 2008; Lewis et al., 2009; Harmelech and Malach, 2013; Guerra-Carrillo et al., 2014; Shannon et al., 2016).

3.5.3 Disuse Impacts Cingulo-opercular Network (CON) Important for Executive Control

The importance of control systems in the human brain has been recognized for several decades (Posner and Petersen, 1990), but our understanding of these systems has changed dramatically over time and continues to evolve (Petersen and Posner, 2012). Disentangling the roles of two functional networks mediating executive control, the cingulo-opercular and frontoparietal networks, has relied largely on complex task designs such as task-switching (Dosenbach et al., 2006) and slow-reveal paradigms (Neta et al., 2017). Here, we have demonstrated that a new approach, whole-brain precision functional mapping combined with anatomically specific disuse paradigms, can shed new light on the network interactions that support human cognition and behavior. Although the brain contains several suspected cognitive control networks beyond the CON, such as the frontoparietal (FPN), dorsal attention (DAN), ventral attention (VAN) and salience (SAL) networks, disused motor regions only increased FC with the CON. The CON is thought to initiate goal-directed behaviors and maintain executive control settings in relation to task objectives (Dosenbach et al., 2007; Dosenbach et al., 2008). The increased FC between disused L-SM1_{ue} and the CON during casting suggests either 1) circuits within the CON were

also disused during casting, 2) the CON helps to maintain disused motor circuitry, or 3) spontaneous activity pulses can spread along functional connections to neighboring brain regions in network space.

Spontaneous activity pulses may have emerged in the CON because its use was also reduced during casting. We previously suggested that spontaneous activity pulses found in motor regions may have been caused by disuse-driven changes in local inhibitory physiology (Wellman et al., 2002; Newbold et al., 2020). The CON is generally thought to represent task sets, abstract parameters and motor programs governing goal-driven behaviors (Dosenbach et al., 2007; Dosenbach et al., 2008). Task sets can be applied to multiple motor effectors (e.g., right hand, left index finger, etc.), so it would be reasonable to think that casting one extremity would not cause disuse of the CON. However, at least two sets of circuits within the CON may have been disused during casting: circuits that represent bimanual behaviors and circuits that convey task sets to effector-specific downstream regions (e.g., L-SM1_{ue}). During casting, many of the task sets previously used to control the dominant upper extremity (e.g., inserting a key into a lock) could have been used to control the non-dominant extremity. However, task sets requiring bimanual coordination (e.g., fastening a belt) could not be applied to an alternative set of motor effectors and may have become disused. Another set of CON circuits that may have been disused are the circuits that convey task set information to effector-specific brain regions. The CON contains both somatotopically organized regions (e.g., SMA, SII) and non-somatotopic regions (e.g., anterior insula). Recent work shows that the SMA and SII, as well as regions of the basal ganglia, may act as hubs that connect the rest of the CON to the somatomotor network (Gordon

et al., 2018; Greene et al., 2020). Such circuits could potentially undergo disuse during casting of one extremity.

An alternative possibility is that inputs from the CON to L-SM1_{uc} served a homeostatic function during disuse, helping to maintain motor circuits that are typically maintained through active use. We previously suggested that spontaneous activity pulses may help to maintain the organization of disused brain circuits (Newbold et al., 2020). Perhaps pulses are triggered by the CON, which is the system typically responsible for initiating activation of the somatomotor network (Dosenbach et al., 2007).

Spontaneous activity pulses may also have originated in the disused somatomotor circuits and spread along functional connections to brain regions that were not affected by casting. The CON is immediately adjacent to the somatomotor network in network space (Fig. 3a). Previous work in mice found that spontaneous activity bursts in somatosensory cortex, caused by local pharmacogenetic suppression of inhibitory interneurons, spread to other functionally connected regions not targeted by the experimental manipulation (Rosenthal et al., 2020). An interesting question for future research is whether the CON would show spontaneous activity pulses following disuse of brain systems other than the somatomotor network, such as networks supporting visual and auditory processing, spatial navigation, or social cognition.

3.5.4 Two Complementary Mechanisms for Functional Network Plasticity

Extensive whole-brain imaging before, during and after casting revealed that disuse-driven spontaneous activity pulses occur not only in primary motor and somatosensory areas, but also in higher-order brain regions responsible for executive control over behavior (i.e., the CON). The emergence of spontaneous activity pulses during casting produced increases in FC that were highly focal in network space, specifically occurring between disused motor regions and the CON. Decreases in connectivity between disused motor circuits and the remainder of the somatomotor system, however, were not explained by spontaneous activity pulses. Thus, disuse may drive network plasticity through two complementary mechanisms. Decreased coactivation of brain regions during disuse might drive Hebbian-like disconnection between disused and still-active somatomotor circuits. Spontaneous activity pulses, which contributed to increased connectivity with the CON, may help preserve disused circuits for future reintegration and use. Together, these two network plasticity mechanisms—Hebbian-like and pulse-mediated—may represent a network-focal “stand-by mode” that allows the brain to isolate disused circuits while simultaneously protecting them from premature functional degradation.

3.6 METHODS

3.6.1 Human Participants

Participants were three healthy, adult volunteers. Details are described in Newbold *et al.* (Newbold et al., 2020).

3.6.2 Experimental Intervention

We constrained the dominant upper extremity for two weeks by fitting each participant with a fiberglass cast. Casts extended from just below the shoulder to past the fingertips. Details are described in Newbold *et al.* (Newbold et al., 2020).

3.6.3 MRI Acquisition

Participants were scanned every day of the experiment for 42-64 consecutive days. We collected 30 minutes of resting-state functional MRI (rs-fMRI) data every day of the experiment, as well as also task fMRI and T1- and T2-weighted structural scans. Acquisition parameters and procedures are detailed in Newbold *et al.* (Newbold et al., 2020).

3.6.4 MR Image Processing

Preprocessing of structural and functional images, denoising of resting-state fMRI data, and cortical surface projection were performed previously (Newbold et al., 2020). Fully processed

data are available in the Derivatives folder of the Cast-Induced Plasticity dataset on OpenNeuro (www.openneuro.org/datasets/ds002766).

3.6.5 ROI Selection

The region of the left primary somatomotor cortex controlling the casted upper extremity (L-SM1_{ue}) was located individually in each participant using task fMRI. Details of the task analysis and region of interest (ROI) selection are described in Newbold *et al.* (Newbold et al., 2020).

The L-SM1_{ue} ROI was used here to generate seed maps (Fig. 2, Supplementary Fig. 1), to analyze spatial specificity of whole-brain functional connectivity changes (Fig. 4b, Supplementary Fig. 3) and to measure FC between L-SM1_{ue} and the dorsal anterior cingulate cortex (dACC) for the removable cast control experiment (Fig. 5), the pulse censoring analysis (Fig. 7) and the pulse addition analysis (Fig. 8, Supplementary Fig. 5).

Individual-specific sets of parcels spanning the entire cerebral cortex were previously generated for each participant using a functional connectivity gradient-based approach, and each parcel was assigned to one of 17 canonical functional networks using a graph theory-based community detection algorithm (Gordon et al., 2017; Newbold et al., 2020). Cortical parcels were used here to display functional connectivity changes in anatomical (Fig. 2, 3, 6-8, Supplementary Fig. 1, 2, 4, 6) and network space (Fig. 3, Supplementary Fig. 2). We also generated a set of subcortical and cerebellar parcels by assigning each voxel to the functional network with which it showed the strongest functional connectivity and then grouping adjacent voxels with matching network assignments into parcels. Sets of cortical, subcortical and cerebellar parcels were used to examine changes in FC between all pairs of brain regions (Fig. 4, Supplementary Fig. 3).

A subset of parcels corresponding to the left primary somatomotor cortex (L-SM1_{uc}) was previously generated by selecting all left-hemisphere parcels assigned to the upper-extremity somatomotor network, excluding any parcels that fell outside of the pre- and post-central gyri (Newbold et al., 2020). Functional connections between L-SM1_{uc} parcels and all other parcels were averaged to generate parcel-wise seed maps (Fig. 2, 3, 6-8, Supplementary Fig. 1, 2, 4, 6) and to quantify the spatial specificity of FC changes between all cortical, subcortical and cerebellar parcels (Fig. 4, Supplementary Fig. 3).

Individual-specific ROIs in the left dorsal anterior cingulate cortex (L-dACC) were selected using pulse analysis of variance (ANOVA) maps, which were previously generated for each participant (Newbold et al., 2020). ROIs were selected within a large anatomical region, automatically labeled by FreeSurfer (union of caudal anterior cingulate gyrus, posterior cingulate gyrus, and superior frontal gyrus). We first located the vertex showing the maximum ANOVA F-statistic and then iteratively expanded the ROI by selecting neighboring vertices in descending order of F-statistic, until the ROI included 100 vertices. The L-dACC ROI was used to measure FC between L-SM1_{uc} and the L-dACC for pulse censoring (Fig. 7) and pulse addition analyses (Fig. 8, Supplementary Fig. 6).

3.6.5 Functional Connectivity Measurement

Mean rs-fMRI time series were extracted from the L-SM1_{uc} ROI and each cortical, subcortical and cerebellar parcel by averaging the time series of all vertices/voxels within the ROI/parcel. Vertex-wise functional connectivity (FC) seed maps were generated for each session by computing a Pearson correlation between the mean rs-fMRI time series from the L-SM1_{uc} ROI

and the time series from every vertex. Frames with high head motion, identified previously (Newbold et al., 2020), were excluded from FC calculations. Vertex-wise seed maps were averaged across sessions before, during and after casting (Pre, Cast, Post; Fig. 2, Supplementary Fig. 1).

FC between all pairs of cortical, subcortical and cerebellar parcels was measured as pairwise correlations of all mean rs-fMRI time series, excluding high-motion frames, producing a correlation matrix for each session. Correlation matrices were averaged over Pre, Cast and Post period. FC changes during casting and recovery were computed as the differences between correlation matrices (casting = Cast – Pre; recovery = Post – Cast). Full Cast – Pre differences matrices are shown in Supplementary Figure 3. Parcel-wise difference seed maps showing changes in L-SM1_{uc} FC during casting and recovery (Fig. 2-3, Supplementary Fig. 1-2) were computed by averaging together columns of the difference matrices corresponding to the L-SM1_{uc} parcels (see *ROI selection*, above).

3.6.6 Spring Embedding

Cortical parcels were displayed in network space using force-directed (“spring-embedded”) graphs (Jacomy et al., 2014), generated with Gephi (<https://gephi.org/>). Graph weights were taken from parcel-wise correlation matrices averaged across all sessions prior to casting (Pre). Graphs were thresholded to include only the top 0.2% of pairwise functional connections. We initially examined graphs using an edge threshold of 0.1%, but several parcels with large FC changes were disconnected from the main graph. Thus, we selected the 0.2% connection threshold to display all key findings (Fig. 3, Supplementary Fig. 2).

3.6.7 Functional Connectivity Changes by Network

To test which functional networks showed large changes in FC with L-SM1_{ue} during casting, parcel-wise L-SM1_{ue} seed maps were compared to individual-specific network maps. Parcel-wise L-SM1_{ue} difference seed maps (Cast – Pre) were thresholded to contain the top 5% of parcels showing FC increases/decreases. FC increases (Cast > Pre) and decreases (Cast < Pre) were examined separately. The number of supra-threshold parcels in each cortical network is shown in Figure 3. Alternative thresholds (top 1%, 10% and 20%) all yielded similar results. Networks containing a greater number of FC increases/decreases than expected by chance were identified by comparing the number of supra-threshold parcels found using each participant's true network map to the number of parcels found using spatially permuted network maps (see *Statistical analyses*, below).

3.6.8 Whole-brain Analyses of Functional Connectivity Changes

The spatial specificity of whole-brain plasticity was examined by comparing changes in FC between all cortical, subcortical and cerebellar parcels to individual-specific functional network maps. We examined the top 50 changes in FC (25 greatest increases and 25 greatest decreases). A change in FC between two parcels was counted as involving L-SM1_{ue} if either of the two parcels was an L-SM1_{ue} parcel. The number L-SM1_{ue} changes found using each participant's true network map was compared to the number of L-SM1_{ue} changes found using spatially permuted network maps (see *Statistical analyses*, below).

To examine whole-brain FC changes at a finer spatial resolution, we examined differences in FC between all cortical, subcortical and cerebellar vertices/voxels. We computed the magnitude of whole-brain FC change between each vertex/voxel as the sum of squared FC changes between that vertex/voxel and every other gray-matter vertex/voxel (Fig. 4, Supplementary Fig. 3). We tested if whole-brain FC change was higher in L-SM1_{ue} than in the rest of the brain by comparing the mean magnitude of whole-brain FC change inside of each participant's true L-SM1_{ue} ROI to the mean magnitude of whole-brain FC change inside of spatially rotated ROIs (see *Statistical analyses*, below).

3.6.9 Spatial and Temporal Comparisons of Pulses and FC Changes

To generate a parcel-wise map of spontaneous activity pulses, we extracted rs-fMRI time series from every cortical, subcortical and cerebellar parcel surrounding each detected pulse (13.2 seconds before to 17.6 seconds after each pulse peak). Pulse peaks were detected previously (Newbold et al., 2020). We then performed an ANOVA on the extracted time series (Fig. 6b). The spatial distribution of ANOVA F-statistics was compared to the spatial distribution of L-SM1_{ue} FC changes using a Pearson correlation across parcels.

We also compared the number of pulses detected during each rs-fMRI scan (Newbold et al., 2020) to the FC measured between L-SM1_{ue} and L-dACC (Fig. 5c), using a Pearson correlation.

3.6.10 Pulse Censoring Analyses

To assess the contribution of large, detectable spontaneous activity pulses (>0.4% rs-fMRI signal

change) to FC changes observed during casting, frames surrounding each pulse (13.2 seconds before to 17.6 seconds after each pulse peak) were excluded from FC calculations. Pulse detection criteria were identical to those used previously (Newbold et al., 2020). We plotted FC measured between L-SM1_{uc} and L-dACC during each session before casting (Pre), during casting (Cast) and during casting with pulses excluded (Cens; Fig. 7b). We compared Cast vs. Pre FC measurements and Cens vs. Cast FC measurements using t-tests (see *Statistical analyses*, below). We also generated difference seed maps showing FC changes between L-SM1_{uc} and all cortical parcels due to censoring (Cens – Cast; Fig. 7c, Supplementary Fig. 4).

3.6.11 Pulse Addition Analyses

To assess the contribution to FC changes of pulses with a hypothetical full magnitude distribution, including pulses that were too small (<0.4% rs-fMRI signal change) to distinguish from ongoing spontaneous activity fluctuations, we created simulated rs-fMRI time series containing a full distribution of pulses. We first generated a histogram showing the magnitude distribution of detected pulses. Magnitudes were grouped into bins with a width of 0.5%-signal-change. We then fit a log-normal distribution to the observed pulse magnitudes using a least-squares approach (Fig. 8a). This provided an estimate of the full pulse magnitude distribution, including pulses that were too small to detect. We then added the mean pulse time series to the baseline (Pre) rs-fMRI time series, drawing pulse magnitudes from the full log-normal distribution (example shown in Fig. 8b). The number of pulses added was selected so that the number of large pulses (>0.4% signal change) would match the number of pulses detected in each participant in an average Cast scan. We then computed FC of the baseline time series (Pre)

and the time series with added pulses (Sim; Fig. 8c). Finally, we applied the same pulse censoring strategy described above to the simulated time series and computed FC after censoring (Cens; Fig. 8c). Because pulse magnitudes were drawn from a full log-normal distribution, only a portion of the added pulses were detected and censored. We compared Sim vs. Pre FC measurements and Cens vs. Sim FC measurements using t-tests (see *Statistical analyses*, below). The simulation and censoring procedures were repeated using triangular and exponential magnitude distributions (Supplementary Fig. 5). We also generated difference seed maps showing FC changes between L-SM1_{ue} and all cortical parcels due to pulse simulation (Sim – Pre; Fig. 8d, Supplementary Fig. 6).

3.6.12 Statistical Analyses

All statistical tests were performed identically for each participant. Whenever appropriate, we used simple parametric statistical tests:

- Spatial similarity between anatomical maps was tested using a Pearson correlation across parcels (Nico: d.f. = 566; Ashley: 578; Omar: 624). Spatial correlations were computed between the following maps:
 - FC changes during casting (Cast – Pre) vs. FC changes during recovery (Post – Cast; Fig. 2b)
 - FC changes during casting (Cast – Pre) vs. pulse ANOVA (F-statistic; Fig. 6)
 - FC changes during casting (Cast – Pre) vs. FC changes due to pulse censoring (Cens – Cast; Fig. 7C, Supplementary Fig. 4)

- FC changes due to pulse censoring (Cens – Cast) vs. residual FC changes after pulse censoring (Cens – Pre; Supplementary Fig. 4)
- FC changes during casting (Cast – Pre) vs. FC changes due to simulated pulses (Sim – Pre; Fig. 8d, Supplementary Fig. 6)
- The number of pulses detected during each scan was compared to the FC measured between L-SM1_{ue} and L-dACC using a Pearson correlation (Nico: d.f. = 45; Ashley: 61; Omar: 40; Fig. 6c).
- FC between L-SM1_{ue} and L-dACC measured during each session of the cast period (Nico: n = 13 sessions; Ashley: 13; Omar: 14) was compared to FC during each session of the pre period (Nico: n = 10; Ashley: 12; Omar: 14) using a two-sided, unpaired t-test (Nico: d.f. = 21, Ashley: 23, Omar: 26; Fig. 7b).
- FC between L-SM1_{ue} and L-dACC measured using the full time series (motion-censored only) of each session of the cast period (Nico: n = 13 sessions; Ashley: 13; Omar: 14) was compared to FC measurements of the same sessions excluding pulses (motion- and pulse-censored) using a one-sided, paired t-test (Nico: d.f. = 24, Ashley: 24, Omar: 26; Fig. 7b).
- FC between L-SM1_{ue} and L-dACC measured during each session of the pre period (Pre; Nico: n = 10; Ashley: 12; Omar: 14) was compared to FC measurements of the same sessions after adding simulated pulses (Sim) using a two-sided, paired t-test (Nico: d.f. = 18, Ashley: 22, Omar: 26; Fig. 8c).
- FC between L-SM1_{ue} and L-dACC measured using the full time simulated series (Sim; motion-censored only; Nico: n = 10; Ashley: 12; Omar: 14) was compared to FC

measurements of the same sessions excluding pulses (motion- and pulse-censored) using a two-sided, paired t-test (Nico: d.f. = 18, Ashley: 22, Omar: 26; Fig. 8c).

When parametric statistical tests were not appropriate to test a specific hypothesis, we tested results against a null distribution generated via permutation resampling. In each case, our null hypothesis was that observed effects had no spatial relationship to ROIs/functional networks and any overlap occurred by chance. For vertex-wise ROIs, we modeled the null hypothesis by rotating the ROI around the cortical surface 1,000 times (Gordon et al., 2016; Gordon et al., 2020). For functional networks, we modeled the null hypothesis by permuting the network assignments of parcels 1,000 times. Each permuted ROI/network map was used exactly as the actual map in order to compute a null distribution for the value of interest. The P-value reported for each test represents the two-sided probability that a value in the null distribution has a greater magnitude than the observed value. Permutation resampling was used to generate null distributions for the following values:

- Overlap of each functional network with increases in L-SM1_{ue} FC during casting (Cast > Pre; number of parcels in top 5%; Fig. 3b)
- Overlap of each functional network with decreases in L-SM1_{ue} FC during casting (Cast > Pre; number of parcels in top 5%; Fig. 3c)
- Overlap of L-SM1_{ue} parcels with the 50 largest changes in FC between all pairs of cortical, subcortical and cerebellar parcels (Fig. 4a, Supplementary Fig. 3)
- Magnitude of whole-brain FC change in the L-SM1_{ue} ROI (Fig. 4b, Supplementary Fig. 3)

Since we tested the overlap of L-SM1_{ue} FC increases/decreases with 17 different functional networks, a Benjamini-Hochberg procedure was applied to correct for multiple comparisons, maintaining false discovery rates < 0.05 . Each of the three participants constituted a separate replication of the experiment, rather than multiple comparisons, so no correction was necessary for tests repeated in each participant.

3.6.13 Data Visualization

Regions of interest and whole-brain pulse maps were shown on cortical surfaces generated by FreeSurfer (Fischl, 2012) and Human Connectome Project (HCP) Workbench software packages (Marcus et al., 2011). These images were rendered using HCP Workbench (Marcus et al., 2011). Figures showing the greatest differences in functional connectivity across the entire brain in inflated anatomical space (Fig. 4, Supplementary Fig. 3) were rendered using Blender, a free and open-source 3D modeling software package (www.blender.org). To make the large number of changed connections included in these images visually compact, connections following similar spatial trajectories were drawn toward each other using a previously published mean-shift edge bundling algorithm (Bottger et al., 2014). All other figures were produced using Matlab (www.mathworks.com).

3.6.14 Data Availability

This study used our previously published dataset (Newbold et al., 2020), available on the OpenNeuro database (www.openneuro.org/datasets/ds002766).

3.6.15 Code Availability

All code needed to reproduce our analyses is available on Gitlab

(<https://gitlab.com/DosenbachGreene/cast-whole-brain>).

3.7 Supplementary Figures

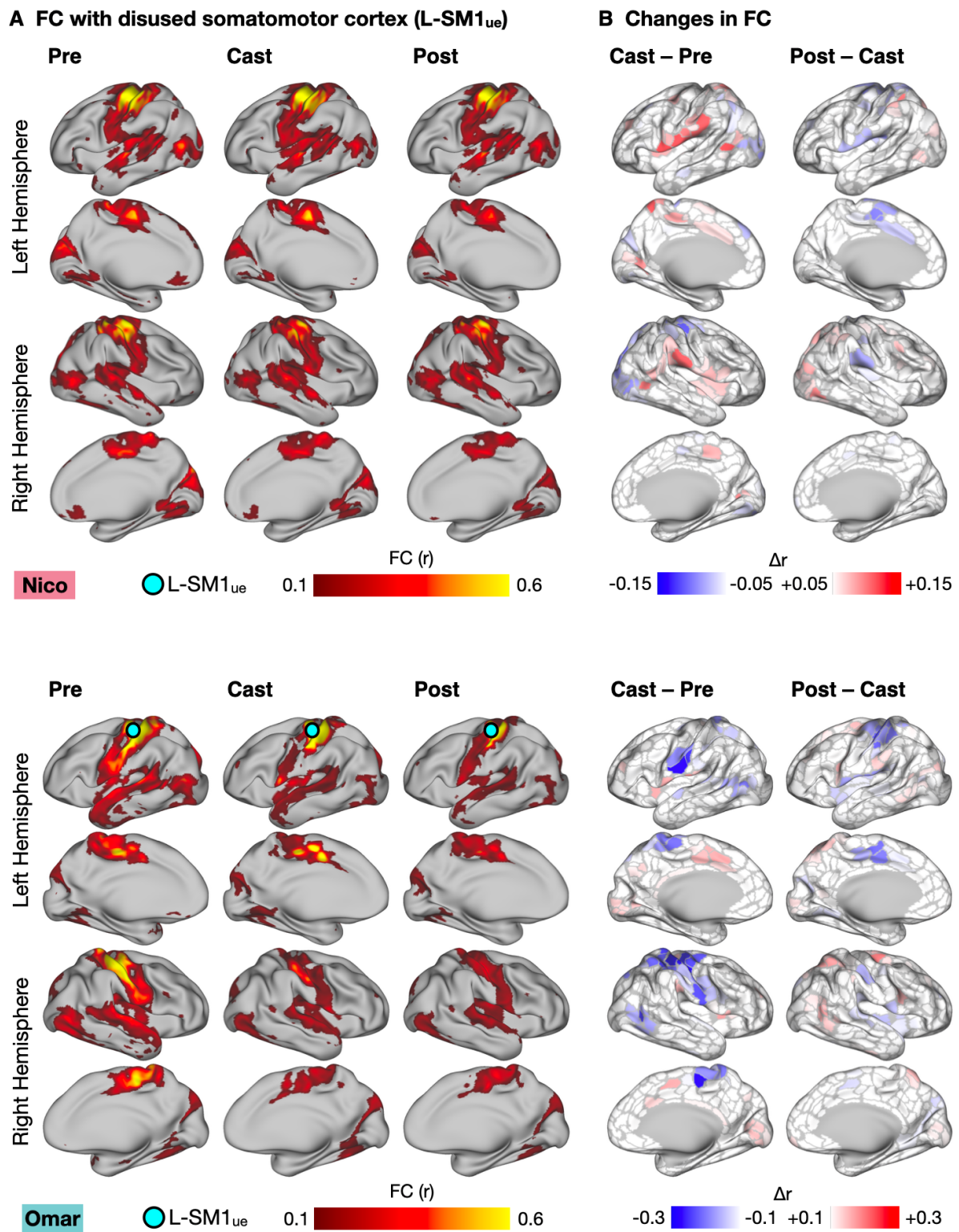


Figure 3-S1: See next page for caption.

Figure 3-S1: Functional Connectivity (FC) Changes Involving the Disused Somatomotor Cortex (L-SM1_{ue}) in Anatomical Space (All Participants), related to Figure 2. **(A)** Seed maps showing FC between L-SM1_{ue} and the remainder of the cerebral cortex in Nico (top) and Omar (bottom). Seed maps were averaged across sessions before, during and after casting (Pre, Cast, Post). **(B)** Subtraction maps showing changes in FC during casting (Cast – Pre) and recovery (Post – Cast). Differences are shown on sets of 506 (Nico) and 626 (Omar) individual-specific cortical parcels. For Nico and Ashley, these parcels were previously generated and published (Gordon, 2017). We applied identical methods to generate a set of parcels for Omar.

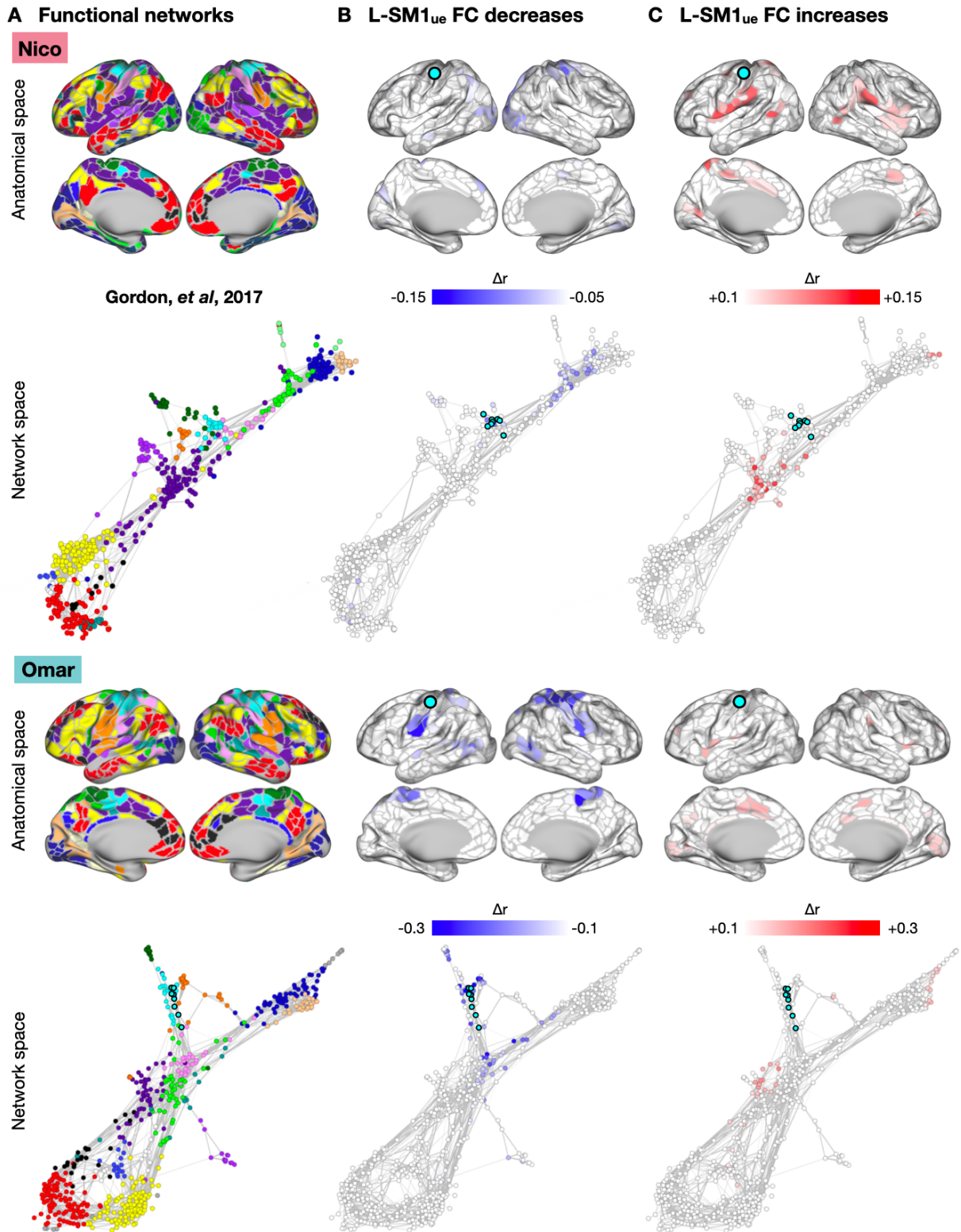
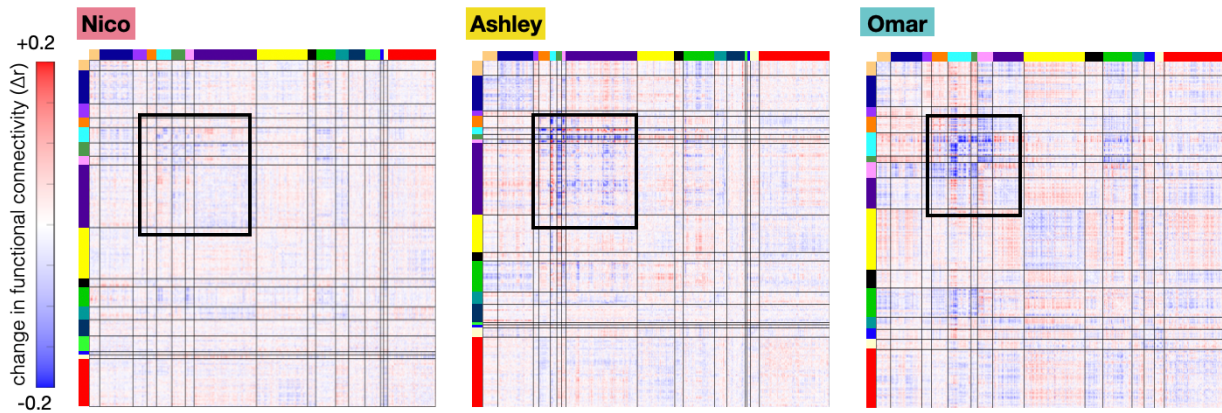


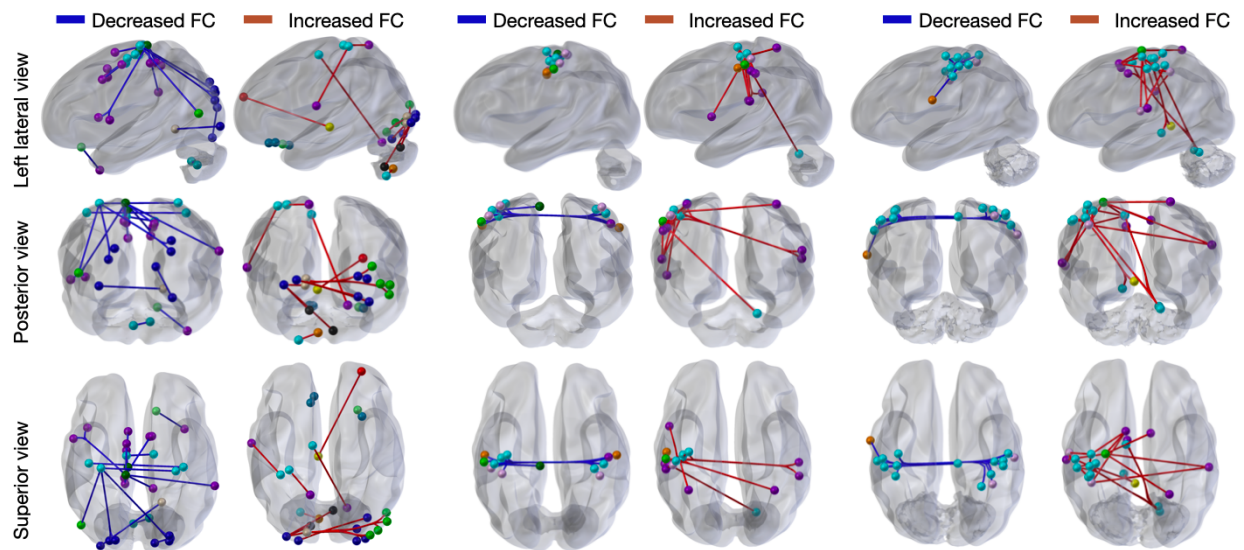
Figure 3-S2: See next page for caption.

Figure 3-S2: Functional Connectivity (FC) Changes Involving the Disused Somatomotor Cortex (L-SM1_{ue}) in Anatomical and Network Space in Nico and Omar, related to Figure 3. **(A)** Maps of 17 canonical functional networks in Nico (top) and Omar (bottom). Networks are shown in anatomical space (inflated cortical surfaces) and network space (spring-embedded graphs based on Pre scans). See Figure 3 for network color key. **(B)** Subtraction maps showing disuse-driven decreases in functional connectivity (FC) with left somatomotor cortex (L-SM1_{ue}) in anatomical space and network space. **(C)** Subtraction maps showing disuse-driven increases in FC with L-SM1_{ue} in anatomical and network space.

A Difference correlation matrices (Cast – Pre)



B Greatest FC changes (top 25 increases + top 25 decreases) in anatomical space



C Regions showing greatest FC changes

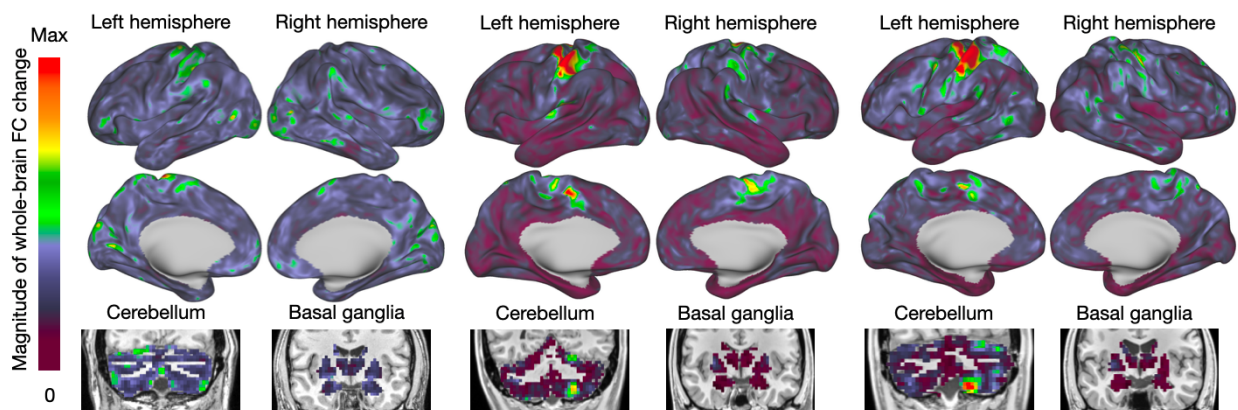
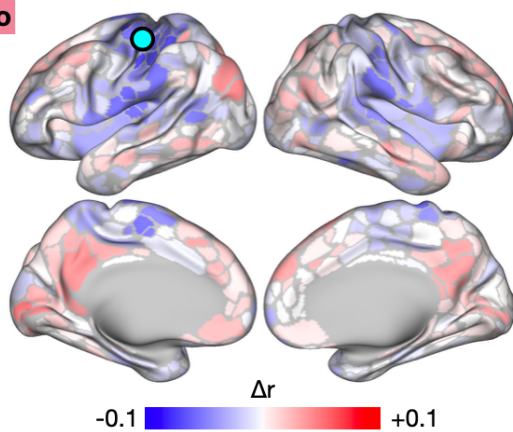


Figure 3-S3: See next page for caption.

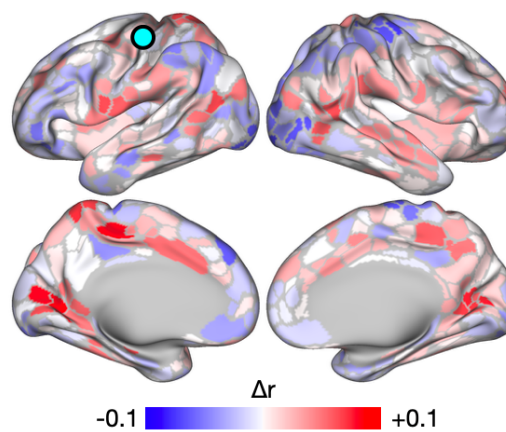
Figure 3-S3: Whole-brain Patterns of Disuse-driven Plasticity, related to Figure 4. **(A)** Matrices showing changes in functional connectivity (FC) between all pairs of individual specific cortical, subcortical and cerebellar parcels during casting (Nico: 744 parcels, Ashley: 733; Omar: 761). **(B)** 50 largest changes in FC shown in anatomical space. **(C)** Magnitude of whole-brain FC change, computed as the sum of squared FC changes between each vertex/voxel and every other gray-matter vertex/voxel

A Effect of pulse censoring (Cens - Cast)

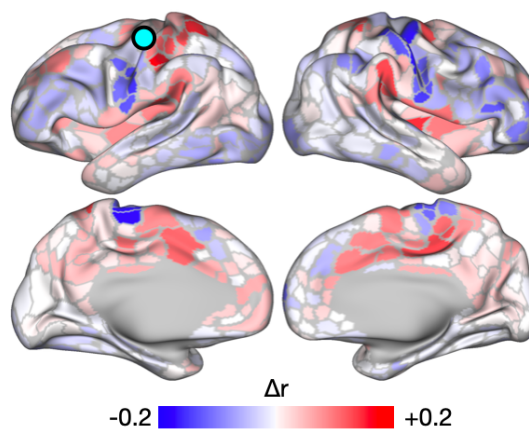
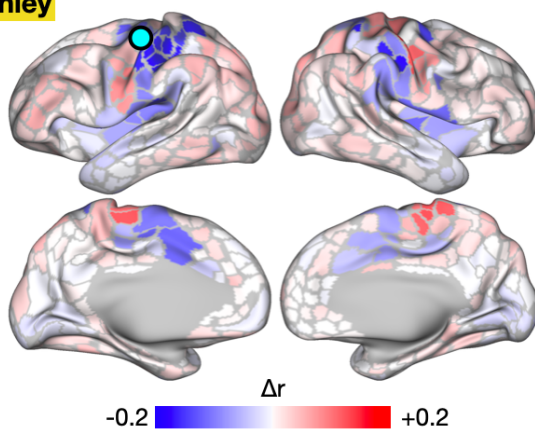
Nico



B Residual effect (Cens - Pre)



Ashley



Omar

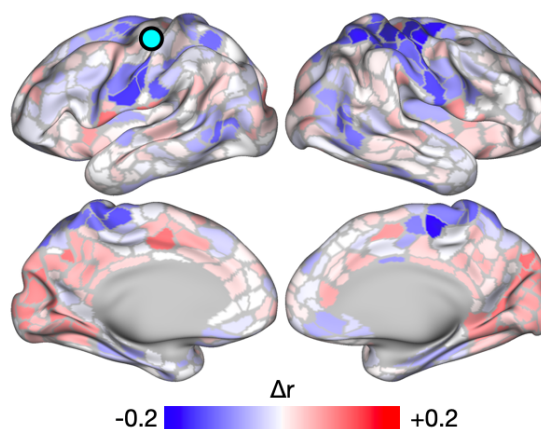
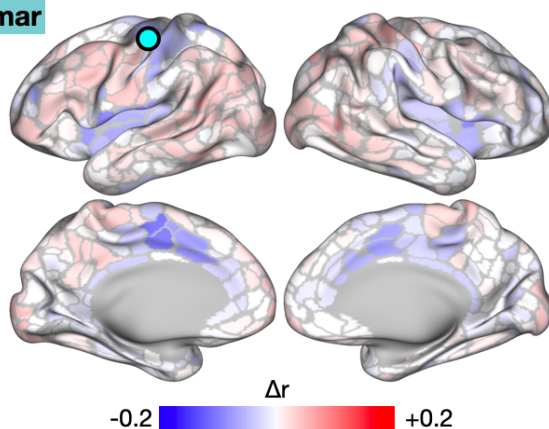
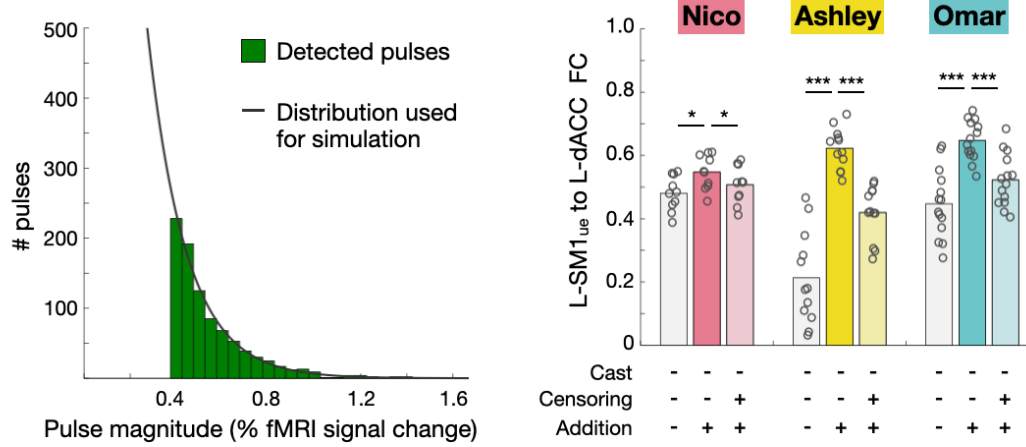


Figure 3-S4: See next page for caption.

Figure 3-S4: Functional Connectivity (FC) Changes Explained by Spontaneous Activity Pulses, related to Figure 7. **(A)** Subtraction map showing changes in L-SM1_{uc} FC due to pulse censoring. The spatial pattern of FC changes due to pulse censoring was negatively correlated with FC changes during casting (Nico: $r = -0.35$, $P < 0.001$; Ashley: $r = -0.90$, $P < 0.001$; Omar: $r = -0.33$, $P < 0.001$). **(B)** Subtraction map showing residual FC changes during casting after pulse censoring. The spatial pattern of residual FC changes was negatively correlated with the effect of pulse censoring (Nico: spatial correlation, $r = -0.23$, $P < 0.001$; Ashley: $r = -0.76$, $P < 0.001$; Omar: $r = -0.18$; $P < 0.001$).

A Exponential distribution



B Triangular distribution

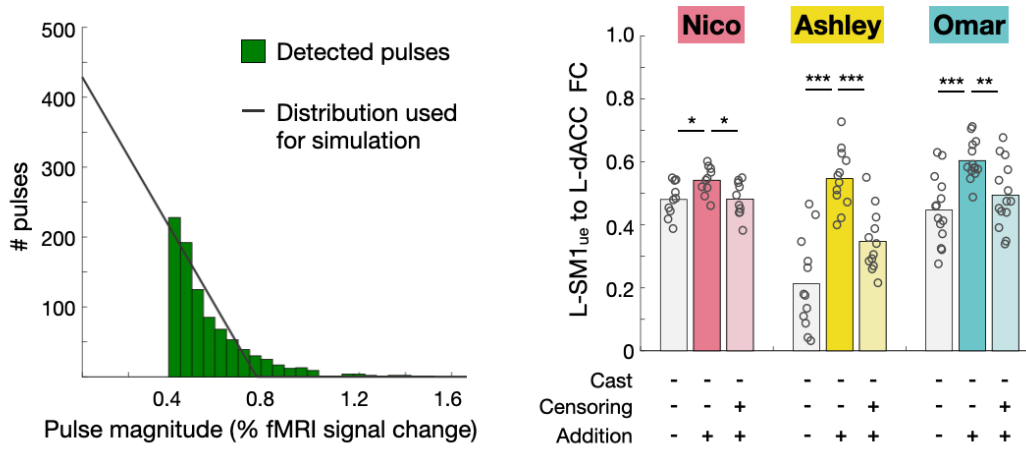
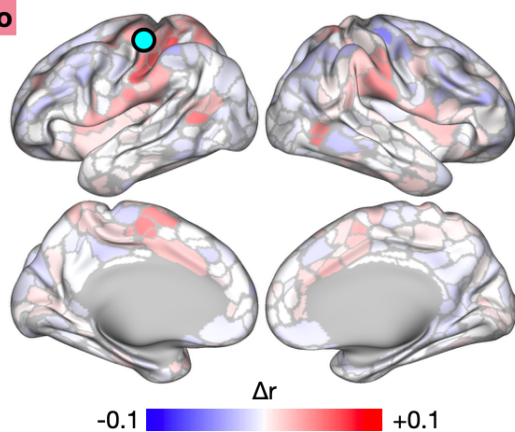


Figure 3-S5: Alternative Distributions for Pulse Magnitudes, related to Figure 8. **(A)** Exponential distribution. *Left*: Histogram of pulse magnitudes (peak fMRI signal), pooled across all participants. An exponential distribution (black line) was fit to the data using a least-squares approach. *Right*: Adding simulated pulses, with magnitudes drawn from the exponential distribution, increased FC between L-SM1_{ue} and L-dACC. Censoring simulated pulses partially reduced FC increases. * $P < 0.05$, *** $P < 0.001$. **(B)** Triangular distribution. *Left*: Histogram of pulse magnitudes (peak fMRI signal), pooled across all participants. A linear distribution (black line) was fit to the data using a least-squares approach. *Right*: Adding simulated pulses, with magnitudes drawn from the linear distribution, increased FC between L-SM1_{ue} and L-dACC. Censoring simulated pulses partially reduced FC increases. * $P < 0.05$, ** $P < 0.01$, *** $P < 0.001$.

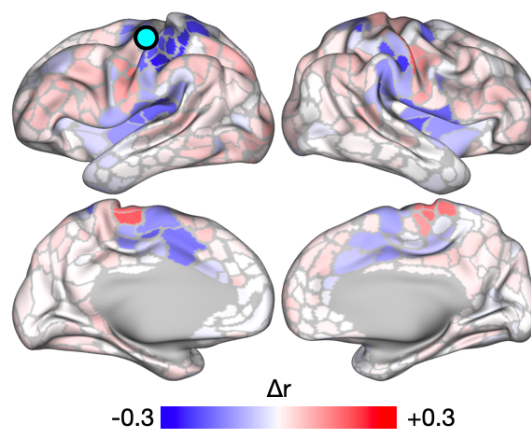
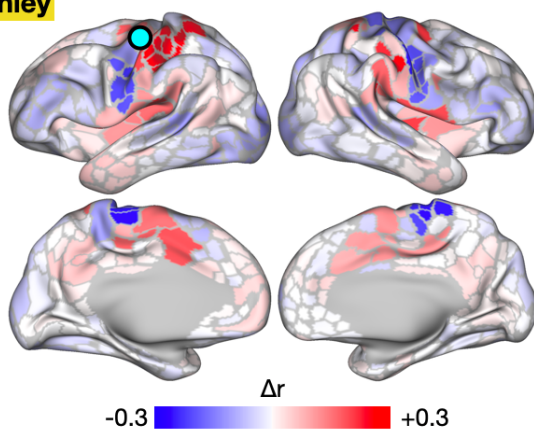
A Effect of simulation (Sim - Pre)

Nico



B Effect of censoring (Cens - Sim)

Ashley



Omar

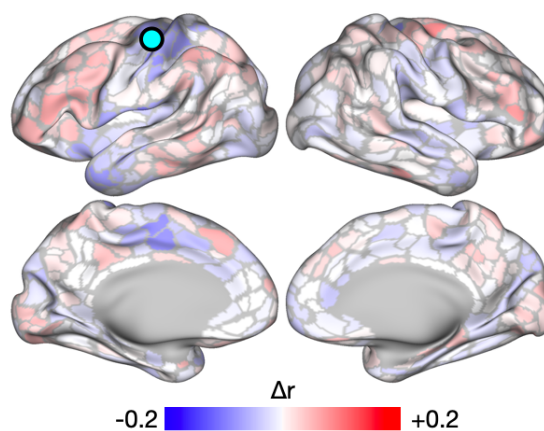
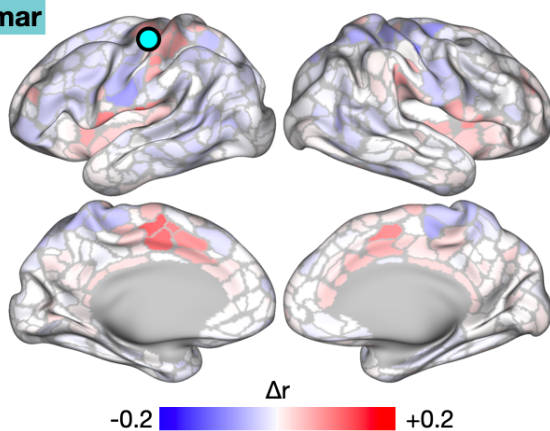
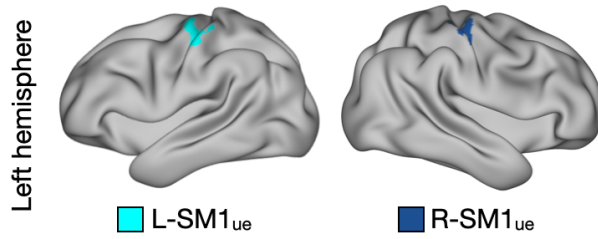


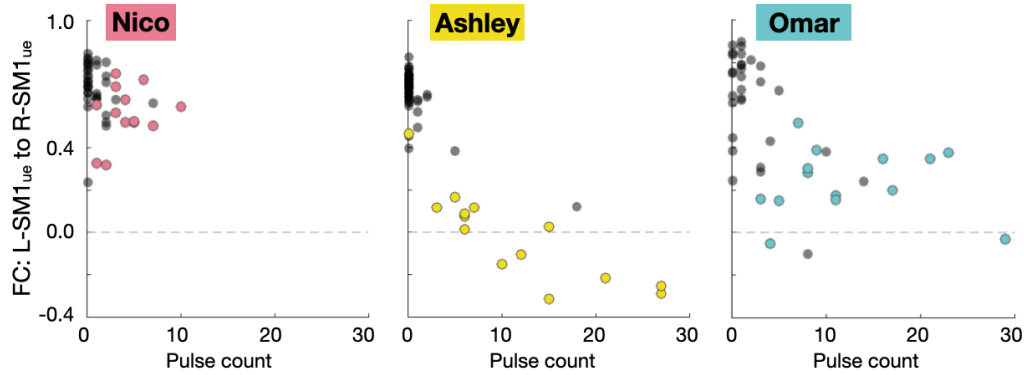
Figure 3-S6: See next page for caption.

Figure 3-S6: Functional Connectivity (FC) Changes Caused by Simulated Spontaneous Activity Pulses (All Participants), related to Figure 8. **(A)** Subtraction map showing changes in L-SM1_{ue} FC due to addition of simulated pulses. FC changes due to pulse addition closely matched FC changes during casting (Nico: spatial correlation, $r = 0.44$, $P < 0.001$; Ashley: $r = 0.95$, $P < 0.001$; Omar: $r = 0.64$, $P < 0.001$). **(B)** Subtraction map showing effect of censoring simulated pulses. Effects of censoring closely complemented the effect of pulse addition (Nico: $r = -0.71$, $P < 0.001$; Ashley: $r = -0.96$, $P < 0.001$; Omar: $r = -0.69$; $P < 0.001$).

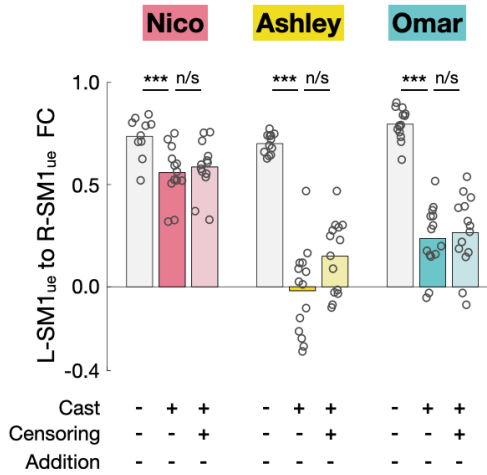
A Left and right motor regions of interest



B Functional connectivity vs. number of pulses detected during each scan



C Effect of pulse censoring



D Effect of pulse addition

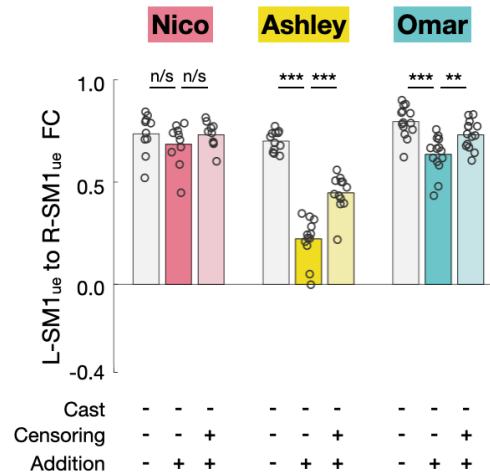


Figure 3-S7: Functional Connectivity (FC) Decreases Were Not Explained by Spontaneous Activity Pulses, related to Figure 8. (A) Example regions of interest (ROIs) in the left and right primary somatomotor cortex (L-SM1_{ue} and R-SM1_{ue}). (B) Relationship of FC between L-SM1_{ue} and R-SM1_{ue} vs. the number of pulses detected. Each dot represents one 30-minute scan. Colored dots represent scans during the cast period. For all participants, FC between L-SM1_{ue} and R-SM1_{ue} was significantly correlated with the number of pulses detected (Nico: $r=0.74$, $P<0.001$; Ashley: $r=0.57$, $P<0.001$; Omar: $r=0.73$, $P<0.001$).

3.7 Acknowledgements

We thank Kristen M. Scheidter and Annie L. Nguyen for help in collecting MRI data and Ryan V. Raut for his comments on the manuscript. This work was supported by NIH grants NS110332 (D.J.N.), NS088590 (N.U.F.D.), TR000448 (N.U.F.D.), MH96773 (N.U.F.D.), MH122066 (N.U.F.D.), MH1000872 (T.O.L.), MH112473 (T.O.L.), NS090978 (B.P.K.), MH104592 (D.J.G.), NS080675 (M.E.R.), NS098577 (to the Neuroimaging Informatics and Analysis Center); the US Department of Veterans Affairs Clinical Sciences Research and Development Service grant 1IK2CX001680 (E.M.G.); Kiwanis Neuroscience Research Foundation (N.U.F.D.); the Jacobs Foundation grant 2016121703 (N.U.F.D.); the Child Neurology Foundation (N.U.F.D.); the McDonnell Center for Systems Neuroscience (D.J.N., T.O.L., A.Z., B.L.S., and N.U.F.D.); the McDonnell Foundation (S.E.P.), the Mallinckrodt Institute of Radiology grant 14-011 (N.U.F.D.); the Hope Center for Neurological Disorders (N.U.F.D., B.L.S., and S.E.P.).

Chapter 4: Conclusions

4.1 Summary of Results

4.1.1 Casting Degraded Strength and Fine Motor Skill

Casting had profound effects on behavior and motor function. Constant behavioral monitoring using accelerometers on both wrists showed large reductions in use of the casted extremity (–50%) and slight increases in use of the un-casted extremity (+20%). Motor assessments completed immediately after cast removal showed large reductions in grip strength (–40 lb) and fine motor skill (–20% performance on Purdue Pegboard) of the casted extremity. We did not observe consistent changes in strength or fine motor skill of the un-casted extremity.

4.1.2 Spontaneous Activity Pulses Propagated through Disused Brain Circuits

Daily resting-state functional MRI (rs-fMRI) acquired before, during and after casting revealed multiple changes in spontaneous activity of disused brain circuits. The most striking observation was of large, spontaneous pulses of activity that occurred in the disused motor circuits during casting. In all participants, virtually no pulse-like events were seen prior to casting, many pulses were observed during the cast period, and a small number of pulses occurred after cast removal. Pulses had a time course resembling a canonical hemodynamic response function, consistent with a brief burst of neural activity. Although pulses showed a wide distribution of magnitudes, many pulses were much larger (>1.5% BOLD signal change) than typical ongoing spontaneous

activity fluctuations ($<0.5\%$ BOLD signal change). This was reflected in a strong increase in amplitude of low-frequency fluctuations (ALFF) of the disused motor cortex during casting.

An analysis of variance (ANOVA) of whole-brain time courses surrounding each detected pulse revealed that, in addition to the disused motor cortex, pulses also occurred in the dorsal anterior cingulate cortex/supplementary motor area (dACC/SMA), frontal operculum, secondary somatosensory cortex (SII), pre- and post-central sulci, angular gyri, putamen, thalamus and cerebellum. Collectively, these regions comprise the somatomotor circuit that normally controls the casted extremity, as well as the cingulo-opercular network (CON). Pulses did not occur simultaneously in all regions. A consistent pattern of propagation was observed, with pulses occurring earliest in the dACC/SMA, then propagating to the motor cortex, then cerebellum, with mean time delays of 200ms and 600ms, respectively. Time delays in other regions were not consistent across participants, which may have been due to lower pulse amplitude or weaker fMRI signal in those structures, especially the putamen and thalamus.

4.1.3 Disuse Caused Rapid, Anatomically Specific Changes in Functional Connectivity

In addition to spontaneous activity pulses, participants also showed highly consistent, rapid, and anatomically specific changes in functional connectivity (FC). The most prominent change was a loss of typical functional connectivity between the disused motor cortex (L-SM1_{ue}) and the homotopic region of the opposite hemisphere (R-SM1_{ue}). All participants showed large effect sizes (Nico: $\Delta r = -0.23$, Ashley: $\Delta r = -0.86$, Omar: $\Delta r = -0.61$). Loss of FC between L-SM1_{ue} and R-SM1_{ue} occurred rapidly during casting, with significant decreases detectable in all participants

within 48 hours of casting. Recovery was also rapid in two participants, but one participant (Omar) continued to show reduced FC for two weeks after cast removal. L-SM1_{ue} disconnected not only from R-SM1_{ue}, but also from the remainder of the somatomotor network. Disconnection was highly specific to L-SM1_{ue} and did not occur in the neighboring lower extremity or face regions of the somatomotor cortex.

Whole-brain analysis of FC changes revealed that L-SM1_{ue} also showed increases in FC with several cortical and subcortical regions. Subcortically, L-SM1_{ue} FC increases were specific to regions of the putamen, thalamus and cerebellum that normally control the casted extremity. In the cortex, L-SM1_{ue} showed increased FC with the dACC/SMA, anterior insula, SII, bilateral pre- and post-central sulci and angular gyri. All of these regions belonged to the CON. FC increases were highly specific to the CON and did not involve any other functional networks.

4.1.4 Functional Connectivity Increases Resulted from Spontaneous Activity Pulses

Increased FC between L-SM1_{ue} and the CON appeared to result from the spontaneous activity pulses that occurred synchronously in both structures. Three results supported this conclusion: spatial and session-wise correlations between pulses and FC increases, partial reduction in cast-driven FC changes after censoring pulses, and recreation of cast-driven FC changes by simulated pulses.

We initially suspected that FC increases may have resulted from spontaneous activity pulses because of spatial and session-wise correlations between the two phenomena. Brain regions

showing pulses were generally the same regions that showed increases in FC with L-SM1_{ue} during the cast period. Additionally, sessions during which more pulses were detected were also the sessions that showed the highest FC between L-SM1_{ue} and the CON.

Two complementary analyses—pulse censoring and pulse addition—also suggested that pulses produced increases in FC. When all detected pulses were excluded from FC calculations, FC increases between L-SM1_{ue} observed during the casting period were partially reduced. This partial reduction may reflect the fact that pulses occurred at a range of magnitudes and only large pulses (>0.4% fMRI signal change) could be detected and censored. To test if smaller pulses could explain the residual effect of casting after pulse censoring, simulated pulses (mean pulse time series scaled at a range of magnitudes) were added to the pre-cast rs-fMRI recordings. This simulation recreated the effect size and anatomical distribution of FC increases observed during casting. Applying the pulse censoring strategy to the simulated pulses partly reduced simulated FC changes, similar to the effect of censoring the actual data. The pulse censoring and pulse additional analyses suggested that pulses did not explain the decreases in FC in the somatomotor system observed during casting.

4.2 Brain Circuits Require Regular Use to Maintain Their Functional Architecture

Despite the utility of FC as a tool in human neuroscience and neurosurgery, little is known about the mechanisms controlling the spatiotemporal organization of resting-state brain activity. There is no consensus regarding the functions served by resting-state activity (Raichle, 2006; Vincent, 2009). Some existing hypotheses concerning the physiological roles of infra-slow spontaneous

activity include constraining higher-frequency activity necessary for online perception and behavior (Lewis et al., 2009) and consolidation of experience- and use-dependent plasticity (Robertson et al., 2004; Klinzing et al., 2019). In many conceptualizations, the spatiotemporal organization of resting-state activity is closely related to its physiological function. For example, in order for spontaneous activity to support memory consolidation, recently modified circuits spanning multiple brain must be reactivated in synchrony (Klinzing et al., 2019). It has also been suggested that resting-state activity may be an epiphenomenal byproduct of maintaining a critical excitatory/inhibitory balance necessary to allow cascades of activity during behavior and experience (Shew et al., 2009). Such epiphenomenal activity would have no physiological “need” for spatiotemporal organization, but correlation structure could arise from synaptic connections between brain regions (Honey et al., 2009). However, two points argue against an epiphenomenal “role” for spontaneous activity. First, spontaneous activity consumes an enormous amount of metabolic energy (Raichle, 2006). The brain makes up 2% of body tissue by mass but it consumes 20% of the body’s energy (50% in children). It is unlikely that evolution would favor such a large energy expenditure for a process that does not serve a key function. Second, spontaneous activity impacts behaviors and perceptions (Fox et al., 2007; Scholvinck et al., 2012). This influence on behavior and perception would be disadvantageous unless it were regulated in a way that improves function. Epiphenomenal spontaneous activity would only reduce the reliability of neural processing.

One prominent hypothesis regarding the spatiotemporal organization of spontaneous activity is that resting-state FC results from prior coactivation of brain regions during behavior and experience (Dosenbach et al., 2008; Lewis et al., 2009; Harmelech and Malach, 2013; Guerra-

Carrillo et al., 2014; Shannon et al., 2016). This is often called a “Hebbian” account of FC.

Hebbian plasticity is the process by which neurons that frequently fire synchronous action potentials form stronger synaptic connections with one another (Hebb, 1949). Hebbian plasticity is only one mechanism by which neurons change their synaptic strengths (Turrigiano et al., 1998; Keck et al., 2013). Although synaptic plasticity leading to changes in FC may involve many Hebbian and non-Hebbian mechanisms, the high-level phenomenon of frequently co-activated brain regions becoming more functionally connected is similar in concept to classical Hebbian plasticity. Thus “Hebbian” or “Hebbian-like” are appropriate terms for co-activation-dependent FC changes, whether or not the synaptic changes involved result from classic Hebbian mechanisms.

At its core, the Hebbian hypothesis of FC is agnostic to the synaptic (or non-synaptic) mechanisms that produce FC changes. It simply states that brain regions that co-activate during behavior show stronger FC during subsequent rest. The Hebbian FC hypothesis is also agnostic to the physiological functions of spontaneous activity. Co-activated brain regions could become more functionally connected because the functions served by spontaneous activity require activity that is correlated across recently activated circuits. Alternatively, epiphenomenal spontaneous activity could become more correlated between recently co-activated brain regions because of altered synaptic connections. Both of these very different mechanistic accounts lead to the same high-level phenomenon: experience- and use-dependent co-activation leading to increases in subsequent resting-state FC.

Even in its abstract formulation, the often-stated Hebbian hypothesis of FC had previously received little experimental support. Many previous studies attempted to induce changes in FC by driving co-activation of brain regions during behavioral training paradigms, but these studies have invariably produced minuscule effect sizes ($\Delta r \sim 0.1$), which were often poorly localized in the brain (Lewis et al., 2009; Harmelech and Malach, 2013; Guerra-Carrillo et al., 2014; Shannon et al., 2016). The massive reduction in FC ($\Delta r \sim 0.8$) following casting represents the strongest evidence gathered to date supporting the Hebbian FC hypothesis.

Results from daily rs-fMRI before, during and after casting has also refined the Hebbian FC hypothesis by revealing a time course by which FC changes can take place. Most prior formulations of the Hebbian FC hypothesis did not state whether co-activation of brain region would lead to FC changes over a period of hours or days or years (Lewis et al., 2009; Harmelech and Malach, 2013; Guerra-Carrillo et al., 2014), although at least one prior report suggested that the effects of co-activation may be accumulated over many years (Shannon et al., 2016). We have now shown that blocking co-use of the left and right upper extremities can produce a complete loss of FC between the left and right motor cortex in a matter of days. Wearing a cast during a 30-minute scan was not sufficient to drive large changes in FC, but changes were detectable in some cases after just 12 of disuse. These observations specify a time constant of Hebbian FC changes and indicate that FC is determined, at least in part, by a person's experiences and behaviors over the past several hours to days. Future work will be needed to determine if this time constant applies to other brain networks and other forms of experience- and use-driven plasticity. Going forward, this time constant may constrain hypotheses concerning the physiological and synaptic mechanisms that produce FC changes.

4.3 Disuse Drives Systems-Level Plasticity of Brain Networks

Changes in FC during casting represent systems-level plasticity of large-scale brain networks. It should first be clarified that these FC changes are in fact plasticity and not a transient change in function due to wearing a cast, as has been observed during drowsiness, sleep and other behavioral states (Tagliazucchi et al., 2012; Tagliazucchi et al., 2013; Gratton et al., 2018). This point was deliberately tested during a control experiment. If FC changes during casting reflected a transient behavioral change related to wearing a cast, then these changes should have been reproduced by placing a temporary cast on participants during scans. This was not the case. Although one participant did show a significant decrease in FC between the left and right motor cortex when wearing a temporary cast during scans, this effect was much smaller than any FC changes observed during prolonged casting. Additionally, one participant showed reduced FC for over a week after cast removal, even though post-cast rs-fMRI did not involve wearing casts during scans. Thus, the observed FC changes depend on a history of having been casted, not a participant's current state of casting. This temporal dissociation of cause and effect is what qualifies disuse-driven changes in FC as plasticity, as opposed to a transient change in state.

Many prior studies have shown that disuse drives plasticity (Wiesel and Hubel, 1963; Merzenich et al., 1983a; Milliken et al., 2013). However, most prior studies of plasticity have used highly focal recording techniques, almost exclusively focused on primary motor and sensory cortex. Whole-brain rs-fMRI before, during and after casting revealed that disuse does not only drive local plasticity, but also causes modifies large-scale functional networks. Disused brain regions functionally disconnected from the remainder of the somatomotor system and become more

strongly connected to executive control regions in the CON. Whole-brain patterns of FC changes showed a striking degree of network-specificity. L-SM1_{ue} FC increases were highly specific to the CON and did not involve any other functional network. Thus, the whole-brain coverage enabled by rs-fMRI revealed a role for executive control regions in somatomotor plasticity and provide new evidence that individual-specific functional networks are a valid unit of brain organization. These findings would have been impossible to appreciate using the focalized recording techniques traditionally employed to study disuse-driven plasticity.

4.4 Precision Functional Mapping Allows Reliable Measurement of Plasticity

The large, clean, anatomically specific changes in FC observed during casting can partly be attributed to the dramatic behavioral manipulation we imposed (two weeks of persistent limb constraint) and the large amount of data we collected on each participant. The reliability of FC measurement increases drastically with increasing duration of recordings (Laumann et al., 2015). Typical studies acquire very little data (often <10 minutes) on each participant. Such short scans yield very noisy measurements of FC and would provide little statistical power to detect FC changes due to an experimental manipulation. The novel experimental design we used to examine FC changes during casting could easily be applied to study other plasticity manipulations, fluctuations in hormone levels (Pritschet et al., 2020), progression of psychiatric and neurological disease, or responses to therapies. In a time when the more common approach of correlating individual-differences with naturally occurring variance in behavioral measures is facing an existential replication crisis (Marek et al., 2020), we hope this approach will provide a new path forward for relating rs-fMRI measures to behavioral and clinical variables.

4.5 Individual Differences in Disuse-Driven Plasticity

Although all participants showed qualitatively similar changes in FC due to casting, there were interesting individual differences in effect size and time course of FC changes. One participant (Ashley) showed a very large decrease in somatomotor FC ($\Delta r > 0.8$) with a rapid (hours to days) onset and recovery. Another participant (Nico) showed a much smaller change in FC ($\Delta r \sim 0.2$) with a more gradual (several days) onset and recovery. The final participant (Omar) showed an intermediate change in FC ($\Delta r \sim 0.6$), a rapid onset (hours) and a very gradual recovery (>week). With three participants, we cannot relate these differences in effect size and time course to inter-individual differences in any explanatory variable. However, we can speculate regarding some possible explanations for these differences, which could be examined in future studies.

Some possible explanatory variables are 1) differences in MRI acquisition methods, 2) movement in the scanner, 3) age, 4) activity level, 5) time of day, and 6) ingested substances. 1) One potential explanation for the smaller FC changes observed in Nico was that he was scanned on an older MRI scanner (Siemens Trio) than the scanner used for Ashley and Omar (Siemens Prisma). Poorer signal to noise and slower acquisition rate due to scanner and sequence differences may have made it harder to detect FC changes in Nico. 2) Although all participants held very still during scans, relative to typical study participants, Ashley had particularly low head motion. Higher head motion in Nico and Omar may have been responsible for the increased fMRI signal fluctuations present prior to casting in these participants and could have made it more difficult to detect decreases in FC during casting. 3) Nico was 35 years old at the time of casting, while Ashley was 25 years old and Omar was 27 years old. There are many reasons to believe that younger participants may undergo greater plasticity in response to disuse or recover

more quickly after resuming normal use. 4) Ashley also was more physically active than Nico and Omar, which also could have contributed to her increased effect size and rate of recovery. (This is a subjective physical activity rating but this could be examined objectively using surveys that each participant completed during the experiment or by accelerometry.) 5) Nico was scanned every morning at 5:00 a.m., while Ashley and Omar were scanned every night at 9:00 p.m. Nico may have shown a smaller effect size because he was typically sleeping immediately prior to each scan while the other two participants were awake and behaving for many hours prior to scanning. Again, this individual difference could be tracked in greater detail using accelerometry. 6) Nico and Omar regularly ingested caffeine prior to scans, while Ashley did not. Some individual differences in effect size and rate of recovery could have resulted from direct effects of caffeine or other ingested substances on spontaneous brain activity or secondary effects on arousal or neurovascular coupling.

All of these possible explanatory variables could be explored in future studies. Different variables lend themselves to different experimental designs. Some variables, including age, physical activity level, and sleep patterns, could be studied using natural population variance. Studies of natural population variance would likely require many participants to achieve reliable results and would be subject to many confounding variables. A more powerful and controlled study design would be to experimentally manipulate variables of interest in a randomized, controlled trial. This approach would be possible for variables such as activity level, neuroactive medications, and sleep. Perhaps the most powerful design for resting-state fMRI would be within individual-comparisons. This design would prevent the need to compare results across individuals, which can be challenging due to differences in structural and functional anatomy.

Within-individual comparisons could be used to study the effects of time of day and sleep, i.e., participants could be scanned in the morning and evening, and changes that occur across waking hours could be compared to changes that occur across sleep.

4.6 Spontaneous Activity Pulses May Help to Maintain Disused Circuits

The brain may have mechanisms that protect circuits during disuse. Adult brain circuits are typically maintained by regular use (Buzsáki, 2019). Disused circuits are deprived of feedback needed to maintain an accurate representation of the outside world. Spontaneous neural activity may protect circuits from disuse-driven functional degradation. Waves of spontaneous activity shape brain circuits early in development (Espinosa and Stryker, 2012), before circuits receive any input from the outside world, and may be important for maintaining circuit organization during disuse.

Spontaneous waves of activity typically cease early in critical periods (Tolonen et al., 2007; Blankenship and Feller, 2010), when the brain begins to rely on external inputs to shape circuits. This shift from spontaneous to externally evoked activity as the primary driver of activity-dependent plasticity is thought to result, at least in part, from increased inhibition by parvalbumin-positive interneurons at critical-period onset (Hensch, 2004; Toyozumi et al., 2013). Increased inhibitory tone remains into adulthood and spontaneous activity in the adult brain typically does not include the transient waves of activity seen in pre-critical period development. However, immediately following the onset of disuse, parvalbumin-expressing interneurons in disused circuits become less active, shifting the excitatory-inhibitory balance in

these circuits towards a more development-like state (Gainey et al., 2018). Focal disinhibition during disuse may permit the reemergence of spontaneous waves of activity in the adult brain. If so, these waves of activity may help maintain the somatotopic organization that is shared by regions throughout the somatomotor system. Closer examination of spontaneous activity pulses may reveal new targets by which to promote maintenance and recovery of function in the setting of clinical disuse or brain injury.

Spontaneous waves of activity are thought to refine topographic organization in brain circuits because adjacent cells in one map tend to be co-activated during wave propagation (Butts et al., 2007). These synchronous action potentials are carried to target regions, which themselves are topographically organized. The key component of slow activity transients that allows them to refine topographic organization is their wave-like propagation. Thus, if pulses are to help maintain topographic organization within the disused somatomotor system in a manner similar to developmental slow activity transients, they must propagate across each region of the disused system. In the case of retinal waves, the best studied case of slow activity transients, propagation across the retinotopic map in V1 occurs over several seconds (Ackman et al., 2012). If pulses propagated across regions of the disused motor system with a similar speed, this propagation should be detectable in rs-fMRI recordings. We have preliminary evidence that disuse-driven spontaneous activity pulses do propagate across the primary motor and somatosensory cortex, supplementary motor area, anterior insula and cerebellum (Figure 4-1). The directions of propagation observed in each region were strikingly similar across participants. On average, pulse propagation across the primary motor cortex required approximately one second. Future work will explore how the direction of propagation in each region relates to that region's

direction of somatotopy and whether the direction of propagation of individual pulses covaries across brain regions.

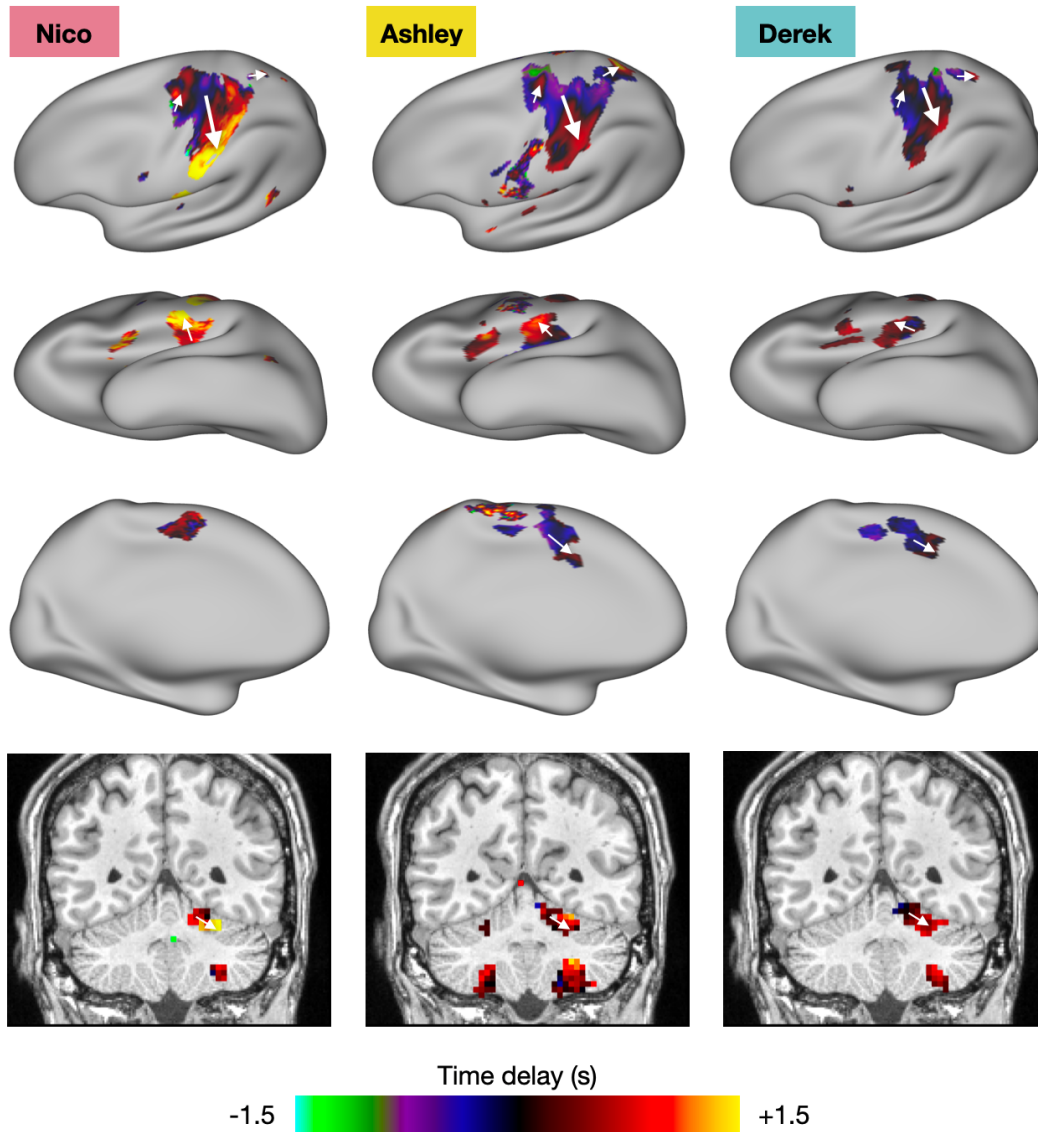


Figure 4-1: Wave-like propagation of spontaneous activity pulses. Time delays of spontaneous activity pulses were estimated for each cortical vertex and cerebellar voxel by parabolic interpolation of the cross correlation with the mean L-SM1_{ue} pulse time series. Time delays were averaged across all pulses to produce a mean time delay map for each participant. White arrows indicate propagation within the primary motor and somatosensory cortex, secondary somatosensory cortex, supplementary motor area, and cerebellum. Directions of propagation are highly consistent across participants.

4.7 Relationship between Pulses and Ongoing Spontaneous Activity

A key question for future research is how the spontaneous activity pulses uncovered by casting relate to typical resting-state activity. One of the key properties that distinguishes pulses from pre-cast resting-state activity is their transient nature. Many recent studies have focused on transient or “dynamic” fluctuations in typical rs-fMRI recordings. The methods used in some prominent dynamics studies (Allen et al., 2014) have been shown to provide insufficient evidence to distinguish genuine dynamics from statistical noise (Laumann et al., 2017). However, interest in dynamic activity patterns in rs-fMRI recordings persists (Esfahlani et al., 2019; Sporns et al., 2020).

At higher temporal frequencies, many transient neural events exist in normal spontaneous brain activity. One of the best studied examples of transient neural events in the resting brain is the sharp-wave ripple, which reactivates recently used hippocampal population sequences (Buzsaki, 2015). Although sharp-wave ripples are often studied during sleep, these events occur regularly in waking animals during periods of inactivity (Buzsaki, 2015). It is not infeasible that transient fluctuations in neural activity could also occur at infra-slow time scales measured by rs-fMRI.

Early in embryonic development, spontaneous activity occurs in a discontinuous fashion, with large, brief activations separated by long periods of cortical silence as recently activated neurons recovery from a refractory state (Tolonen et al., 2007). Later in development, spontaneous activity becomes increasingly continuous in nature. Perhaps these changes in neural dynamics through development result from increasing segregation of neural circuits, leading spontaneous

activations later in development to spread only to small subsets of neurons in a given brain regions. This would leave most of the neuronal population still primed to participate in subsequent activations. Thus, multiple parallel circuits within a brain region could show transient activations at non-overlapping times. If activations in each circuit produce fluctuations in BOLD signal, then these many transient (non-Gaussian) activation time series could sum together into one stationary-appearing (Gaussian) rs-fMRI time series. Thus, the stationarity normally observed in rs-fMRI recordings may represent a sum of many non-stationary processes.

If disuse were to dampen some processes or amplify others, this may allow some non-stationary processes to dominate the rs-fMRI signal, enabling the detection of individual transient pulses. Under this view, the pulses observed during disuse are not necessarily a unique physiological feature that emerges during disuse but a process that is always present in the adult brain, made visible by disuse. In this case, the topographic refinement functions that may be served by disuse-driven spontaneous activity pulses may also occur in under baseline conditions, and spontaneous activity in the adult brain may be a key mechanism that maintains circuits throughout life.

References

- Ackman, J.B., Burbridge, T.J., and Crair, M.C. (2012). Retinal waves coordinate patterned activity throughout the developing visual system. *Nature* 490, 219-225.
- Albert, N.B., Robertson, E.M., and Miall, R.C. (2009). The resting human brain and motor learning. *Curr Biol* 19, 1023-1027.
- Allen, E.A., Damaraju, E., Plis, S.M., Erhardt, E.B., Eichele, T., and Calhoun, V.D. (2014). Tracking whole-brain connectivity dynamics in the resting state. *Cereb Cortex* 24, 663-676.
- Barch, D.M., Burgess, G.C., Harms, M.P., Petersen, S.E., Schlaggar, B.L., Corbetta, M., Glasser, M.F., Curtiss, S., Dixit, S., Feldt, C., *et al.* (2013). Function in the human connectome: task-fMRI and individual differences in behavior. *Neuroimage* 80, 169-189.
- Behzadi, Y., Restom, K., Liao, J., and Liu, T.T. (2007). A component based noise correction method (CompCor) for BOLD and perfusion based fMRI. *Neuroimage* 37, 90-101.
- Berger, H. (1929). Über das elektroencephalogramm des menschen. *Archiv für Psychiatrie* 87, 527-570.
- Biswal, B., Yetkin, F.Z., Haughton, V.M., and Hyde, J.S. (1995). Functional connectivity in the motor cortex of resting human brain using echo-planar MRI. *Magn Reson Med* 34, 537-541.
- Blankenship, A.G., and Feller, M.B. (2010). Mechanisms underlying spontaneous patterned activity in developing neural circuits. *Nat Rev Neurosci* 11, 18-29.
- Blumberg, M.S., Marques, H.G., and Iida, F. (2013). Twitching in sensorimotor development from sleeping rats to robots. *Curr Biol* 23, R532-537.
- Bottger, J., Schafer, A., Lohmann, G., Villringer, A., and Margulies, D.S. (2014). Three-dimensional mean-shift edge bundling for the visualization of functional connectivity in the brain. *IEEE Trans Vis Comput Graph* 20, 471-480.
- Braga, R.M., and Buckner, R.L. (2017). Parallel Interdigitated Distributed Networks within the Individual Estimated by Intrinsic Functional Connectivity. *Neuron* 95, 457-471 e455.
- Bullmore, E., and Sporns, O. (2009). Complex brain networks: graph theoretical analysis of structural and functional systems. *Nat Rev Neurosci* 10, 186-198.
- Bush, G., Frazier, J.A., Rauch, S.L., Seidman, L.J., Whalen, P.J., Jenike, M.A., Rosen, B.R., and Biederman, J. (1999). Anterior cingulate cortex dysfunction in attention-deficit/hyperactivity disorder revealed by fMRI and the Counting Stroop. *Biol Psychiatry* 45, 1542-1552.
- Butts, D.A., Kanold, P.O., and Shatz, C.J. (2007). A burst-based "Hebbian" learning rule at retinogeniculate synapses links retinal waves to activity-dependent refinement. *PLoS Biol* 5, e61.

- Buzsaki, G. (2015). Hippocampal sharp wave-ripple: A cognitive biomarker for episodic memory and planning. *Hippocampus* 25, 1073-1188.
- Buzsáki, G. (2019). *The brain from inside out* (New York, NY: Oxford University Press).
- Cang, J., Renteria, R.C., Kaneko, M., Liu, X., Copenhagen, D.R., and Stryker, M.P. (2005). Development of precise maps in visual cortex requires patterned spontaneous activity in the retina. *Neuron* 48, 797-809.
- Carter, A.R., Patel, K.R., Astafiev, S.V., Snyder, A.Z., Rengachary, J., Strube, M.J., Pope, A., Shimony, J.S., Lang, C.E., Shulman, G.L., and Corbetta, M. (2012). Upstream dysfunction of somatomotor functional connectivity after corticospinal damage in stroke. *Neurorehabil Neural Repair* 26, 7-19.
- Clare, S., Humberstone, M., Hykin, J., Blumhardt, L.D., Bowtell, R., and Morris, P. (1999). Detecting activations in event-related fMRI using analysis of variance. *Magn Reson Med* 42, 1117-1122.
- Clark, B.C., Issac, L.C., Lane, J.L., Damron, L.A., and Hoffman, R.L. (2008). Neuromuscular plasticity during and following 3 wk of human forearm cast immobilization. *J Appl Physiol* (1985) 105, 868-878.
- Colonnese, M.T., and Khazipov, R. (2010). "Slow activity transients" in infant rat visual cortex: a spreading synchronous oscillation patterned by retinal waves. *J Neurosci* 30, 4325-4337.
- Cordes, D., Haughton, V.M., Arfanakis, K., Carew, J.D., Turski, P.A., Moritz, C.H., Quigley, M.A., and Meyerand, M.E. (2001). Frequencies contributing to functional connectivity in the cerebral cortex in "resting-state" data. *AJNR Am J Neuroradiol* 22, 1326-1333.
- Davis, H., Davis, P.A., Loomis, A.L., Harvey, E.N., and Hobart, G. (1937). Changes in Human Brain Potentials during the Onset of Sleep. *Science* 86, 448-450.
- Dhond, R.P., Yeh, C., Park, K., Kettner, N., and Napadow, V. (2008). Acupuncture modulates resting state connectivity in default and sensorimotor brain networks. *Pain* 136, 407-418.
- Diamond, M.E., Armstrong-James, M., and Ebner, F.F. (1993). Experience-dependent plasticity in adult rat barrel cortex. *Proc Natl Acad Sci U S A* 90, 2082-2086.
- Dosenbach, N.U., Fair, D.A., Cohen, A.L., Schlaggar, B.L., and Petersen, S.E. (2008). A dual-networks architecture of top-down control. *Trends Cogn Sci* 12, 99-105.
- Dosenbach, N.U., Fair, D.A., Miezin, F.M., Cohen, A.L., Wenger, K.K., Dosenbach, R.A., Fox, M.D., Snyder, A.Z., Vincent, J.L., Raichle, M.E., *et al.* (2007). Distinct brain networks for adaptive and stable task control in humans. *Proc Natl Acad Sci U S A* 104, 11073-11078.
- Dosenbach, N.U., Nardos, B., Cohen, A.L., Fair, D.A., Power, J.D., Church, J.A., Nelson, S.M., Wig, G.S., Vogel, A.C., Lessov-Schlaggar, C.N., *et al.* (2010). Prediction of individual brain maturity using fMRI. *Science* 329, 1358-1361.

- Dosenbach, N.U., Visscher, K.M., Palmer, E.D., Miezin, F.M., Wenger, K.K., Kang, H.C., Burgund, E.D., Grimes, A.L., Schlaggar, B.L., and Petersen, S.E. (2006). A core system for the implementation of task sets. *Neuron* 50, 799-812.
- Dosenbach, N.U.F., Koller, J.M., Earl, E.A., Miranda-Dominguez, O., Klein, R.L., Van, A.N., Snyder, A.Z., Nagel, B.J., Nigg, J.T., Nguyen, A.L., *et al.* (2017). Real-time motion analytics during brain MRI improve data quality and reduce costs. *Neuroimage* 161, 80-93.
- Drager, U.C. (1975). Receptive fields of single cells and topography in mouse visual cortex. *J Comp Neurol* 160, 269-290.
- Dreyfus-Brisac, C., and Larroche, J.C. (1971). [Discontinuous electroencephalograms in the premature newborn and at term. Electro-anatomo-clinical correlations]. *Rev Electroencephalogr Neurophysiol Clin* 1, 95-99.
- Eisenberger, N.I., Lieberman, M.D., and Williams, K.D. (2003). Does rejection hurt? An fMRI study of social exclusion. *Science* 302, 290-292.
- Engel, S.A., Rumelhart, D.E., Wandell, B.A., Lee, A.T., Glover, G.H., Chichilnisky, E.J., and Shadlen, M.N. (1994). fMRI of human visual cortex. *Nature* 369, 525.
- Esfahlani, F.Z., Jo, Y., Faskowitz, J., Byrge, L., Kennedy, D.P., Sporns, O., and Betzel, R.F. (2019). High-amplitude co-fluctuations in cortical activity drive functional connectivity. *bioRxiv*.
- Espinosa, J.S., and Stryker, M.P. (2012). Development and plasticity of the primary visual cortex. *Neuron* 75, 230-249.
- Fagiolini, M., and Hensch, T.K. (2000). Inhibitory threshold for critical-period activation in primary visual cortex. *Nature* 404, 183-186.
- Fair, D.A., Miranda-Dominguez, O., Snyder, A.Z., Perrone, A., Earl, E.A., Van, A.N., Koller, J.M., Feczko, E., Tisdall, M.D., van der Kouwe, A., *et al.* (2020). Correction of respiratory artifacts in MRI head motion estimates. *Neuroimage* 208, 116400.
- Feldheim, D.A., and O'Leary, D.D. (2010). Visual map development: bidirectional signaling, bifunctional guidance molecules, and competition. *Cold Spring Harb Perspect Biol* 2, a001768.
- Feldman, D.E., and Brecht, M. (2005). Map plasticity in somatosensory cortex. *Science* 310, 810-815.
- Fischl, B. (2012). FreeSurfer. *Neuroimage* 62, 774-781.
- Fox, M.D., Corbetta, M., Snyder, A.Z., Vincent, J.L., and Raichle, M.E. (2006). Spontaneous neuronal activity distinguishes human dorsal and ventral attention systems. *Proc Natl Acad Sci U S A* 103, 10046-10051.

- Fox, M.D., Snyder, A.Z., Vincent, J.L., Corbetta, M., Van Essen, D.C., and Raichle, M.E. (2005). The human brain is intrinsically organized into dynamic, anticorrelated functional networks. *Proc Natl Acad Sci U S A* 102, 9673-9678.
- Fox, M.D., Snyder, A.Z., Vincent, J.L., and Raichle, M.E. (2007). Intrinsic fluctuations within cortical systems account for intertrial variability in human behavior. *Neuron* 56, 171-184.
- Fuchs, J.L., and Salazar, E. (1998). Effects of whisker trimming on GABA(A) receptor binding in the barrel cortex of developing and adult rats. *J Comp Neurol* 395, 209-216.
- Gainey, M.A., Aman, J.W., and Feldman, D.E. (2018). Rapid Disinhibition by Adjustment of PV Intrinsic Excitability during Whisker Map Plasticity in Mouse S1. *J Neurosci* 38, 4749-4761.
- Galli, L., and Maffei, L. (1988). Spontaneous impulse activity of rat retinal ganglion cells in prenatal life. *Science* 242, 90-91.
- Garraghty, P.E., LaChica, E.A., and Kaas, J.H. (1991). Injury-induced reorganization of somatosensory cortex is accompanied by reductions in GABA staining. *Somatosens Mot Res* 8, 347-354.
- Garraghty, P.E., and Muja, N. (1996). NMDA receptors and plasticity in adult primate somatosensory cortex. *J Comp Neurol* 367, 319-326.
- Gordon, E.M., Laumann, T.O., Adeyemo, B., Huckins, J.F., Kelley, W.M., and Petersen, S.E. (2016). Generation and Evaluation of a Cortical Area Parcellation from Resting-State Correlations. *Cereb Cortex* 26, 288-303.
- Gordon, E.M., Laumann, T.O., Gilmore, A.W., Newbold, D.J., Greene, D.J., Berg, J.J., Ortega, M., Hoyt-Drazen, C., Gratton, C., Sun, H., *et al.* (2017). Precision Functional Mapping of Individual Human Brains. *Neuron* 95, 791-807 e797.
- Gordon, E.M., Laumann, T.O., Marek, S., Raut, R.V., Gratton, C., Newbold, D.J., Greene, D.J., Coalson, R.S., Snyder, A.Z., Schlaggar, B.L., *et al.* (2020). Default mode network streams for coupling to language and control systems. *Proc Natl Acad Sci U S A* In press.
- Gordon, E.M., Lynch, C.J., Gratton, C., Laumann, T.O., Gilmore, A.W., Greene, D.J., Ortega, M., Nguyen, A.L., Schlaggar, B.L., Petersen, S.E., *et al.* (2018). Three Distinct Sets of Connector Hubs Integrate Human Brain Function. *Cell Rep* 24, 1687-1695 e1684.
- Grafstein, B. (1971). Transneuronal transfer of radioactivity in the central nervous system. *Science* 172, 177-179.
- Gratton, C., Koller, J.M., Shannon, W., Greene, D.J., Maiti, B., Snyder, A.Z., Petersen, S.E., Perlmuter, J.S., and Campbell, M.C. (2019). Emergent Functional Network Effects in Parkinson Disease. *Cereb Cortex* 29, 2509-2523.
- Gratton, C., Laumann, T.O., Nielsen, A.N., Greene, D.J., Gordon, E.M., Gilmore, A.W., Nelson, S.M., Coalson, R.S., Snyder, A.Z., Schlaggar, B.L., *et al.* (2018). Functional Brain Networks Are

Dominated by Stable Group and Individual Factors, Not Cognitive or Daily Variation. *Neuron* 98, 439-452 e435.

Grayson, D.S., Bliss-Moreau, E., Machado, C.J., Bennett, J., Shen, K., Grant, K.A., Fair, D.A., and Amaral, D.G. (2016). The Rhesus Monkey Connectome Predicts Disrupted Functional Networks Resulting from Pharmacogenetic Inactivation of the Amygdala. *Neuron* 91, 453-466.

Grayson, D.S., and Fair, D.A. (2017). Development of large-scale functional networks from birth to adulthood: A guide to the neuroimaging literature. *Neuroimage* 160, 15-31.

Greene, D.J., Marek, S., Gordon, E.M., Siegel, J.S., Gratton, C., Laumann, T.O., Gilmore, A.W., Berg, J.J., Nguyen, A.L., Dierker, D., *et al.* (2020). Integrative and Network-Specific Connectivity of the Basal Ganglia and Thalamus Defined in Individuals. *Neuron* 105, 742-758 e746.

Greene, J.D., Sommerville, R.B., Nystrom, L.E., Darley, J.M., and Cohen, J.D. (2001). An fMRI investigation of emotional engagement in moral judgment. *Science* 293, 2105-2108.

Greicius, M.D., Flores, B.H., Menon, V., Glover, G.H., Solvason, H.B., Kenna, H., Reiss, A.L., and Schatzberg, A.F. (2007). Resting-state functional connectivity in major depression: abnormally increased contributions from subgenual cingulate cortex and thalamus. *Biol Psychiatry* 62, 429-437.

Greicius, M.D., Krasnow, B., Reiss, A.L., and Menon, V. (2003). Functional connectivity in the resting brain: a network analysis of the default mode hypothesis. *Proc Natl Acad Sci U S A* 100, 253-258.

Greiner, J.V., and Weidman, T.A. (1980). Histogenesis of the cat retina. *Exp Eye Res* 30, 439-453.

Guerra-Carrillo, B., Mackey, A.P., and Bunge, S.A. (2014). Resting-state fMRI: a window into human brain plasticity. *Neuroscientist* 20, 522-533.

Hahamy, A., Sotiropoulos, S.N., Henderson Slater, D., Malach, R., Johansen-Berg, H., and Makin, T.R. (2015). Normalisation of brain connectivity through compensatory behaviour, despite congenital hand absence. *Elife* 4.

Hamburger, V. (1963). Some aspects of the embryology of behavior. *Quarterly Review of Biology* 38, 342-365.

Hanganu, I.L., Ben-Ari, Y., and Khazipov, R. (2006). Retinal waves trigger spindle bursts in the neonatal rat visual cortex. *J Neurosci* 26, 6728-6736.

Harauzov, A., Spolidoro, M., DiCristo, G., De Pasquale, R., Cancedda, L., Pizzorusso, T., Viegi, A., Berardi, N., and Maffei, L. (2010). Reducing intracortical inhibition in the adult visual cortex promotes ocular dominance plasticity. *J Neurosci* 30, 361-371.

- Harmelech, T., and Malach, R. (2013). Neurocognitive biases and the patterns of spontaneous correlations in the human cortex. *Trends Cogn Sci* 17, 606-615.
- Harmelech, T., Preminger, S., Wertman, E., and Malach, R. (2013). The day-after effect: long term, Hebbian-like restructuring of resting-state fMRI patterns induced by a single epoch of cortical activation. *J Neurosci* 33, 9488-9497.
- He, B.J., Zempel, J.M., Snyder, A.Z., and Raichle, M.E. (2010). The temporal structures and functional significance of scale-free brain activity. *Neuron* 66, 353-369.
- Hebb, D.O. (1949). *The organization of behavior; a neuropsychological theory* (New York,: Wiley).
- Hedrich, T., Pellegrino, G., Kobayashi, E., Lina, J.M., and Grova, C. (2017). Comparison of the spatial resolution of source imaging techniques in high-density EEG and MEG. *Neuroimage* 157, 531-544.
- Hensch, T.K. (2004). Critical period regulation. *Annu Rev Neurosci* 27, 549-579.
- Hensch, T.K., Fagiolini, M., Mataga, N., Stryker, M.P., Baekkeskov, S., and Kash, S.F. (1998). Local GABA circuit control of experience-dependent plasticity in developing visual cortex. *Science* 282, 1504-1508.
- Herscovitch, P., Markham, J., and Raichle, M.E. (1983). Brain blood flow measured with intravenous H₂(15)O. I. Theory and error analysis. *J Nucl Med* 24, 782-789.
- Honey, C.J., Sporns, O., Cammoun, L., Gigandet, X., Thiran, J.P., Meuli, R., and Hagmann, P. (2009). Predicting human resting-state functional connectivity from structural connectivity. *Proc Natl Acad Sci U S A* 106, 2035-2040.
- Hoyt, C.R., Van, A.N., Ortega, M., Koller, J.M., Everett, E.A., Nguyen, A.L., Lang, C.E., Schlaggar, B.L., and Dosenbach, N.U.F. (2019). Detection of Pediatric Upper Extremity Motor Activity and Deficits With Accelerometry. *JAMA Netw Open* 2, e192970.
- Hubel, D.H., and Wiesel, T.N. (1959). Receptive fields of single neurones in the cat's striate cortex. *J Physiol* 148, 574-591.
- Hubel, D.H., and Wiesel, T.N. (1970). The period of susceptibility to the physiological effects of unilateral eye closure in kittens. *J Physiol* 206, 419-436.
- Hubel, D.H., and Wiesel, T.N. (1972). Laminar and columnar distribution of geniculo-cortical fibers in the macaque monkey. *J Comp Neurol* 146, 421-450.
- Jacomy, M., Venturini, T., Heymann, S., and Bastian, M. (2014). ForceAtlas2, a continuous graph layout algorithm for handy network visualization designed for the Gephi software. *PLoS One* 9, e98679.

- Jasper, H., and Kershman, J. (1941). ELECTROENCEPHALOGRAPHIC CLASSIFICATION OF THE EPILEPSIES. *Arch NeurPsych* 45, 903-943.
- Jenkinson, M., Beckmann, C.F., Behrens, T.E., Woolrich, M.W., and Smith, S.M. (2012). *Fsl*. *Neuroimage* 62, 782-790.
- Katz, L.C., and Shatz, C.J. (1996). Synaptic activity and the construction of cortical circuits. *Science* 274, 1133-1138.
- Keck, T., Keller, G.B., Jacobsen, R.I., Eysel, U.T., Bonhoeffer, T., and Hubener, M. (2013). Synaptic scaling and homeostatic plasticity in the mouse visual cortex in vivo. *Neuron* 80, 327-334.
- Kelly, M.K., Carvell, G.E., Kodger, J.M., and Simons, D.J. (1999). Sensory loss by selected whisker removal produces immediate disinhibition in the somatosensory cortex of behaving rats. *J Neurosci* 19, 9117-9125.
- Khazipov, R., and Luhmann, H.J. (2006). Early patterns of electrical activity in the developing cerebral cortex of humans and rodents. *Trends Neurosci* 29, 414-418.
- Khazipov, R., Sirota, A., Leinekugel, X., Holmes, G.L., Ben-Ari, Y., and Buzsaki, G. (2004). Early motor activity drives spindle bursts in the developing somatosensory cortex. *Nature* 432, 758-761.
- Kim, J., Song, M., Jang, J., and Paik, S. (2020). Spontaneous retinal waves can generate long-range horizontal connectivity in visual cortex. *J Neurosci* in press.
- Klinzing, J.G., Niethard, N., and Born, J. (2019). Mechanisms of systems memory consolidation during sleep. *Nat Neurosci* 22, 1598-1610.
- Kraft, A.W., Mitra, A., Bauer, A.Q., Snyder, A.Z., Raichle, M.E., Culver, J.P., and Lee, J.M. (2017). Visual experience sculpts whole-cortex spontaneous infraslow activity patterns through an Arc-dependent mechanism. *Proc Natl Acad Sci U S A* 114, E9952-E9961.
- Kucyi, A., and Parvizi, J. (2020). Pupillary dynamics link spontaneous and task-evoked activations recorded directly from human insula. *J Neurosci*.
- Lancaster, J., Glass, T.G., Lankipalli, B.R., Downs, H., Mayberg, H., and Fox, P.T. (1995). A modality-independent approach to spatial normalization of tomographic images of the human brain. *Hum Brain Mapp* 3, 209-223.
- Laumann, T.O., Gordon, E.M., Adeyemo, B., Snyder, A.Z., Joo, S.J., Chen, M.Y., Gilmore, A.W., McDermott, K.B., Nelson, S.M., Dosenbach, N.U., *et al.* (2015). Functional System and Areal Organization of a Highly Sampled Individual Human Brain. *Neuron* 87, 657-670.
- Laumann, T.O., Snyder, A.Z., Mitra, A., Gordon, E.M., Gratton, C., Adeyemo, B., Gilmore, A.W., Nelson, S.M., Berg, J.J., Greene, D.J., *et al.* (2017). On the Stability of BOLD fMRI Correlations. *Cereb Cortex* 27, 4719-4732.

- Letzkus, J.J., Wolff, S.B., and Luthi, A. (2015). Disinhibition, a Circuit Mechanism for Associative Learning and Memory. *Neuron* 88, 264-276.
- LeVay, S., Hubel, D.H., and Wiesel, T.N. (1975). The pattern of ocular dominance columns in macaque visual cortex revealed by a reduced silver stain. *J Comp Neurol* 159, 559-576.
- Lewis, C.M., Baldassarre, A., Committeri, G., Romani, G.L., and Corbetta, M. (2009). Learning sculpts the spontaneous activity of the resting human brain. *Proc Natl Acad Sci U S A* 106, 17558-17563.
- Liepert, J., Storch, P., Fritsch, A., and Weiller, C. (2000). Motor cortex disinhibition in acute stroke. *Clin Neurophysiol* 111, 671-676.
- Lindquist, M.A., Meng Loh, J., Atlas, L.Y., and Wager, T.D. (2009). Modeling the hemodynamic response function in fMRI: efficiency, bias and mis-modeling. *Neuroimage* 45, S187-198.
- Lowe, M.J., Mock, B.J., and Sorenson, J.A. (1998). Functional connectivity in single and multislice echoplanar imaging using resting-state fluctuations. *Neuroimage* 7, 119-132.
- Makin, T.R., Scholz, J., Filippini, N., Henderson Slater, D., Tracey, I., and Johansen-Berg, H. (2013). Phantom pain is associated with preserved structure and function in the former hand area. *Nat Commun* 4, 1570.
- Marcus, D.S., Harwell, J., Olsen, T., Hodge, M., Glasser, M.F., Prior, F., Jenkinson, M., Laumann, T., Curtiss, S.W., and Van Essen, D.C. (2011). Informatics and data mining tools and strategies for the human connectome project. *Front Neuroinform* 5, 4.
- Marek, S., and Dosenbach, N.U.F. (2019). Control networks of the frontal lobes. *Handb Clin Neurol* 163, 333-347.
- Marek, S., Siegel, J.S., Gordon, E.M., Raut, R.V., Gratton, C., Newbold, D.J., Ortega, M., Laumann, T.O., Adeyemo, B., Miller, D.B., *et al.* (2018). Spatial and Temporal Organization of the Individual Human Cerebellum. *Neuron* 100, 977-993 e977.
- Marek, S., Trevo-Clemmens, B., Calabro, F.J., Montez, D.F., Kay, B.P., Hatoum, A.S., Donohue, M.R., Foran, W., Miller, R.L., Feczko, E., *et al.* (2020). Towards Reproducible Brain-Wide Association Studies. *bioRxiv*.
- Meister, M., Wong, R.O., Baylor, D.A., and Shatz, C.J. (1991). Synchronous bursts of action potentials in ganglion cells of the developing mammalian retina. *Science* 252, 939-943.
- Merzenich, M.M., Kaas, J.H., Wall, J., Nelson, R.J., Sur, M., and Felleman, D. (1983a). Topographic reorganization of somatosensory cortical areas 3b and 1 in adult monkeys following restricted deafferentation. *Neuroscience* 8, 33-55.

- Merzenich, M.M., Kaas, J.H., Wall, J.T., Sur, M., Nelson, R.J., and Felleman, D.J. (1983b). Progression of change following median nerve section in the cortical representation of the hand in areas 3b and 1 in adult owl and squirrel monkeys. *Neuroscience* 10, 639-665.
- Merzenich, M.M., Nelson, R.J., Stryker, M.P., Cynader, M.S., Schoppmann, A., and Zook, J.M. (1984). Somatosensory cortical map changes following digit amputation in adult monkeys. *J Comp Neurol* 224, 591-605.
- Milh, M., Kaminska, A., Huon, C., Lapillonne, A., Ben-Ari, Y., and Khazipov, R. (2007). Rapid cortical oscillations and early motor activity in premature human neonate. *Cereb Cortex* 17, 1582-1594.
- Milliken, G.W., Plautz, E.J., and Nudo, R.J. (2013). Distal forelimb representations in primary motor cortex are redistributed after forelimb restriction: a longitudinal study in adult squirrel monkeys. *J Neurophysiol* 109, 1268-1282.
- Mitra, A., Snyder, A.Z., Hacker, C.D., and Raichle, M.E. (2014). Lag structure in resting-state fMRI. *J Neurophysiol* 111, 2374-2391.
- Molunby, M.J., Anderson, R.M., Newbold, D.J., Koblesky, N.K., Garrett, A.M., Schreiner, D., Radley, J.J., and Weiner, J.A. (2017). gamma-Protocadherins Interact with Neuroligin-1 and Negatively Regulate Dendritic Spine Morphogenesis. *Cell Rep* 18, 2702-2714.
- Mueller, S., Wang, D., Fox, M.D., Yeo, B.T., Sepulcre, J., Sabuncu, M.R., Shafee, R., Lu, J., and Liu, H. (2013). Individual variability in functional connectivity architecture of the human brain. *Neuron* 77, 586-595.
- Murphy, T.H., and Corbett, D. (2009). Plasticity during stroke recovery: from synapse to behaviour. *Nat Rev Neurosci* 10, 861-872.
- Neta, M., Nelson, S.M., and Petersen, S.E. (2017). Dorsal Anterior Cingulate, Medial Superior Frontal Cortex, and Anterior Insula Show Performance Reporting-Related Late Task Control Signals. *Cereb Cortex* 27, 2154-2165.
- Newbold, D.J., Laumann, T.O., Hoyt, C.R., Hampton, J.M., Montez, D.F., Raut, R.V., Ortega, M., Mitra, A., Nielsen, A.N., Miller, D.B., *et al.* (2020). Plasticity and spontaneous activity pulses in disused human brain circuits. *Neuron* In press.
- Newman, M.E. (2004). Analysis of weighted networks. *Phys Rev E Stat Nonlin Soft Matter Phys* 70, 056131.
- Nielsen, A.N., Gratton, C., Church, J.A., Dosenbach, N.U.F., Black, K.J., Petersen, S.E., Schlaggar, B.L., and Greene, D.J. (2020). Atypical Functional Connectivity in Tourette Syndrome Differs Between Children and Adults. *Biol Psychiatry* 87, 164-173.
- Nielsen, A.N., Greene, D.J., Gratton, C., Dosenbach, N.U.F., Petersen, S.E., and Schlaggar, B.L. (2019). Evaluating the Prediction of Brain Maturity From Functional Connectivity After Motion Artifact Denoising. *Cereb Cortex* 29, 2455-2469.

Ogawa, S., Lee, T.M., Kay, A.R., and Tank, D.W. (1990). Brain magnetic resonance imaging with contrast dependent on blood oxygenation. *Proc Natl Acad Sci U S A* 87, 9868-9872.

Oldfield, R.C. (1971). The assessment and analysis of handedness: the Edinburgh inventory. *Neuropsychologia* 9, 97-113.

Pawela, C.P., Biswal, B.B., Hudetz, A.G., Li, R., Jones, S.R., Cho, Y.R., Matloub, H.S., and Hyde, J.S. (2010). Interhemispheric neuroplasticity following limb deafferentation detected by resting-state functional connectivity magnetic resonance imaging (fcMRI) and functional magnetic resonance imaging (fMRI). *Neuroimage* 49, 2467-2478.

Penfield, W., and Boldrey, E. (1937). SOMATIC MOTOR AND SENSORY REPRESENTATION IN THE CEREBRAL CORTEX OF MAN AS STUDIED BY ELECTRICAL STIMULATION. *Brain* 60, 389-443.

Petersen, S.E., Fox, P.T., Posner, M.I., Mintun, M., and Raichle, M.E. (1988). Positron emission tomographic studies of the cortical anatomy of single-word processing. *Nature* 331, 585-589.

Petersen, S.E., and Posner, M.I. (2012). The attention system of the human brain: 20 years after. *Annu Rev Neurosci* 35, 73-89.

Petersson, P., Waldenstrom, A., Fahraeus, C., and Schouenborg, J. (2003). Spontaneous muscle twitches during sleep guide spinal self-organization. *Nature* 424, 72-75.

Poldrack, R.A., Laumann, T.O., Koyejo, O., Gregory, B., Hover, A., Chen, M.Y., Gorgolewski, K.J., Luci, J., Joo, S.J., Boyd, R.L., *et al.* (2015). Long-term neural and physiological phenotyping of a single human. *Nat Commun* 6, 8885.

Posner, M.I., and Petersen, S.E. (1990). The attention system of the human brain. *Annu Rev Neurosci* 13, 25-42.

Power, J.D. (2017). A simple but useful way to assess fMRI scan qualities. *Neuroimage* 154, 150-158.

Power, J.D., Barnes, K.A., Snyder, A.Z., Schlaggar, B.L., and Petersen, S.E. (2012). Spurious but systematic correlations in functional connectivity MRI networks arise from subject motion. *Neuroimage* 59, 2142-2154.

Power, J.D., Cohen, A.L., Nelson, S.M., Wig, G.S., Barnes, K.A., Church, J.A., Vogel, A.C., Laumann, T.O., Miezin, F.M., Schlaggar, B.L., and Petersen, S.E. (2011). Functional network organization of the human brain. *Neuron* 72, 665-678.

Preyer, W.T. (1885). *Specielle physiologie des embryo: Untersuchungen über die lebenserscheinungen vor der geburt.*

Pritschet, L., Santander, T., Taylor, C.M., Layher, E., Yu, S., Miller, M.B., Grafton, S.T., and Jacobs, E.G. (2020). Functional reorganization of brain networks across the human menstrual cycle. *Neuroimage* 220, 117091.

- Provine, R.R. (1972). Ontogeny of bioelectric activity in the spinal cord of the chick embryo and its behavioral implications. *Brain Res* 41, 365-378.
- Raichle, M.E. (1979). Quantitative in vivo autoradiography with positron emission tomography. *Brain Res* 180, 47-68.
- Raichle, M.E. (2006). Neuroscience. The brain's dark energy. *Science* 314, 1249-1250.
- Raichle, M.E., MacLeod, A.M., Snyder, A.Z., Powers, W.J., Gusnard, D.A., and Shulman, G.L. (2001). A default mode of brain function. *Proc Natl Acad Sci U S A* 98, 676-682.
- Raichle, M.E., Martin, W.R., Herscovitch, P., Mintun, M.A., and Markham, J. (1983). Brain blood flow measured with intravenous H₂(15)O. II. Implementation and validation. *J Nucl Med* 24, 790-798.
- Ramachandran, V.S., Rogers-Ramachandran, D., and Stewart, M. (1992). Perceptual correlates of massive cortical reorganization. *Science* 258, 1159-1160.
- Raut, R.V., Mitra, A., Marek, S., Ortega, M., Snyder, A.Z., Tanenbaum, A., Laumann, T.O., Dosenbach, N.U.F., and Raichle, M.E. (2020). Organization of Propagated Intrinsic Brain Activity in Individual Humans. *Cereb Cortex* 30, 1716-1734.
- Raut, R.V., Mitra, A., Snyder, A.Z., and Raichle, M.E. (2019). On time delay estimation and sampling error in resting-state fMRI. *Neuroimage in press*.
- Reynolds, J.N., Hyland, B.I., and Wickens, J.R. (2001). A cellular mechanism of reward-related learning. *Nature* 413, 67-70.
- Robertson, E.M., Pascual-Leone, A., and Miall, R.C. (2004). Current concepts in procedural consolidation. *Nat Rev Neurosci* 5, 576-582.
- Robinson, E.C., Jbabdi, S., Glasser, M.F., Andersson, J., Burgess, G.C., Harms, M.P., Smith, S.M., Van Essen, D.C., and Jenkinson, M. (2014). MSM: a new flexible framework for Multimodal Surface Matching. *Neuroimage* 100, 414-426.
- Rosenthal, Z.P., Raut, R.V., Yan, P., Koko, D., Kraft, A.W., Czerniewski, L., Acland, B., Mitra, A., Snyder, L.H., Bauer, A.Q., *et al.* (2019). Local perturbations of cortical excitability propagate differentially through large-scale functional networks. *Cereb Cortex in press*.
- Rosenthal, Z.P., Raut, R.V., Yan, P., Koko, D., Kraft, A.W., Czerniewski, L., Acland, B., Mitra, A., Snyder, L.H., Bauer, A.Q., *et al.* (2020). Local Perturbations of Cortical Excitability Propagate Differentially Through Large-Scale Functional Networks. *Cereb Cortex* 30, 3352-3369.
- Rosvall, M., and Bergstrom, C.T. (2008). Maps of random walks on complex networks reveal community structure. *Proc Natl Acad Sci U S A* 105, 1118-1123.

- Sami, S., Robertson, E.M., and Miall, R.C. (2014). The time course of task-specific memory consolidation effects in resting state networks. *J Neurosci* 34, 3982-3992.
- Scholvinck, M.L., Friston, K.J., and Rees, G. (2012). The influence of spontaneous activity on stimulus processing in primary visual cortex. *Neuroimage* 59, 2700-2708.
- Seeley, W.W., Menon, V., Schatzberg, A.F., Keller, J., Glover, G.H., Kenna, H., Reiss, A.L., and Greicius, M.D. (2007). Dissociable intrinsic connectivity networks for salience processing and executive control. *J Neurosci* 27, 2349-2356.
- Seitzman, B.A., Gratton, C., Laumann, T.O., Gordon, E.M., Adeyemo, B., Dworesky, A., Kraus, B.T., Gilmore, A.W., Berg, J.J., Ortega, M., *et al.* (2019). Trait-like variants in human functional brain networks. *Proc Natl Acad Sci U S A* 116, 22851-22861.
- Seo, D.O., Funderburk, S.C., Bhatti, D.L., Motard, L.E., Newbold, D., Girven, K.S., McCall, J.G., Krashes, M., Sparta, D.R., and Bruchas, M.R. (2016). A GABAergic Projection from the Centromedial Nuclei of the Amygdala to Ventromedial Prefrontal Cortex Modulates Reward Behavior. *J Neurosci* 36, 10831-10842.
- Shannon, B.J., Dosenbach, R.A., Su, Y., Vlassenko, A.G., Larson-Prior, L.J., Nolan, T.S., Snyder, A.Z., and Raichle, M.E. (2013). Morning-evening variation in human brain metabolism and memory circuits. *J Neurophysiol* 109, 1444-1456.
- Shannon, B.J., Vaishnavi, S.N., Vlassenko, A.G., Shimony, J.S., Rutlin, J., and Raichle, M.E. (2016). Brain aerobic glycolysis and motor adaptation learning. *Proc Natl Acad Sci U S A* 113, E3782-3791.
- Schatz, C.J., and Stryker, M.P. (1988). Prenatal tetrodotoxin infusion blocks segregation of retinogeniculate afferents. *Science* 242, 87-89.
- Sheline, Y.I., Barch, D.M., Donnelly, J.M., Ollinger, J.M., Snyder, A.Z., and Mintun, M.A. (2001). Increased amygdala response to masked emotional faces in depressed subjects resolves with antidepressant treatment: an fMRI study. *Biol Psychiatry* 50, 651-658.
- Shew, W.L., Yang, H., Petermann, T., Roy, R., and Plenz, D. (2009). Neuronal avalanches imply maximum dynamic range in cortical networks at criticality. *J Neurosci* 29, 15595-15600.
- Shulman, G.L., Ollinger, J.M., Linenweber, M., Petersen, S.E., and Corbetta, M. (2001). Multiple neural correlates of detection in the human brain. *Proc Natl Acad Sci U S A* 98, 313-318.
- Siegel, J.S., Seitzman, B.A., Ramsey, L.E., Ortega, M., Gordon, E.M., Dosenbach, N.U.F., Petersen, S.E., Shulman, G.L., and Corbetta, M. (2018). Re-emergence of modular brain networks in stroke recovery. *Cortex* 101, 44-59.
- Smyser, C.D., Inder, T.E., Shimony, J.S., Hill, J.E., Degnan, A.J., Snyder, A.Z., and Neil, J.J. (2010). Longitudinal analysis of neural network development in preterm infants. *Cereb Cortex* 20, 2852-2862.

- Southwell, D.G., Froemke, R.C., Alvarez-Buylla, A., Stryker, M.P., and Gandhi, S.P. (2010). Cortical plasticity induced by inhibitory neuron transplantation. *Science* 327, 1145-1148.
- Sporns, O., Faskowitz, J., Teixeira, S., and Betzel, R.F. (2020). Dynamic Expression of Brain Functional Systems Disclosed by Fine-Scale Analysis of Edge Time Series. *bioRxiv*.
- Sylvester, C.M., Yu, Q., Srivastava, A.B., Marek, S., Zheng, A., Alexopoulos, D., Smyser, C.D., Shimony, J.S., Ortega, M., Dierker, D.L., *et al.* (2020). Individual-specific functional connectivity of the amygdala: A substrate for precision psychiatry. *Proc Natl Acad Sci U S A* 117, 3808-3818.
- Tagliazucchi, E., von Wegner, F., Morzelewski, A., Borisov, S., Jahnke, K., and Laufs, H. (2012). Automatic sleep staging using fMRI functional connectivity data. *Neuroimage* 63, 63-72.
- Tagliazucchi, E., von Wegner, F., Morzelewski, A., Brodbeck, V., Jahnke, K., and Laufs, H. (2013). Breakdown of long-range temporal dependence in default mode and attention networks during deep sleep. *Proc Natl Acad Sci U S A* 110, 15419-15424.
- Talairach, J., and Tournoux, P. (1988). Co-planar stereotaxic atlas of the human brain : 3-dimensional proportional system : an approach to cerebral imaging (Stuttgart ; New York: Georg Thieme).
- Tang, Y., Stryker, M.P., Alvarez-Buylla, A., and Espinosa, J.S. (2014). Cortical plasticity induced by transplantation of embryonic somatostatin or parvalbumin interneurons. *Proc Natl Acad Sci U S A* 111, 18339-18344.
- Tatum, W.O., Rubboli, G., Kaplan, P.W., Mirsatari, S.M., Radhakrishnan, K., Gloss, D., Caboclo, L.O., Drislane, F.W., Koutroumanidis, M., Schomer, D.L., *et al.* (2018). Clinical utility of EEG in diagnosing and monitoring epilepsy in adults. *Clin Neurophysiol* 129, 1056-1082.
- Tiffin, J., and Asher, E.J. (1948). The Purdue pegboard; norms and studies of reliability and validity. *J Appl Psychol* 32, 234-247.
- Tolonen, M., Palva, J.M., Andersson, S., and Vanhatalo, S. (2007). Development of the spontaneous activity transients and ongoing cortical activity in human preterm babies. *Neuroscience* 145, 997-1006.
- Toyozumi, T., Miyamoto, H., Yazaki-Sugiyama, Y., Atapour, N., Hensch, T.K., and Miller, K.D. (2013). A theory of the transition to critical period plasticity: inhibition selectively suppresses spontaneous activity. *Neuron* 80, 51-63.
- Turrigiano, G.G., Leslie, K.R., Desai, N.S., Rutherford, L.C., and Nelson, S.B. (1998). Activity-dependent scaling of quantal amplitude in neocortical neurons. *Nature* 391, 892-896.
- Vahdat, S., Darainy, M., Milner, T.E., and Ostry, D.J. (2011). Functionally specific changes in resting-state sensorimotor networks after motor learning. *J Neurosci* 31, 16907-16915.

- Van der Loos, H., and Woolsey, T.A. (1973). Somatosensory cortex: structural alterations following early injury to sense organs. *Science* 179, 395-398.
- van der Pas, S.C., Verbunt, J.A., Breukelaar, D.E., van Woerden, R., and Seelen, H.A. (2011). Assessment of arm activity using triaxial accelerometry in patients with a stroke. *Arch Phys Med Rehabil* 92, 1437-1442.
- Vincent, J.L. (2009). Learning and memory: while you rest, your brain keeps working. *Curr Biol* 19, R484-486.
- Wager, T.D., Rilling, J.K., Smith, E.E., Sokolik, A., Casey, K.L., Davidson, R.J., Kosslyn, S.M., Rose, R.M., and Cohen, J.D. (2004). Placebo-induced changes in fMRI in the anticipation and experience of pain. *Science* 303, 1162-1167.
- Wang, D., Buckner, R.L., Fox, M.D., Holt, D.J., Holmes, A.J., Stoecklein, S., Langs, G., Pan, R., Qian, T., Li, K., *et al.* (2015). Parcellating cortical functional networks in individuals. *Nat Neurosci* 18, 1853-1860.
- Welker, E., Soriano, E., and Van der Loos, H. (1989). Plasticity in the barrel cortex of the adult mouse: effects of peripheral deprivation on GAD-immunoreactivity. *Exp Brain Res* 74, 441-452.
- Wellman, C.L., Arnold, L.L., Garman, E.E., and Garraghty, P.E. (2002). Acute reductions in GABAA receptor binding in layer IV of adult primate somatosensory cortex after peripheral nerve injury. *Brain Res* 954, 68-72.
- Wenger, E., Kuhn, S., Verrel, J., Martensson, J., Bodammer, N.C., Lindenberger, U., and Lovden, M. (2017). Repeated Structural Imaging Reveals Nonlinear Progression of Experience-Dependent Volume Changes in Human Motor Cortex. *Cereb Cortex* 27, 2911-2925.
- Wiesel, T.N., and Hubel, D.H. (1963). Single-Cell Responses in Striate Cortex of Kittens Deprived of Vision in One Eye. *J Neurophysiol* 26, 1003-1017.
- Wiesel, T.N., and Hubel, D.H. (1965). Comparison of the effects of unilateral and bilateral eye closure on cortical unit responses in kittens. *J Neurophysiol* 28, 1029-1040.
- Wiesel, T.N., and Hubel, D.H. (1974). Ordered arrangement of orientation columns in monkeys lacking visual experience. *J Comp Neurol* 158, 307-318.
- Wong, R.O. (1999). Retinal waves and visual system development. *Annu Rev Neurosci* 22, 29-47.
- Yeo, B.T., Krienen, F.M., Sepulcre, J., Sabuncu, M.R., Lashkari, D., Hollinshead, M., Roffman, J.L., Smoller, J.W., Zollei, L., Polimeni, J.R., *et al.* (2011). The organization of the human cerebral cortex estimated by intrinsic functional connectivity. *J Neurophysiol* 106, 1125-1165.
- Zang, Y.F., He, Y., Zhu, C.Z., Cao, Q.J., Sui, M.Q., Liang, M., Tian, L.X., Jiang, T.Z., and Wang, Y.F. (2007). Altered baseline brain activity in children with ADHD revealed by resting-state functional MRI. *Brain Dev* 29, 83-91.

Zhang, Y., Brady, M., and Smith, S. (2001). Segmentation of brain MR images through a hidden Markov random field model and the expectation-maximization algorithm. *IEEE Trans Med Imaging* 20, 45-57.